Mechanisms Shaping Excitatory Transmission at the Developing Retinogeniculate Synapse

Citation

Permanent link

Terms of Use

Share Your Story

**Mechanisms Shaping Excitatory Transmission at the
Developing Retinogeniculate Synapse**

A dissertation presented

by

Jessica Lauren Hauser

to

The Division of Medical Sciences

in partial fulfillment of the requirements

for the degree of

Doctor of Philosophy

in the subject of

Neuroscience

Harvard University

Cambridge, Massachusetts

July 2014

**Mechanisms Shaping Excitatory Transmission at the
Developing Retinogeniculate Synapse**

Abstract

The retinogeniculate synapse, the connection between retinal ganglion cells (RGCs) and thalamic relay neurons, undergoes extensive remodeling and refinement in the first few postnatal weeks. While many studies have focused on this process, little is known about the factors that influence excitatory transmission during this dynamic period. A major goal of my dissertation research was to identify mechanisms that regulate glutamate release and clearance at the developing synapse. First, we investigated the role of glutamate transporters and metabotropic glutamate receptors (mGluRs) in shaping excitatory transmission. Early in synapse development, we found that presynaptic group II/III mGluRs are present and are activated by glutamate released from RGCs following optic tract stimulation at natural frequencies. This response was found to diminish with age, but glutamate transporters continued to shape synaptic currents throughout development. The finding that glutamate is able to escape the synaptic cleft and bind extrasynaptic high-affinity mGluRs led us to speculate that glutamate might also diffuse to neighboring synapses and bind ionotropic glutamate receptors opposing quiescent release sites. Excitatory currents recorded from immature, but not mature, retinogeniculate synapses display a prolonged decay timecourse. We found evidence that both asynchronous release of glutamate as well as spillover of glutamate between neighboring synapses contributes to slowly decaying synaptic currents. Furthermore, we uncovered and characterized a novel, purely spillover-mediated current from immature relay neurons, which strongly supports the presence of glutamate spillover between boutons of different RGCs. These results indicate that far more RGCs contribute to relay neuron firing than would be predicted by the anatomy alone. Finally, in an ongoing study, we investigated the functional role of the neuronal glutamate transporter GLT-1 at the immature retinogeniculate

synapse. While GLT-1 has been found in both neurons and glia, excitatory currents at the retinogeniculate synapse were largely unaffected in mice lacking neuronal GLT-1, suggesting non-neuronal glutamate transporters are responsible for the majority of glutamate removal from the developing synapse. Taken together, these results provide insight into the synaptic environment of the developing retinogeniculate synapse and identify a number of mechanisms that shape excitatory transmission during this period of synaptic maturation and refinement.

Table of Contents

Tables and Figures

DEDICATION

This dissertation is dedicated to my parents Beverly and Kevin Hauser
my sister Jaclyn and my grandfather "Pa"
With their endless support, unconditional love and encouragement, I've been able to accomplish
things I never could have imagined. And to Pa, who I know tried his best to see this
day, thank you for sitting at the kitchen table with me and playing gin rummy.
Thank you and I love you.

<u>Acknowledgements</u>

I begin with my deep appreciation and thanks for my PhD advisor **Chinfei Chen** for all of her help and support through the years. Even before joining her lab, while I was a technician in Michael Greenberg's lab across the hall, she was exceptionally generous toward me and gave me the support and guidance I needed to pursue my educational goals. This generosity continued throughout my graduate career. I thank her for helping me grow as a scientist, challenging me to think creatively and making me practice public talks *ad nauseam*. Without her the completion of this thesis would not have been possible. It has been an honor to be in her lab and her confidence in me will continue to be a source of strength as I pursue the next step in my career.

I am also very grateful for and wish to thank my labmates, past and present- **Andrew Thompson, Liza Litvina, Kevin Park, Joseph Leffler, Erin Kang, Evi Hock, David Lin, Mac Hooks, Mallorie Stanley and Matthew Taylor** for their patience, scientific advice and a million other things like checking mice on the weekends and creating a great supportive working environment. In addition I'd like to thank my collaborator and mentor, **Paul Rosenberg** for his guidance and intellectual input on my projects.

I would like to thank my committee: **Wade Regehr, Bruce Bean** and **Beth Stevens** for their scientific guidance and support. In addition I'd like to thank the Program in Neuroscience, **Karen Harmin, Rick Born** and **Rachel Wilson** for organizing a supportive environment and individually providing me with substantial support and guidance throughout my PhD. I'd like to thank **Michael Greenberg** and **Yingxi Lin** for inspiring me to pursue science, **Michaela Fagiolini** for her encouragement and **David Cardozo** for all of his kind support, advice and faith in me even when I didn't have it myself. Also, I'd like to express my gratitude to the entire

Page intentionally left blank

CHAPTER 1

INTRODUCTION

INTRODUCTION

Synapses are specialized connections between neurons that allow one neuron to communicate with another. Synaptic transmission, the signaling between neurons, is one of the fundamental processes of the nervous system. The average neuron in the human brain is estimated to make and receive thousands of these connections, and with 10^{11} neurons in the central nervous system (CNS), there are a thousand-fold more synapses in our brain than there are stars in our galaxy (Kandel et al., 2000). Considering the enormous number of neurons and synaptic connections in the nervous system, a critical task of the developing brain is to ensure their correct wiring. Often, the initial formation of these connections is imprecise and redundant. However, over time, neural circuits undergo significant refinement, resulting in the mature connectivity that ultimately carries out all the functions of the adult brain, from simple reflexes to perception and learning.

To understand the processes involved in the proper development of synaptic connections, one must first consider some of the dynamic mechanisms responsible for shaping synaptic transmission. After initial neuronal differentiation, migration, and axon guidance, the immature contacts undergo further modifications based on both spontaneous neuronal activity and sensory experience (Katz and Shatz, 1996; Huberman, 2007; Blankenship and Feller, 2010; Hong and Chen, 2011). Examining the mechanisms that sculpt early synapses and the functional significance of synaptic differences over development provides the groundwork to identify potential mechanisms governing plasticity of an established circuit. In addition, work over the last several years has made it increasingly clear that the basis of many neurological and psychiatric disorders are linked to defects in the structure and/or function of synapses (Cohen and Greenberg, 2008), further underscoring the reach and potential of basic synaptic research.

Part I: Chemical Synapses

Chemical synapses can be divided into three compartments based on anatomy: the presynaptic terminal, the synaptic cleft, and the postsynaptic cell. The presynaptic terminal contains neurotransmitter-filled vesicles poised for release from a specialized region called the active zone. When an action potential invades the terminal, it triggers the opening of voltage-gated calcium channels. Rapid influx of calcium through these channels increases the probability of vesicle fusion to presynaptic membranes and neurotransmitter exocytosis. Once released from the presynaptic membrane, neurotransmitter diffuses across the synaptic cleft, binds receptors and channels in the opposing postsynaptic density (PSD) of the target cell, and influences the membrane potential of the postsynaptic cell through the opening or closing of channels. The synaptic response is then terminated by removal of neurotransmitter from the synaptic cleft, by diffusion, transmitter uptake, or enzymatic breakdown.

In the CNS, glutamate is the major neurotransmitter responsible for fast excitatory transmission. Glutamate binds two major classes of receptors: ligand-gated ion channels and metabotropic glutamate receptors (mGluRs). Fast excitatory transmission is mediated through non-selective cation ligand-gated channels (Dingledine et al., 1999), while the more modulatory influences of glutamate are mediated through mGluR-G protein-coupled receptor signaling (Pin and Duvoisin, 1995). Several features influence the strength of a synapse. The size of the postsynaptic response is determined by the number of release sites (N), the probability of vesicle release (P_R), and the quantal response, the amplitude of the postsynaptic response following release of a single vesicle (Del Castillo and Katz, 1954). While the original work describing synaptic transmission was performed using the squid giant axon and at the large peripheral synapse of the neuromuscular junction formed between motor neuron axons and skeletal muscles (Katz and Miledi, 1965), advances in the patch-clamp technique now (Neher and Sakmann, 1976) allow for the recording of central neurons in their intact synaptic environments. Using this

technique, the time course of signaling has been shown to vary considerably between different synapses (Jonas, 2000). When one considers the remarkable number of synapses in the brain, it is no surprise that there exists such diversity of contacts. Investigating their similarities and differences has built a foundation for understanding the basic functional unit of nervous system organization. Based on extensive work over the last several decades, we can begin to appreciate some of the major sources of this diversity.

Here, I briefly outline some of the mechanisms that are known to shape the time course of excitatory glutamatergic signaling in the CNS, roughly based on the anatomical location of the synapse. Next, I introduce an essential synapse in the visual system, the retinogeniculate synapse, which is the connection between retinal ganglion cells (RGCs) of the eye and relay neurons in the lateral geniculate nucleus (LGN) of the thalamus. The retinogeniculate synapse has been a very important model system for studying functional changes in synaptic strength over development. While numerous studies have focused on the process of synaptic refinement at the retinogeniculate contact, less is known about the mechanisms responsible for shaping excitatory transmission at the immature synapse. One of the major goals of my thesis work was to explore the immature retinogeniculate synaptic environment and to investigate the mechanisms responsible for shaping excitatory transmission during a dynamic period of synapse development.

The Presynaptic Release of Neurotransmitter

The evoked release of neurotransmitter is contingent on several events: the invasion of an action potential into the presynaptic terminal, the opening of voltage-gated calcium (Ca^{2+}) channels and subsequent Ca^{2+} influx into the terminal, and the binding of Ca^{2+} to calcium sensors associated with release machinery which ultimately triggers the exocytosis of transmitter. All of these events occur within a synaptic delay of less than a millisecond (Sabatini

4

and Regehr, 1999). Essential to the release process is the influx of Ca^{2+} into the presynaptic terminal. Therefore, mechanisms that alter the concentration or time course of Ca^{2+} in the terminal influence the dynamics of transmitter release and thereby shape the time course of the postsynaptic response.

Two types of evoked release have been described in the CNS: synchronous and delayed (asynchronous) release. Synchronous release is driven by high concentrations of Ca^{2+} (Ca^{2+}_{local}) near open channels, whereas asynchronous release is driven by residual Ca^{2+} (Ca^{2+}_{res}), in the latter case additional quantal or multiquantal release can persist for several milliseconds (Kaeser and Regehr, 2014). While a majority of CNS synaptic release is synchronous, high-frequency patterns of presynaptic activity can cause the build-up of Ca^{2+}_{res} and lead to increased asynchrony (Zengel and Magleby, 1981; Zucker and Lara-Estrella, 1983; Sakaba, 2006). In addition, broadening of the action potential waveform, especially during its repolarization phase, can prolong Ca^{2+} entry into the presynaptic terminal and reduce synchrony. The shape of the action potential, its amplitude and width, has been shown to vary considerably in the CNS, and the resulting effects on Ca^{2+} influx support the idea that these differences can affect the timing and strength of synaptic transmission (Sabatini and Regehr, 1999; Geiger and Jonas, 2000; Bean, 2007).

Another mechanism that can influence the release of neurotransmitter is the physical distance between the Ca^{2+} channels and the Ca^{2+} sensors associated with the vesicular release machinery. For example, at the young calyx of Held, a large glutamatergic synapse in the auditory system, the distance between Ca^{2+} channel and sensor is larger early in development than later (Fedchyshyn and Wang, 2005). Corresponding with a change in coupling distance from loose ("microdomain") to tight ("nanodomain") is an increase in the strength and efficiency of synaptic transmission with age (Eggermann et al., 2012). More recently this phenomenon has

been shown to occur at a mature hippocampal synapse, the mossy fiber to CA3 pyramidal neuron contact (Vyleta and Jonas, 2014). Here, loose coupling of the calcium channels and sensors allows the probability of release to be influenced by endogenous Ca^{2+} buffers in the terminals (Vyleta and Jonas, 2014). Therefore, the spacing of calcium channels and the presence of endogenous calcium buffers and/or calcium reuptake mechanisms can all influence neurotransmitter release, and therefore the shape of excitatory currents in the CNS, both during development and in mature circuits.

Presynaptic Ca^{2+} entry into the terminal can also be modulated by activation of a number of other pathways, including presynaptic cannabinoid type 1 receptors (Wilson and Nicoll, 2001; Foldy et al., 2006), $GABA_B$ receptors (Dittman and Regehr, 1996; Isaacson, 1998), adenosine receptors (Dittman and Regehr, 1996), muscarinic receptors (Howe and Surmeier, 1995), serotonin receptors (Chen and Regehr, 2003), and metabotropic glutamate receptors (Glaum and Miller, 1995; Min et al., 1998). These pathways can reduce or increase the influx of Ca^{2+} into the presynaptic terminal, and, acting through direct or indirect G-protein mediated mechanisms, decrease or enhance the probability of transmitter release.

The Time Course of Glutamate in the Synaptic Cleft

Once the vesicles fuse and release their contents into the synaptic cleft, the time course and concentration of glutamate in the cleft can influence the excitatory response of the postsynaptic cell. In cultured hippocampal neurons the peak concentration of glutamate in the cleft can reach approximately 1 mM and decay with a time constant of 1 ms (Clements et al., 1992), another CNS synapse, the climbing fiber to Purkinje cell synapse, release of multiple vesicles can cause the peak glutamate concentration in the cleft to reach as high as 10mM (Clements et al., 1992; Wadiche and Jahr, 2001). In the peripheral nervous system, at the neuromuscular junction, the neurotransmitter acetylocholine is enzymatically broken down in the cleft, thereby terminating its

influence on the muscle. However, at excitatory glutamatergic synapses in the CNS, no such enzymes are present to remove active transmitter. Rather, the concentration profile of glutamate is determined by two major mechanisms: clearance through diffusion and removal by high-affinity glutamate transporters.

Diffusion of glutamate across the narrow synaptic cleft (~20 nm) only takes tens of microseconds (Sabatini and Regehr, 1999). However, synapse geometry can have a major influence on diffusion (Bergles et al., 1999). Simple morphology and extensive extracellular space surrounding small synaptic contacts facilitate rapid clearance of glutamate by diffusion. Conversely, broad contacts with multiple release sites surrounded by dense extracellular space or glial sheaths impede transmitter diffusion and prolong the time course of glutamate binding to postsynaptic receptors (Sykova and Nicholson, 2008). A prime example of the latter is the mossy fiber- unipolar brush cell contact of the cerebellum, where glutamate becomes trapped in the cleft and causes dramatically prolonged synaptic currents (Kinney et al., 1997). Interestingly, changes in synaptic anatomy have been shown to contribute to the developmental acceleration of postsynaptic currents. At the mossy fiber-granule cell synapse in the cerebellum, developmental changes in the size and location of the postsynaptic density and surrounding neuropil underlie the speeding of currents with age (Cathala et al., 2005). In addition, in the rat hypothalamic supraoptic nucleus, glutamate clearance and activation of extrasynaptic receptors is determined by the extent of glial coverage (Oliet et al., 2001). Therefore, physically impeding glutamate escape into the extrasynaptic space can have a significant influence on synaptic transmission by prolonging the activation of both metabotropic and ionotropic glutamate receptors.

Fast excitatory synaptic transmission is often thought to occur in a "point-to-point" manner, where release of glutamate from a single active zone diffuses across the cleft to exclusively bind

to directly opposing ionotropic receptors in the postsynaptic density. This impression of transmission is often disregarded particularly at synapses with multiple closely arranged release sites (Sykova and Nicholson, 2008). Closely spaced release sites with high probability of release can increase the chances of glutamate pooling or spillover between release sites, or even between independent synaptic contacts. In addition, prolonged, high concentrations of glutamate can be reached through the concomitant release of multiple vesicles from a single release site, termed multivesicular release, or following trains of stimuli (Trussell et al., 1993; Carter and Regehr, 2000; Wadiche and Jahr, 2001; Rudolph et al., 2011). Thus, the concentration and spread of glutamate within the synaptic microenvironment can influence the extent of receptor activation and the time course of the postsynaptic response.

In addition to diffusion, the removal of glutamate through high-affinity glutamate transporters contributes to the time course of peak glutamate concentration at the synapse (Diamond and Jahr, 1997). One major role of glutamate transporters is to maintain low concentrations of ambient glutamate (approximately ~25 nM; (Herman and Jahr, 2007). The location and density of glutamate transporters matter, as several studies have now shown that glutamate transporters can limit the extent of glutamate spillover to neighboring synapses and the activation of extrasynaptic receptors. At climbing fiber to Purkinje cell synapses of the cerebellum, Bergmann glial cells closely oppose contacts and prevent glutamate spillover between release sites. In addition, also in the cerebellum, neuronal glutamate transporters shield activation of postsynaptic mGluRs, thereby influencing synaptic plasticity (Brasnjo and Otis, 2001; Wadiche and Jahr, 2005). At hippocampal synapses, neuronal glutamate transporters have been shown to regulate glutamate clearance and activation of extrasynaptic receptors through glutamate buffering as well (Diamond, 2001; Scimemi et al., 2009).

Therefore, glutamate clearance from the synaptic cleft, through diffusion, buffering or reuptake by high affinity glutamate transporters, can influence the extent to which both metabotropic and ionotropic glutamatergic receptors are activated, shaping the time course of synaptic transmission in CNS synapses.

Properties of Postsynaptic Receptors

The shape of the postsynaptic response is also influenced by the composition and properties of postsynaptic receptors. Three major classes of ionotropic glutamate receptor channels are found postsynaptic to excitatory synaptic terminals: α-amino-3-hydroxy-5-methyl-4-isoxazolepropionic acid receptors (AMPARs), kainate receptors (KARs) and *N*-methyl-D-aspartate receptors (NMDARs)(Dingledine et al., 1999) Most excitatory synapses in the CNS contain both postsynaptic AMPAR and NMDARs. Not many synapses have postsynaptic KAR, although KARs are sometimes present on presynaptic terminals (Chittajallu et al., 1996).

AMPA receptors are composed of four subunits: GluA1 -4 (Dingledine et al., 1999). The fast component of excitatory postsynaptic currents (EPSCs) in neurons is mediated by the low affinity AMPARs, whereas the slower decay of the EPSC is mediated by NMDARs. Since AMPARs have a much lower affinity for glutamate than NMDARs, glutamate unbinds rapidly from these receptors, which quickly close in a process called deactivation (Dingledine et al., 1999). Even if glutamate is not removed from the cleft, AMPARs close and become desensitized, no longer responding to additional exposure of glutamate until they have recovered (Raman and Trussell, 1992). The majority of AMPAR channels are permeable to both sodium and potassium cations but are impermeable to calcium. Posttranscriptional editing of the GluR2 mRNA causes a single amino acid change that renders these channels impermeable to calcium, but a fraction of AMPA receptors lack the GluR2 subunit and are calcium permeable. The expression of calcium permeable and impermeable AMPARs has been shown to change

9

with age at some synapses (Ho et al., 2007; Takeuchi et al., 2012; Hauser et al., 2014). Another developmental change that occurs at a number of synapses is the ratio of AMPARs to NMDARs, with the number of AMPARs in the postsynaptic membrane increasing there is an increase in the quantal response to glutamate (Hsia et al., 1998; Chen and Regehr, 2000).

NMDARs, unlike AMPARs, have a much higher affinity for glutamate and slower channel kinetics. A classic experiment showed that NMDARs can stay activated even hundreds of milliseconds after glutamate is removed from the extracellular solution (Lester et al., 1990). NMDARs are composed of four subunits: two obligatory GluN1 subunits that bind glycine, combined with two GluN2 (A-D) subunits that bind glutamate (Dingledine et al., 1999). Glycine is often present in saturating concentrations, so glutamate is the neurotransmitter required for receptor activation. NMDARs have been termed 'coincidence detectors' because they display voltage-dependent block by extracellular Mg^{2+} ions. In order for current to flow through the receptor there must be both the presynaptic release of glutamate and sufficient depolarization of the postsynaptic membrane to relieve the Mg^{2+} block. Different GluN2 subunits display varying sensitivities to Mg^{2+} block, with NR2C/D subunits being less sensitive than NR2A/B (Kirson et al., 1999; Misra et al., 2000). In addition, high affinity to glutamate predisposes NMDARs to saturate at some CNS synapses when there are fewer receptors available following repeated exposure to glutamate. In fact, both receptor desensitization and saturation have been shown to shape short-term plasticity at the mature retinogeniculate synapse (Chen et al., 2002; Budisantoso et al., 2012).

Taken together, several mechanisms in the presynaptic membrane, the synaptic cleft, and postsynaptic membranes influence the shape of excitatory synaptic transmission. Differences in release, glutamate diffusion, and receptor composition all contribute to the astonishing diversity

of synapses in the CNS. Moreover, many of these features are modified over development and serve as substrates of synaptic plasticity in the mature nervous system.

PART II: The Retinogeniculate Synapse

Essential to our understanding of the complexity of neural circuits in the adult brain is the investigation of how patterns of connectivity emerge over development. During the initial stages of development, synaptic connections undergo robust changes in strength and wiring (Huberman, 2007; Hong and Chen, 2011). The proper development of many neural circuits relies on the propagation of spontaneous activity throughout the network (Katz and Shatz, 1996; Kirkby et al., 2013), so information used to sculpt mature specificity is being relayed via immature synapses during this dynamic period of circuit formation (Mooney et al., 1996; Weliky and Katz, 1999; Furman and Crair, 2012). The visual system is one of the classical model systems used to understand this process.

In the adult, a visual scene represented by patterns of photons is translated into patterns of spikes in retinal ganglion cells (RGCs). RGCs send their projections to relay neurons of the lateral geniculate nucleus (LGN) of the thalamus, which in turn project to primary visual cortex, where the cortical processing of visual information begins (Kandel et al., 2000). However, well before the onset of vision, spontaneous retinal activity propagates through the LGN to the developing cortex (Furman and Crair, 2012). The glutamatergic contact between RGCs and relay neurons of the LGN, the retinogeniculate synapse, has been shown to undergo extensive synaptic remodeling over the first four postnatal weeks (in mice). Three major stages of development have been described. First, RGCs originating from each eye project axons to overlapping territories in the LGN, with axonal arbors undergoing large-scale refinement and segregation into eye-specific zones by p8 in mice (Ziburkus et al., 2003; Jaubert-Miazza et al., 2005; Huberman, 2007). This initial stage of refinement has been shown to require spontaneous

11

activity, or retinal waves, in the form of high-frequency bursts synchronized among neighboring RGCs in the developing retina (Torborg and Feller, 2005; Blankenship and Feller, 2010). Eye-specific segregation results from a competitive process of pruning inappropriate axonal branches and the growth of appropriately targeted axons (Huberman, 2007).

After this initial eye-specific segregation, a second stage of robust functional synaptic remodeling occurs. During this stage, between p8 and p20, the number of RGCs that innervate each relay neuron dramatically declines, while the synaptic strength of the remaining inputs increases (Figure 1.1;(Chen and Regehr, 2000). While these first two stages have been shown to rely on spontaneous retinal activity, a third stage of refinement that requires visual experience occurs between p20 and 30. During this last stage, retinogeniculate inputs stabilize to their mature state (Hooks and Chen, 2006; Hong and Chen, 2011). Ultimately, the output of a relay neuron is dominated by a single RGC input, and the two cells share similar receptive fields (Tavazoie and Reid, 2000; Sincich et al., 2009).

What synaptic mechanisms underlie the developmental changes in this visual circuit? Using minimal stimulation of the optic tract, it has been shown that the strength of a single fiber response increases from tens of picoamperes to nanoamperes following eye opening (Chen and Regehr, 2000). This coincides with a small but significant increase in quantal size (q), most likely due to the insertion of AMPARs with age. However, the most influential mechanism of synaptic strengthening that occurs at the retinogeniculate synapse is the re-arrangement of release sites. While the total number of release sites onto a given relay neuron does not significantly change with age, rearrangement of these release sites, such that they come from a few RGCs rather than many, significantly increases the strength of retinogeniculate contacts. In fact, at the mature retinogeniculate contact, presynaptic boutons of RGC axons make broad contacts onto the proximal dendrites of LGN relay neurons and contain multiple release sites for
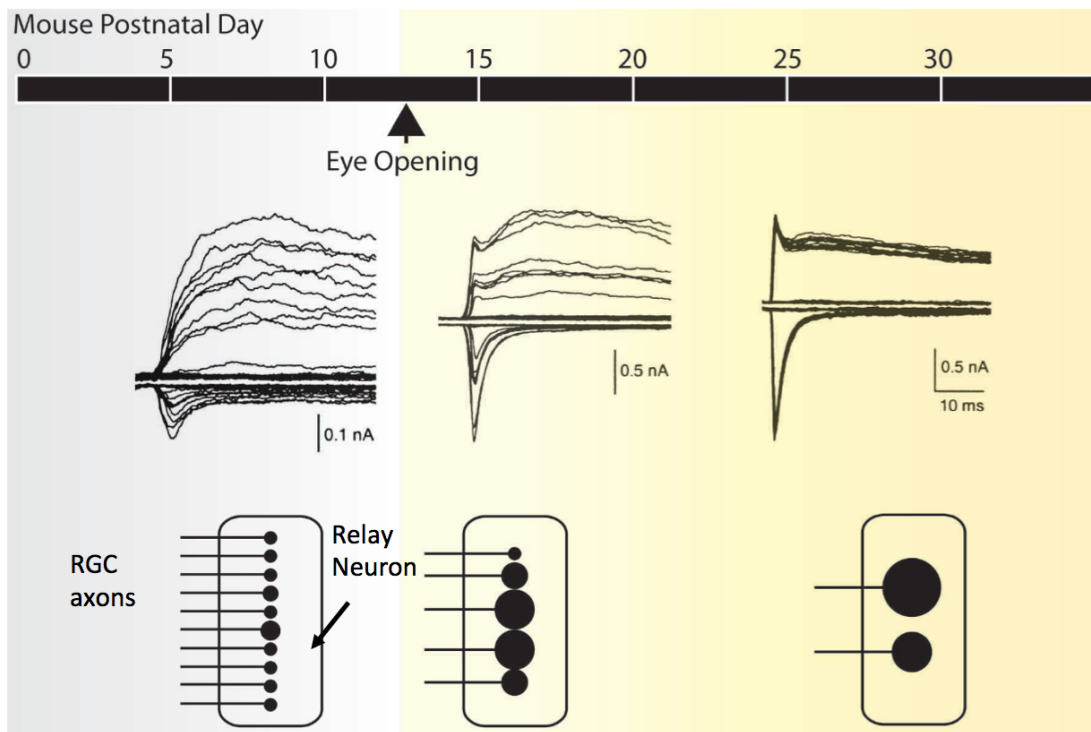
Figure 1.1: Functional development of the mouse retinogeniculate synapse
(Top) Representative excitatory synaptic responses to incremental increases of optic nerve stimulation from p11, 17 and 28 mice. Currents are recorded while alternating the holding potential between V_n=-70 and +40mV to measure both AMPAR and NMDAR currents, respectively. (Bottom) Schematic representation of synaptic refinement drawn to symbolize the experimental data where a number of inputs of different strengths are represented by the sizes of the circles. With normal development, synaptic strength increases 20-fold and the afferent inputs decrease from many to few. Figure adapted from (Hong and Chen, 2011)

glutamate—according to one estimate, an average of 27 release sites within a single RGC bouton in the adult LGN (Rafols and Valverde, 1973; Budisantoso et al., 2012). Further, new evidence from the Chen lab suggests that boutons of RGCs expand and cluster in a fashion that parallels the functional remodeling, and that the spatial organization of these boutons can respond to sensory experience (Hong et al. in revision).

Despite the dramatic changes in synaptic connectivity and strength taking place during the first postnatal month, retinal activity propagates throughout the developing visual circuit (Mooney et al., 1996; Furman and Crair, 2012). This is somewhat surprising given that individual synapses are often too weak to reliably drive relay neuron firing alone (Seeburg et al., 2004; Liu and Chen, 2008). While several studies have focused on the synaptic refinement of this contact, less is known regarding the basic synaptic properties in place that influence synaptic transmission. The major objective of my dissertation research was to identify mechanisms at the immature retinogeniculate synapse that influence the shape of excitatory transmission during this dynamic period.

Aim of this study

This thesis investigates the properties of the developing retinogeniculate synapse that influence the concentration of glutamate at and around the synapse. Moreover, I address how these mechanisms influence the shape of relay neuron synaptic currents. To examine synaptic transmission at the retinogeniculate synapse, I used whole-cell patch clamp of relay neurons in an acute parasagittal mouse slice that preserves both the optic tract and the LGN. Using this preparation I addressed the following questions:

(1) Are glutamate transporters present at the retinogeniculate synapse, and can they shape the time course of synaptic currents?

(2) What role do metabotropic glutamate receptors play at the developing synapse?

(3) Does spillover of glutamate occur early in development, and how extensive is the spillover (e.g. is there inter-bouton spillover)?

(4) Does the glutamate transient change over development? And does the nature of glutamate spillover change with age?

(5) Do changes in the subunit composition of ionotropic glutamate receptors account for the developmental acceleration of the synaptic current?

(6) Is the glutamate transporter GLT1 expressed in neurons of the developing

   retinogeniculate synapse, and if so, does it shape the time course of the glutamate

   transient?

(7) Is GLT1 expressed in glia surrounding the developing retinogeniculate synapse, and

   if so, does it shape the time course of the glutamate transient?

REFERENCES

Bean BP (2007) The action potential in mammalian central neurons. Nature reviews Neuroscience 8:451-465.

Bergles DE, Diamond JS, Jahr CE (1999) Clearance of glutamate inside the synapse and beyond. Current opinion in neurobiology 9:293-298.

Blankenship AG, Feller MB (2010) Mechanisms underlying spontaneous patterned activity in developing neural circuits. Nature reviews Neuroscience 11:18-29.

Brasnjo G, Otis TS (2001) Neuronal glutamate transporters control activation of postsynaptic metabotropic glutamate receptors and influence cerebellar long-term depression. Neuron 31:607-616.

Budisantoso T, Matsui K, Kamasawa N, Fukazawa Y, Shigemoto R (2012) Mechanisms underlying signal filtering at a multisynapse contact. The Journal of neuroscience : the official journal of the Society for Neuroscience 32:2357-2376.

Carter AG, Regehr WG (2000) Prolonged synaptic currents and glutamate spillover at the parallel fiber to stellate cell synapse. The Journal of neuroscience : the official journal of the Society for Neuroscience 20:4423-4434.

Cathala L, Holderith NB, Nusser Z, DiGregorio DA, Cull-Candy SG (2005) Changes in synaptic structure underlie the developmental speeding of AMPA receptor-mediated EPSCs. Nature neuroscience 8:1310-1318.

Chen C, Regehr WG (2000) Developmental remodeling of the retinogeniculate synapse. Neuron 28:955-966.

Chen C, Regehr WG (2003) Presynaptic modulation of the retinogeniculate synapse. The Journal of neuroscience : the official journal of the Society for Neuroscience 23:3130-3135.

Chen C, Blitz DM, Regehr WG (2002) Contributions of receptor desensitization and saturation to plasticity at the retinogeniculate synapse. Neuron 33:779-788.

Chittajallu R, Vignes M, Dev KK, Barnes JM, Collingridge GL, Henley JM (1996) Regulation of glutamate release by presynaptic kainate receptors in the hippocampus. Nature 379:78-81.

Clements JD, Lester RA, Tong G, Jahr CE, Westbrook GL (1992) The time course of glutamate in the synaptic cleft. Science 258:1498-1501.

Cohen S, Greenberg ME (2008) Communication between the synapse and the nucleus in neuronal development, plasticity, and disease. Annual review of cell and developmental biology 24:183-209.

Del Castillo J, Katz B (1954) Quantal components of the end-plate potential. The Journal of physiology 124:560-573.

Diamond JS (2001) Neuronal glutamate transporters limit activation of NMDA receptors by neurotransmitter spillover on CA1 pyramidal cells. The Journal of neuroscience : the official journal of the Society for Neuroscience 21:8328-8338.

Diamond JS, Jahr CE (1997) Transporters buffer synaptically released glutamate on a submillisecond time scale. The Journal of neuroscience : the official journal of the Society for Neuroscience 17:4672-4687.

Dingledine R, Borges K, Bowie D, Traynelis SF (1999) The glutamate receptor ion channels. Pharmacological reviews 51:7-61.

Dittman JS, Regehr WG (1996) Contributions of calcium-dependent and calcium-independent mechanisms to presynaptic inhibition at a cerebellar synapse. The Journal of neuroscience : the official journal of the Society for Neuroscience 16:1623-1633.

Eggermann E, Bucurenciu I, Goswami SP, Jonas P (2012) Nanodomain coupling between Ca(2)(+) channels and sensors of exocytosis at fast mammalian synapses. Nature reviews Neuroscience 13:7-21.

Fedchyshyn MJ, Wang LY (2005) Developmental transformation of the release modality at the calyx of Held synapse. The Journal of neuroscience : the official journal of the Society for Neuroscience 25:4131-4140.

Foldy C, Neu A, Jones MV, Soltesz I (2006) Presynaptic, activity-dependent modulation of cannabinoid type 1 receptor-mediated inhibition of GABA release. The Journal of neuroscience : the official journal of the Society for Neuroscience 26:1465-1469.

Furman M, Crair MC (2012) Synapse maturation is enhanced in the binocular region of the retinocollicular map prior to eye opening. Journal of neurophysiology 107:3200-3216.

Geiger JR, Jonas P (2000) Dynamic control of presynaptic Ca(2+) inflow by fast-inactivating K(+) channels in hippocampal mossy fiber boutons. Neuron 28:927-939.

Glaum SR, Miller RJ (1995) Presynaptic metabotropic glutamate receptors modulate omega-conotoxin-GVIA-insensitive calcium channels in the rat medulla. Neuropharmacology 34:953-964.

Hauser JL, Liu X, Litvina EY, Chen C (2014) Prolonged Synaptic Currents Increase Relay Neuron Firing at the Developing Retinogeniculate Synapse. Journal of neurophysiology.

Herman MA, Jahr CE (2007) Extracellular glutamate concentration in hippocampal slice. The Journal of neuroscience : the official journal of the Society for Neuroscience 27:9736-9741.

Ho MT, Pelkey KA, Topolnik L, Petralia RS, Takamiya K, Xia J, Huganir RL, Lacaille JC, McBain CJ (2007) Developmental expression of Ca2+-permeable AMPA receptors underlies depolarization-induced long-term depression at mossy fiber CA3 pyramid synapses. The Journal of neuroscience : the official journal of the Society for Neuroscience 27:11651-11662.

Hong YK, Chen C (2011) Wiring and rewiring of the retinogeniculate synapse. Current opinion in neurobiology 21:228-237.

Hooks BM, Chen C (2006) Distinct roles for spontaneous and visual activity in remodeling of the retinogeniculate synapse. Neuron 52:281-291.

Howe AR, Surmeier DJ (1995) Muscarinic receptors modulate N-, P-, and L-type Ca2+ currents in rat striatal neurons through parallel pathways. The Journal of neuroscience : the official journal of the Society for Neuroscience 15:458-469.

Hsia AY, Malenka RC, Nicoll RA (1998) Development of excitatory circuitry in the hippocampus. Journal of neurophysiology 79:2013-2024.

Huberman AD (2007) Mechanisms of eye-specific visual circuit development. Current opinion in neurobiology 17:73-80.

Isaacson JS (1998) GABAB receptor-mediated modulation of presynaptic currents and excitatory transmission at a fast central synapse. Journal of neurophysiology 80:1571-1576.

Jaubert-Miazza L, Green E, Lo FS, Bui K, Mills J, Guido W (2005) Structural and functional composition of the developing retinogeniculate pathway in the mouse. Visual neuroscience 22:661-676.

Jonas P (2000) The Time Course of Signaling at Central Glutamatergic Synapses. News in physiological sciences : an international journal of physiology produced jointly by the International Union of Physiological Sciences and the American Physiological Society 15:83-89.

Kaeser PS, Regehr WG (2014) Molecular mechanisms for synchronous, asynchronous, and spontaneous neurotransmitter release. Annual review of physiology 76:333-363.

Kandel ER, Schwartz JH, Jessell TM (2000) Principles of neural science, 4th Edition. New York: McGraw-Hill, Health Professions Division.

Katz B, Miledi R (1965) Release of acetylcholine from a nerve terminal by electric pulses of variable strength and duration. Nature 207:1097-1098.

Katz LC, Shatz CJ (1996) Synaptic activity and the construction of cortical circuits. Science 274:1133-1138.

Kinney GA, Overstreet LS, Slater NT (1997) Prolonged physiological entrapment of glutamate in the synaptic cleft of cerebellar unipolar brush cells. Journal of neurophysiology 78:1320-1333.

Kirkby LA, Sack GS, Firl A, Feller MB (2013) A role for correlated spontaneous activity in the assembly of neural circuits. Neuron 80:1129-1144.

Kirson ED, Schirra C, Konnerth A, Yaari Y (1999) Early postnatal switch in magnesium sensitivity of NMDA receptors in rat CA1 pyramidal cells. The Journal of physiology 521 Pt 1:99-111.

18

Lester RA, Clements JD, Westbrook GL, Jahr CE (1990) Channel kinetics determine the time course of NMDA receptor-mediated synaptic currents. Nature 346:565-567.

Liu X, Chen C (2008) Different roles for AMPA and NMDA receptors in transmission at the immature retinogeniculate synapse. Journal of neurophysiology 99:629-643.

Min MY, Rusakov DA, Kullmann DM (1998) Activation of AMPA, kainate, and metabotropic receptors at hippocampal mossy fiber synapses: role of glutamate diffusion. Neuron 21:561-570.

Misra C, Brickley SG, Farrant M, Cull-Candy SG (2000) Identification of subunits contributing to synaptic and extrasynaptic NMDA receptors in Golgi cells of the rat cerebellum. The Journal of physiology 524 Pt 1:147-162.

Mooney R, Penn AA, Gallego R, Shatz CJ (1996) Thalamic relay of spontaneous retinal activity prior to vision. Neuron 17:863-874.

Neher E, Sakmann B (1976) Single-channel currents recorded from membrane of denervated frog muscle fibres. Nature 260:799-802.

Oliet SH, Piet R, Poulain DA (2001) Control of glutamate clearance and synaptic efficacy by glial coverage of neurons. Science 292:923-926.

Pin JP, Duvoisin R (1995) The metabotropic glutamate receptors: structure and functions. Neuropharmacology 34:1-26.

Rafols JA, Valverde F (1973) The structure of the dorsal lateral geniculate nucleus in the mouse. A Golgi and electron microscopic study. The Journal of comparative neurology 150:303-332.

Raman IM, Trussell LO (1992) The kinetics of the response to glutamate and kainate in neurons of the avian cochlear nucleus. Neuron 9:173-186.

Rudolph S, Overstreet-Wadiche L, Wadiche JI (2011) Desynchronization of multivesicular release enhances Purkinje cell output. Neuron 70:991-1004.

Sabatini BL, Regehr WG (1999) Timing of synaptic transmission. Annual review of physiology 61:521-542.

Sakaba T (2006) Roles of the fast-releasing and the slowly releasing vesicles in synaptic transmission at the calyx of held. The Journal of neuroscience : the official journal of the Society for Neuroscience 26:5863-5871.

Scimemi A, Tian H, Diamond JS (2009) Neuronal transporters regulate glutamate clearance, NMDA receptor activation, and synaptic plasticity in the hippocampus. The Journal of neuroscience : the official journal of the Society for Neuroscience 29:14581-14595.

Seeburg DP, Liu X, Chen C (2004) Frequency-dependent modulation of retinogeniculate transmission by serotonin. The Journal of neuroscience : the official journal of the Society for Neuroscience 24:10950-10962.

Sincich LC, Horton JC, Sharpee TO (2009) Preserving information in neural transmission. The Journal of neuroscience : the official journal of the Society for Neuroscience 29:6207-6216.

Sykova E, Nicholson C (2008) Diffusion in brain extracellular space. Physiological reviews 88:1277-1340.

Takeuchi Y, Yamasaki M, Nagumo Y, Imoto K, Watanabe M, Miyata M (2012) Rewiring of afferent fibers in the somatosensory thalamus of mice caused by peripheral sensory nerve transection. The Journal of neuroscience : the official journal of the Society for Neuroscience 32:6917-6930.

Tavazoie SF, Reid RC (2000) Diverse receptive fields in the lateral geniculate nucleus during thalamocortical development. Nature neuroscience 3:608-616.

Torborg CL, Feller MB (2005) Spontaneous patterned retinal activity and the refinement of retinal projections. Progress in neurobiology 76:213-235.

Trussell LO, Zhang S, Raman IM (1993) Desensitization of AMPA receptors upon multiquantal neurotransmitter release. Neuron 10:1185-1196.

Vyleta NP, Jonas P (2014) Loose coupling between Ca2+ channels and release sensors at a plastic hippocampal synapse. Science 343:665-670.

Wadiche JI, Jahr CE (2001) Multivesicular release at climbing fiber-Purkinje cell synapses. Neuron 32:301-313.

Wadiche JI, Jahr CE (2005) Patterned expression of Purkinje cell glutamate transporters controls synaptic plasticity. Nature neuroscience 8:1329-1334.

Weliky M, Katz LC (1999) Correlational structure of spontaneous neuronal activity in the developing lateral geniculate nucleus in vivo. Science 285:599-604.

Wilson RI, Nicoll RA (2001) Endogenous cannabinoids mediate retrograde signalling at hippocampal synapses. Nature 410:588-592.

Zengel JE, Magleby KL (1981) Changes in miniature endplate potential frequency during repetitive nerve stimulation in the presence of Ca2+, Ba2+, and Sr2+ at the frog neuromuscular junction. The Journal of general physiology 77:503-529.

Ziburkus J, Lo FS, Guido W (2003) Nature of inhibitory postsynaptic activity in developing relay cells of the lateral geniculate nucleus. Journal of neurophysiology 90:1063-1070.

Zucker RS, Lara-Estrella LO (1983) Post-tetanic decay of evoked and spontaneous transmitter release and a residual-calcium model of synaptic facilitation at crayfish neuromuscular junctions. The Journal of general physiology 81:355-372.

CHAPTER 2:

Materials and Methods

Brain dissection and Slice Preparation

Postnatal day (p)8-34 C57/BL/6 mice (C57BL/6J from Jackson Laboratory, ME) of either sex were anesthetized with isoflurane inhalation and decapitated. All procedures were performed in accordance with federal guidelines and protocols approved by Boston Children's Hospital. Dissecting scissors (World Precision Instruments) were used to make a single centerline cut through the base of the skull and brainstem extending over the olfactory bulb with the blade held laterally to minimize damage to the cortex while cutting the skull. A pair of forceps was used to remove the bone and expose the brain. Two coronal block cuts were made using a standard steel razor blade- one just caudal the olfactory bulb and the other rostral the cerebellum. Following these cuts the brain was removed and placed in ice cold choline-based dissection solution containing the following (in mM): 130 Choline chloride, 26 NaHCO3, 1.25 NaH2PO4, 2.5 KCl, 7.0 MgCl2, 0.5 CaCl2 and 25 glucose (Sigma, St. Louis MO) that was saturated with 95% O_2 / 5% CO_2.

An additional block cut was made in a near parasagittal plane between the centerline and the left hemisphere at a 10° angle from the rostral midsagittal plane. The surface from this block cut was used as the surface glued to the vibratome cutting block, with the dorsal cortical surface upright. The cutting block used was a plexiglass wedge cut at an 18° angle. Brains were sectioned on a VT1000 Leica vibratome using a blade from Delaware Diamond Knives (DDK) that was previously found to improve cell viability. Parasagittal sections 250μm thick were cut using a relatively slow cutting speed at high frequency. The major advantage of this slice orientation is that it preserves a much greater amount of the optic tract fibers than a coronal slice. Moreover, it reduces the amount of contamination from corticothalamic fibers and brainstem inputs (Figure 2.1). It was originally described for rat in (Turner and Salt, 1998) and modified for mouse by Dr. Chen (Chen and Regehr, 2000). Following sectioning, acute slices

were bathed in the choline cutting solution at 31°C for 20 minutes, and then normal aCSF at

31°C for 20 minutes or until use.
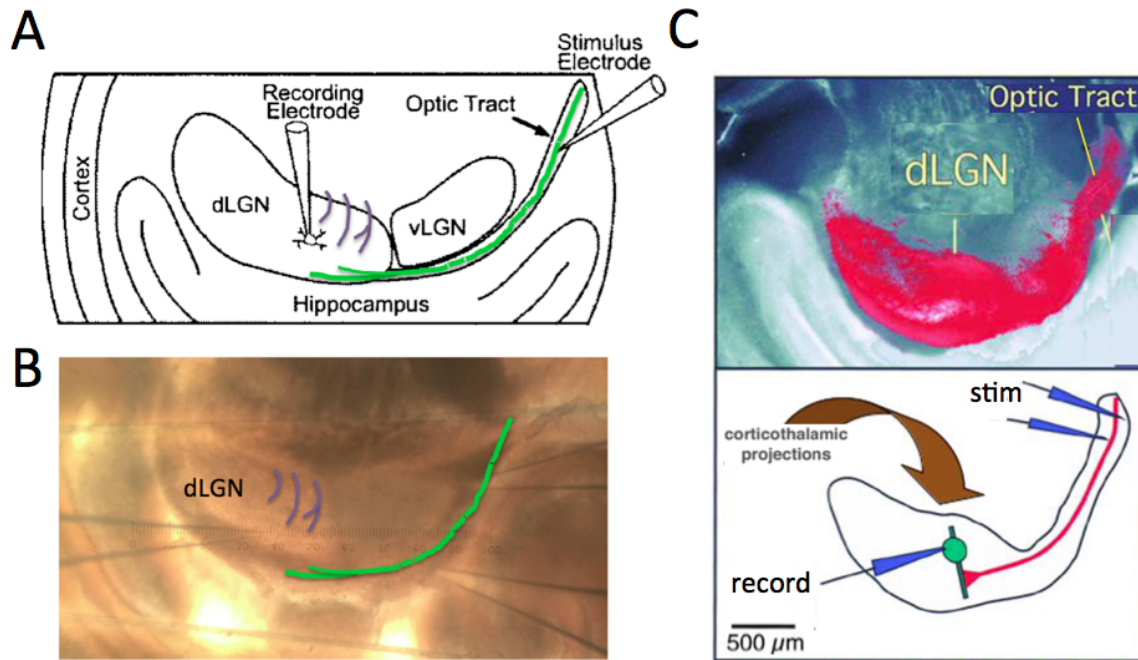
Figure 2.1: Acute Slice Preparation of the mouse LGN
(A) Schematic illustration of the near parasaggital brain slice preparation (from Blitz and Regehr, 2003) and (B) image of acute slice in similar orientation demonstrating placement of recording and stimulus electrode and modified to show retinal ganglion cell axons (green) and corticothalamic inputs (purple). (C, *top*) DiI-labelled (red) retinal ganglion cell axons from the contralateral eye enter the LGN (from Chen and Regehr, 2000), (*bottom*) schematic showing location of stimulating and recording electrodes, retinogeniculate axon (red), relay neuron (green) and where corticothalamic fibers enter the LGN (brown arrow).

Whole Cell Recordings

Electrophysiology. Whole-cell recordings of thalamic relay neurons were acquired using glass

patch pipettes (1.0-2.0 MΩ resistance) filled with internal solution containing (in mM): 35 CsF,

100 CsCl, 10 EGTA, 10 HEPES, the L-type calcium channel antagonist, 0.1 methoxyverapamil

hydrochloride (Sigma, St. Louis, MO) and adjusted to 290-300 mOsm, pH 7.3 for voltage clamp

experiments. This solution was designed to minimize the contributions from postsynaptic

intrinsic membrane conductance and second messenger systems. Relay neurons were visualized using DIC optics (Olympus). Voltage clamp recordings were made using an Axopatch 200B or Multiclamp 700A amplifier (Axon Instruments, Foster City, CA), filtered at 1kHz and digitized at 4-50 kHz with an ITC-16 interface (InstruTECH, Port Washington, NY). EPSCs were evoked by current pulses delivered to the intact optic tract (Figure 2.1) by a pair of aCSF filled glass micropipettes (Drummond Scientific, Broomall, PA), connected to a stimulus isolator (World Precision Instruments, Sarasota, FL), with intensities that ranged from 10-150 μA. The membrane potential of the relay neuron was clamped at either -70 mV or +40 mV (for AMPAR mediated EPSCs and NMDAR mediated EPSCs respectively) during stimulation of the optic tract, and was held at 0 mV between stimulation trials. For baseline recordings, optic tract was stimulated at a frequency of 0.025 Hz for NMDAR- EPSCs and 0.05 Hz for AMPA-EPSCs. To ensure consistent access resistance (R_s) of the recording electrode throughout the entire experiment, we monitored the peak amplitude of a brief (10 ms) hyperpolarizing test pulse (5 mV) given prior to the optic tract stimulation. R_s was <10MΩ (average 5 MΩ), cells were excluded if R_S changed more than 10% during an experiment. Most experiments were performed at 35 ± 1°C, temperature was controlled using an in-line heating device SH27B and Temperature controller TC324B (Warner Instrument, Hamden CT).

Data Acquisition and Analysis. Voltage-clamp recordings were acquired with a Multiclamp 700A amplifier (Axon Instruments, CA) filtered at 1 kHz and digitized at 10-20 kHz with an ITC-16 interface (Instrutech, NY). Data analysis was performed using Igor software (Wavemetrics, OR), Excel (Microsoft, WA) and Prism (GraphPad Software, Inc.). All data are summarized as mean ± SEM, using the two-tailed paired t-test unless otherwise indicated.

Solutions

Table 2.1: External Solutions:

Salt (mM)	aCSF	Cutting solution I	Cutting solution II
NaCl	125		87
NaHCO$_3$	26	26	25
NaH$_2$PO$_4$	1.25	1.25	1.25
KCl	2.5	2.5	2.5
MgCl$_2$	1	7	7
CaCl$_2$	2	0.5	0.5
Glucose	25	25	25
Choline chloride		130	37.5

Table 2.2: Internal Solutions

Salt (mM)	Internal Solution	Current Clamp
CsF	35	
CsCl	100	
EGTA	10	0.5
HEPES	10	20
KMeSO$_4$		116
KCl		6
NaCl		20
Na phosphocreatine		10
MgATP		4
NaGTP		0.3
pH	7.3 with CsOH	7.25 with KOH

Table 2.3: Pharmacology

Drug name	Concentration	Action
Bicuculline	20 µM	$GABA_A$-receptor antagonist
NBQX	200nM, 5 µM	Competitive high AMPA-receptor antagonist
Cyclothiazide	50 µM	AMPAR-selective desensitization inhibitor
TBOA	10-50 µM	Glutamate transporter antagonist
L-AP5	1 mM	Low-affinity NMDAR antagonist
D-AP5	50-100 µM	High-affinity NMDAR antagonist
(R)-CPP	20 µM	High-affinity NMDAR antagonist
g-DGG	1-3 mM	Low-affinity AMPAR antagonist
GYKI 52466	50 µM	AMPAR-selective high affinity antagonist
DPCPX	10 µM	A_1 adenosine receptor antagonist
CGP55845	2 µM	$GABA_B$ receptor antagonist
LY341495	50 µM	Group II/III mGluR antagonist
(S)-DHPG	1-25 µM	Selective group I mGluR agonist
APDC	1-30 µM	Selective group II mGluR agonist
L-AP4	10-500 µM	Selective group III mGluR agonist
EGTA-AM	50 µM	Membrane permeable calcium chelator
Methoxyverapamil hydrochloride	100 µM	L-type calcium channel antagonist

Mice

All experiments were approved by the institutional animal use and care committee at Boston Children's Hospital and were in accordance with NIH guidelines for the humane treatment of animals. For the majority of the experiments, p8-35 C57BL/6J mice (Jax stock no. 000664) of either sex were used. While these mice are known to develop age related hearing loss (around 10 months), they do not express any of the known mutations that lead to retinal degeneration.

GLT-1 conditional knockout mice were generated in the lab of Dr. Paul Rosenberg. Briefly, loxP sites were inserted 217 bp upstream and 419 bp downstream of Slc1a2 gene exon 4. A previously established full GLT1 knockout showed that removal of exon 4 from Slc1a2 results in an mRNA transcript that prevents production of GLT-1 protein in the brains of mutant mice (Tanaka et al., 1997). To generate a neuronal knockout of GLT-1 male mice carrying the conditional GLT-1 knockout allele (GLT1$^{flox/flox}$), GLT1$^{flox/flox}$ male mice were mated with female mice, also GLT1$^{flox/flox}$, that carried the synapsin I promoter-driven Cre recombinase allele,

(Synapsin/Cre, (Rempe et al., 2006); Jax stock no. 003966). For control experiments,

synapsin/Cre mice were crossed with c57bl/6 wildtype males. Detailed description of the

generation and validation of neuronal- specific knockouts of GLT1 can be found in (Petr, Sun et

al. *submitted 2014*).

PCR

PCR reactions were assembled for GLT1 and control gapdh using 4 µL of cDNA per reaction.

P8 RGC cDNA was a generous gift from Dr. Allison Rosen Bialas. RGCs were acutely isolated

using an immunopanning technique described in (Bialas and Stevens, 2013).

Primer design: Primers for RT PCR reactions against GLT1 (SLc1a2) were designed to

recognize the transcripts of all 3 variant mRNAs. To make sure primers did not recognize

genomic DNA, they were designed over regions that spanned across exon/introns. Primers

were ordered from IDT (Integrated DNA Technologies, Inc) and designed using sequencher

(Gene codes corporation) and the Primer-BLAST tool available on the National Center for

Biotechnology Information (NCBI) on-line resource.

Forward primers for detecting GLT-1

transcript: *Reverse primers:*

[F2]: 5'-GGGAAAAATCTCCTGCTCTCAC   [B1]: GGCAATGATGGTCGTGGAC

[F4]: CCTGCTCTCACTGACTGTGTTTG   [B5]: AATCTGCTGGAAACAGGCTTG

[F7]: CGGGAAGAAGAACGACGAG   [B11]: GACCGCCTTGGTGGTATTG

[F12]: GCCTGTTTCCAGCAGATTCAG

Primer pairing and predicted sizes

[F2]&[B1] predicted size 270 bp

[F4]&[B1] predicted size 259 bp

[F7]&[B5] predicted size 100 bp

[F12]&[B11] predicted size 84 bp

Antibodies and immunocytochemistry

To detect the presence of GLT-1 by light and electron microscopic (EM) immunocytochemistry, a monoclonal antibody directed against the C-terminus of GLT-1a (anti-GLT-a, 1:10,000) was used that was generously provided by Dr. Jeffrey Rothstein (Johns Hopkins University). EM experiments were performed by Dr. Chiye Aoki, (New York University) in collaboration with Paul Rosenberg (Boston Children's Hospital).

Procedures for electron microscopic detection of GLT-1. GLT-1$^{+/+}$ and GLT-1$^{-/-}$ mice (Tanaka et al., 1997) were deeply anesthetized using urethane (i.p., 0.34g/g body weight), then euthanized by transcardial perfusion with 200ml of 0.1M phosphate buffer (PB, pH 7.4) containing 4% paraformaldehyde and 0.1% glutaraldehyde, delivered using a peristaltic pump set at a flow rate of 20ml/min. On the day after transcardial perfusion, brains were sectioned using a vibratome at a thickness setting of 50µm, then treated for 30min with 1% sodium borohydride in 0.1M PB within four hours after vibratome sectioning, so as to terminate the aldehyde fixation. After immersion for 30min, sections were rinsed repeatedly in 0.1M PB, so as to remove unreacted sodium borohydride. Vibratome sections containing the LGN of different genotypes of mice were cut on the same day, collected in 0.01M PB containing 0.9% sodium chloride (PBS), set at a pH 7.4. These vibratome sections were stored free-floating in a cold room (4°C) in PBS containing 0.05% sodium azide as preservative.

To visualize GLT-1-immunoreactive processes, vibratome sections were incubated overnight at room temperature under constant agitation in a buffer consisting of PBS-azide with 1% bovine serum albumin (BSA), together with the GLT-1 antibody at the following concentration: 1:10,000. Unbound antibodies were removed by rinsing sections in PBS, then incubated for 1 hour at room temperature in the PBS-azide/BSA buffer containing biotinylated goat anti-mouse IgG (Vector) at a dilution of 1:200. Sections were rinsed again, then incubated in the A+B

solution from Vector's ABC Elite kit. Following rinses in PBS to remove unbound secondary antibodies, sections were immersed in PBS containing 3,3'-diaminobenzidine HCl (DAB, 10mg tablets from Sigma Chem, dissolved in 44ml of PBS) The peroxidase reaction product was begun by adding hydrogen peroxide (4μl of 30% hydrogen peroxide per 44ml of DAB solution) and terminated at the end of 12 minutes by rinsing sections repeatedly in PBS. Vibratome sections were post-fixed using 2% glutaraldehyde in PBS.

Following this immunocytochemical procedure, the vibratome sections were processed by a conventional electron microscopic procedure, consisting of post-fixation by immersion in 1% osmium tetroxide/0.1M phosphate buffer for 1 hour, then dehydrated using graded concentrations of alcohol, up to 70%, then post-fixed overnight using 1% uranyl acetate, dissolved in 70% ethanol. On the following day, dehydration continued up to 100%, then was rinsed in acetone, and infiltrated in EPON 812 (EM Sciences), which was cured by heating the tissue at 60°C, while sandwiched between two sheets of Aclar plastic, with lead weights placed on top of the Aclar sheets, so as to ensure flatness of the EPON-embedded sections. These flat-embedded vibratome sections were re-embedded in Beem capsules (EM Sciences) filled with EPON 812, then ultrathin-sectioned at a plane tangential to the vibratome sections. The number of ultrathin sections collected from any one animal's brain section depended on the natural curvature that the section took on, even while cured under lead weights. Usually, a minimum of ten ultrathin sections needed to be collected from each vibratome section, so as to ensure that the surface-most portions of the vibratome section, where immunoreactivity was expected to be maximal, were sampled for LGN. The ultrathin sections were collected onto formvar-coated, 400 mesh thin-bar nickel grids (EM Sciences).

Quantification of the expression level of GLT-1 in presynaptic axon terminals and astrocytes. Digital electron microscopic images were captured from ultrathin sections by an

experimenter that was kept blind about the genotype of the animal from which brain tissue was collected. Images were captured using a 1.2 megapixel Hamamatsu CCD camera from AMT (Boston, MA) from the JEOL 1200XL electron microscope. Images were captured strictly from regions of the ultrathin section where the vibratome section surface could be verified by the transition of neural tissue to purely EPON matrix. Asymmetric synapses were identified based on the cluster of round clear vesicles on the presynaptic side and the presence of prominently electron-dense postsynaptic densities (PSDs) along the intracellular surface of the membrane facing the vesicle-containing axon terminals. Once these asymmetric synapses were identified, the synapse was scored as containing the DAB reaction product within the axon terminal. Whenever present, the fine astrocytic processes that immediately abutted the asymmetric synapses were scored as exhibiting immunoreactivity or not. Other astrocytic processes in the same micrograph (5μm x 5μm in area, captured at a magnification of 40000x) were evaluated as containing or not containing DAB reaction product along the membrane or intracellularly. All axon terminals forming asymmetric synapses were analyzed, strictly in the order that they were encountered, so as to maximize randomness of sampling.

Synaptosomal uptake of (^{3}H)-L-glutamate and (^{3}H)-D-aspartate.

Sodium-dependent transport of (^{3}H)-L-glutamate and (^{3}H)-D-aspartate was measured as previously described (Petr et al., 2013) and performed by Jianlin Wang (Paul Rosenberg laboratory, Boston Children's Hospital). Mice were anesthetized using ether, brains were removed, and the forebrain dissected, weighed and homogenized in 20 X ice-cold 0.32M sucrose. Samples were centrifuged at 800g for 10min at 4°C. The supernatant was poured into a fresh tube and centrifuged at 20,000g for 20min at 4°C. The pellet was then resuspended in 40× ice-cold 0.32M sucrose and centrifuged at 20, 000g for 20min at 4°C. The washed pellet was then resuspended in 50 X ice-cold 0.32M sucrose by homogenization. The isolated crude synaptosomes were kept on ice and used immediately for uptake assay. Glass tubes containing

450µl of buffer (in mM: NaCl, 140 or choline chloride, 140; KCl, 2.5; CaCl$_2$, 1.2; MgCl$_2$, 1.2; K$_2$HPO$_4$, 1.2; glucose, 10; Tris base, 5; HEPES, 10) with 10µM L-glutamate or D-aspartate (9.995 µM L-glutamate or D-aspartate and 0.005µM (^{3}H)-L-glutamate or (^{3}H)-D-aspartate (PerkinElmer, Boston, MA, USA]) were preincubated for 5min at 37°C in the absence or presence of inhibitors. Glutamate uptake into synaptosomes was initiated by adding 50µl of crude synaptosomes to each tube and incubating at 37°C for 30s. To stop uptake activity, 2ml of ice-cold choline buffer was added to the tube, vortexed and plunged into ice-water slurry. The samples were filtered through Whatman GF/C filter paper pre-wetted with 2ml choline buffer and then the filters were washed three times with 2ml choline buffer. Radioactivity on the filters was measured by liquid scintillation counting (TRI-CARB 2200CA, PACKARD; Long Island Scientific) the radioactivity taken up by the synaptosomes in the absence of sodium was subtracted from that taken up in the presence of sodium to isolate Na$^+$-dependent transport. Inhibitors of glutamate transporters DL-*threo*-β-Benzyloxyaspartic acid (TBOA) was obtained from Tocris Bioscience (UK), low affinity antagonists L-(+)-2-Amino-5-phosphonopentanoic acid (L-AP5) and γ-D-Glutamylgycine (γ-DGG) were purchased from Tocris Bioscience, MO. Nigericin (Sigma-Aldrich, USA) was used to isolate the net uptake component in the synaptosomal assay. To test nigericin sensitive uptake in synaptosomes, we pre-incubated the uptake system (uptake buffer and synaptosomes) with or without nigericin (3 µM) for 5 min at 37°C, and then added 10µM glutamate (including 0.005 µM (^{3}H]-L-glutamate) into each reaction tube to start the uptake (37°C, 30s).

References

Bialas AR, Stevens B (2013) TGF-beta signaling regulates neuronal C1q expression and developmental synaptic refinement. Nature neuroscience 16:1773-1782.

Blitz DM, Regehr WG (2003) Retinogeniculate synaptic properties controlling spike number and timing in relay neurons. Journal of neurophysiology 90:2438-2450.

Chen C, Regehr WG (2000) Developmental remodeling of the retinogeniculate synapse. Neuron 28:955-966.

Petr GT, Schultheis LA, Hussey KC, Sun Y, Dubinsky JM, Aoki C, Rosenberg PA (2013) Decreased expression of GLT-1 in the R6/2 model of Huntington's disease does not worsen disease progression. The European journal of neuroscience 38:2477-2490.

Rempe D, Vangeison G, Hamilton J, Li Y, Jepson M, Federoff HJ (2006) Synapsin I Cre transgene expression in male mice produces germline recombination in progeny. Genesis 44:44-49.

Tanaka K, Watase K, Manabe T, Yamada K, Watanabe M, Takahashi K, Iwama H, Nishikawa T, Ichihara N, Kikuchi T, Okuyama S, Kawashima N, Hori S, Takimoto M, Wada K (1997) Epilepsy and exacerbation of brain injury in mice lacking the glutamate transporter GLT-1. Science 276:1699-1702.

Turner JP, Salt TE (1998) Characterization of sensory and corticothalamic excitatory inputs to rat thalamocortical neurones in vitro. The Journal of physiology 510 (Pt 3):829-843.

CHAPTER 3:

Metabotropic Glutamate Receptors and Glutamate Transporters Shape Transmission at the Developing Retinogeniculate Synapse

Metabotropic Glutamate Receptors and Glutamate Transporters Shape Transmission at the Developing Retinogeniculate Synapse

Jessica L. Hauser[§], Eleanore B. Edson[§], Bryan M. Hooks and Chinfei Chen*

Department of Neurology, F.M. Kirby Neurobiology Center, Children's Hospital, Boston,
300 Longwood Avenue, Boston, MA 02115
and
Program in Neuroscience, Harvard Medical School,
220 Longwood Avenue, Boston, MA 02115

§ these authors contributed equally to this work

*To whom correspondence should be addressed:
Phone: 617-919-2685, Fax: 617-730-0242
chinfei.chen@childrens.harvard.edu

ABSTRACT

Over the first few postnatal weeks, extensive remodeling occurs at the developing murine retinogeniculate synapse, the connection between retinal ganglion cells (RGC) and the visual thalamus. While numerous studies have described the role of activity in the refinement of this connection, little is known about the mechanisms that regulate glutamate concentration at and around the synapse over development. Here we show that interactions between glutamate transporters and metabotropic glutamate receptors (mGluRs) dynamically control the peak and time course of the EPSC at the immature synapse. Inhibiting glutamate transporters by bath application of TBOA (DL-*threo-β-*Benzyloxyapartic acid) prolonged the decay kinetics of both AMPAR and NMDAR-currents at all ages. Moreover, at the immature synapse, TBOA-induced increases in glutamate concentration led to the activation of group II/III mGluRs and a subsequent reduction in neurotransmitter release at RGC terminals. Inhibition of this negative-feedback mechanism resulted in a small but significant increase in peak NMDAR EPSCs during basal stimulation, and a substantial increase in the peak with co-application of TBOA. Activation of mGluRs also shaped the synaptic response during high frequency trains of stimulation that mimic spontaneous RGC activity. At the mature synapse, however, the group II mGluRs and the group III mGluR7-mediated response are down-regulated. Our results suggest that transporters reduce spillover of glutamate, shielding NMDARs and mGluRs from the neurotransmitter. Furthermore, mechanisms of glutamate clearance and release interact dynamically to control the glutamate transient at the developing retinogeniculate synapse.

INTRODUCTION

Fast excitatory neurotransmission in the CNS is primarily mediated by the presynaptic release of glutamate and its clearance from the synaptic cleft. At the retinogeniculate synapse, glutamate is released from RGCs onto thalamic relay neurons in the lateral geniculate nucleus (LGN). Over development, information is continuously relayed through this synapse to cortex (Akerman et al. 2002; Huttenlocher 1967; Krug et al. 2001; Moseley et al. 1988). Prior to eye opening, around postnatal day (P)12 in mice, information is encoded in correlated spontaneous retinal activity characterized by prolonged bursts of spiking reaching frequencies greater than 20 Hz (Demas et al. 2003; Torborg et al. 2005). At this time, relay neurons receive synaptic contacts from more than ten RGCs (Chen and Regehr 2000; Jaubert-Miazza et al. 2005). Consistent with this immature circuitry and patterns of retinal activity, relay neurons are exposed to episodic barrages of glutamate lasting seconds at a time (Mooney et al. 1996). Little is known about the mechanisms present at the immature synapse that handle potentially high concentrations of glutamate.

Two mechanisms of glutamate clearance are diffusion and removal or buffering of the neurotransmitter by high affinity glutamate transporters (Diamond and Jahr 1997; Tzingounis and Wadiche 2007). Glutamate concentration at the cleft can also be reduced through a metabotropic glutamate receptor (mGluR)-mediated decrease in neurotransmitter release (Conn and Pin 1997; Min et al. 1998; Oliet et al. 2001; Renden et al. 2005; Scanziani et al. 1997). The relative roles of these three mechanisms have been shown to change over development at other CNS synapses (Cathala et al. 2005; Renden et al. 2005; Thomas et al. 2011). For example, in the hippocampus, increased neuropil density with age impedes diffusion and corresponds with a greater role of glutamate transporters (Diamond 2005; Thomas et al. 2011). At the Calyx of Held, increased fenestration of the presynaptic terminal at older ages enhances diffusion and reduces the need for presynaptic mGluRs (Renden et al. 2005; Taschenberger et

al. 2002). At the developing rodent retinogeniculate synapse, ultrastructural studies show extensive extracellular space before P4. By P8, this space is replaced by neuropil, and 'coarse glial processes' are seen near RGC terminals (Aggelopoulos et al. 1989; Bickford et al. 2010). These structures are distinct from the adult synapse, where some glia form glomeruli around aggregates of presynaptic terminals (Budisantoso et al. 2012; Lieberman 1973; Rafols and Valverde 1973). At the mature synapse, diffusion is generally restricted to two dimensions because of the large contact size of the RGC bouton (Budisantoso et al. 2012). While the structural detail of the immature synapse has been described, little is known concerning glutamate transporter function or how glutamate release is regulated during bursts of retinal activity.

Our results demonstrate that glutamate transporters actively shape synaptic currents at the retinogeniculate synapse. In addition, inhibiting transporters at the immature synapse leads to the activation of group II/III mGluRs that, in turn, decrease neurotransmitter release from RGC terminals. Frequencies that occur during retinal waves are sufficient to activate these mGluRs. Lastly, we show down regulation of this mGluR-mediated response with age suggesting neurotransmission is tightly controlled throughout this developmental period.

MATERIALS AND METHODS

Slice preparation and extracellular solutions. Parasagittal slices (250 µm) that preserved optic tract and visual thalamus were prepared from P8-12 or P26-34 C57BL/6 or Black Swiss mice (Charles River, Wilmington MA or Taconic Farms, Germantown, NY) of either sex, as described previously (Chen and Regehr 2000) and in accordance with federal guidelines and protocols approved by Children's Hospital Boston. Slices were prepared in ice-cold choline-based dissection solution containing the following (in mM): 130 Choline chloride, 26 $NaHCO_3$, 1.25 NaH_2PO_4, 2.5 KCl, 7.0 $MgCl_2$, 0.5 $CaCl_2$ and 25 glucose. Slices were incubated in this

solution at 32^0C for 15-20 minutes followed by additional 10 minutes in artificial cerebral spinal

fluid (aCSF) containing (in mM): 125 NaCl, 26 $NaHCO_3$, 1.25 NaH_2PO_4, 2.5 KCl, 1.0 $MgCl_2$,

2.0 $CaCl_2$, and 25 glucose (Sigma, St. Louis MO). aCSF was adjusted to 310-315 mOsm.

Slices were then transferred into the recording chamber superfused with aCSF at 2-3 mL/min.

All experiments were performed at 35±1°C, unless otherwise indicated. aCSF and choline

dissection solutions were saturated with 95% O_2 / 5% CO_2. Slices were used for up to 5 hrs

after preparation. Experiments were performed with aCSF containing: the γ-aminobutyric acid

type A ($GABA_A$)-receptor antagonist bicuculline (20µM) or picrotoxin (Sigma, 50µM), the

$GABA_B$-receptor antagonist 3-N-[1-(S)-3,4-dichlorophenyl)ethyl]amino-2-(S)- hydroxypropyl-P-

benzyl-phosphinic acid (CGP55845, 2µM) and the A_1 adenosine receptor antagonist 8-

Cyclopentyl-1,3-dipropylxanthine (DPCPX, 10µM). In order to isolate the NMDAR EPSC, 2,3-

Dihydro-6-nitro-7-sulfamoyl-benzol[f]quinozaline-2,3- dione (NBQX, 5µM) was included while

holding the cell at +40mV. To isolate the AMPAR EPSC, we included 3-[(R)-2-carboxypiperazin-

4-yl]-propyl-1-phosphonic acid (*(R)*-CPP, 20µM) and D-(-)-2-Amino-5-phosphonopentanoic acid

(D-AP5, 50-100µM) in the bath while holding the cell at -70 mV. For some experiments, AMPAR

desensitization was inhibited by including 6-Chloro-3,4-dihydro-3-(5-norbornen-2-yl)-2H-1,2,4-

benzothiazidiazine-7-sulfonamide-1,1-dioxide (cyclothiazide, 50µM) in the bath. To inhibit

glutamate transport 10-50µM DL-threo-β-benzyloxyaspartic acid (TBOA) was added to the

superfusion solution. These agents were also added depending on the experiment: the

antagonist to metabotropic glutamate receptors (2S-2-amino-2-(1S,2S-2-carboxycycloprop-1-

yl)-3-(xanth-9- yl)propanoic acid (LY341495 50µM), agonists to group I, II, and III mGluRs,

respectively: (S)-3,5-dihydroxyphenylglycine (*(S)*-DHPG, 1-10µM), (2R,4R)-4- aminopyrrolidine-

2,4,-dicarboxylate (APDC, 1-30µM), and L-(+)-2-amino-4- phosphonobutyric acid (L-AP4, 10-

50µM) and the low affinity NMDAR antagonist L-(+)-2-Amino-5-phosphonopentanoic acid (L-

AP5, 1mM). Stock solutions of pharmacological agents were stored at -20°C and diluted

according to the final concentrations immediately prior to experiments. All pharmacological agents were purchased from Tocris, MO unless otherwise indicated.

Electrophysiology. Whole-cell recordings of thalamic relay neurons were acquired using glass patch pipettes (1.1-1.7 MΩ resistance) filled with internal solution containing (in mM): 35 CsF, 100 CsCl, 10 EGTA, 10 HEPES, the L-type calcium channel antagonist, 0.1 methoxyverapamil hydrochloride (Sigma, St. Louis, MO) and adjusted to 290-300 mOsm, pH 7.3. This solution is designed to minimize postsynaptic contributions to synaptic transmission. Cesium blocks K^+ channels and thus optimizes voltage-clamp, while EGTA and fluoride inactivate many second messenger systems. Relay neurons were visualized using DIC optics (Olympus). Voltage clamp recordings were made using an Axopatch 200B or Multiclamp 700A amplifier (Axon Instruments, Foster City, CA), filtered at 1kHz and digitized at 4-50 kHz with an ITC-16 interface (InstruTECH, Port Washington, NY). EPSCs were evoked by current pulses delivered to the intact optic tract by a pair of aCSF filled glass micropipettes (Drummond Scientific, Broomall, PA), connected to a stimulus isolator (World Precision Instruments, Sarasota, FL), with intensities that ranged from 10-150 µA. The membrane potential of the relay neuron was clamped at either -70 mV or +40 mV (for AMPAR mediated EPSCs and NMDAR mediated EPSCs respectively) during stimulation of the optic tract, and was held at 0 mV between stimulation trials. For baseline recordings optic tract was stimulated at a frequency of 0.025Hz for NMDAR- EPSC and 0.05Hz for AMPA-EPSCs. To ensure consistent access resistance of the recording electrode throughout the entire experiment, we monitored the peak amplitude of a brief (10 ms) hyperpolarizing test pulse (-5mV) given prior to the optic tract stimulation. Access resistances of relay neurons were <15 MΩ.

Analysis. Data acquisition and analysis was performed using custom software written in IgorPro (Wave-Metrics, Portland, OR), Prism (GraphPad Software, Inc.) and Excel (Microsoft, Redmond, WA). EPSCs were analyzed as the average of 5-10 waves. The decay timecourse

of the AMPAR EPSC is well fit with a double exponential function $f(x) = y_0 + A_1 e(-x/\tau_{fast}) + A_2 e(-x/\tau_{slow})$, and is quantified as the weighted tau: $\tau = [\tau_{fast} \times A_1/(A_1 + A_2)] + [\tau_{slow} \times A_2/(A_1 + A_2)]$. At the immature synapse, the slow component τ_s contributes to a significant component of the EPSC waveform (Liu and Chen 2008) and is the component most sensitive to TBOA. For experiments involving trains of stimuli, stimulus sets were performed using randomized, interleaved trains at frequencies of 10, 20 and 50 Hz. EPSC amplitudes following the first EPSC, $EPSC_{2-5}$ were quantified as the difference between the peak EPSC and the baseline current immediately after the stimulus artifact. Data are summarized as mean ± SEM, using the two-tailed paired t-test unless otherwise indicated.

RESULTS

Glutamate transporters shape the synaptic waveform at the immature retinogeniculate synapse

To investigate the role of glutamate transporters at the immature retinogeniculate synapse we tested the effects of the competitive non-transportable blocker of glutamate transporters, TBOA, on acute slices prepared from P8-12 mice. Whole cell recordings were made with patch electrodes in voltage-clamp mode from relay neurons in the LGN, and synaptic responses were evoked by stimulating optic tract fibers (Chen and Regehr 2000). Figure 3.1 illustrates the effects of bath application of TBOA (50μM) while recording either NMDAR-mediated or AMPAR-mediated EPSCs.

When we inhibited glutamate transport with TBOA, the NMDAR-EPSC amplitude was reduced to 56 ± 4% of control (n=5, p=0.01) and the time course of decay was significantly prolonged (half-decay time ($T_{1/2}$): 542.9 ± 156.9% of control, n=5, p<0.05, Figure 3.1A, C). The remaining
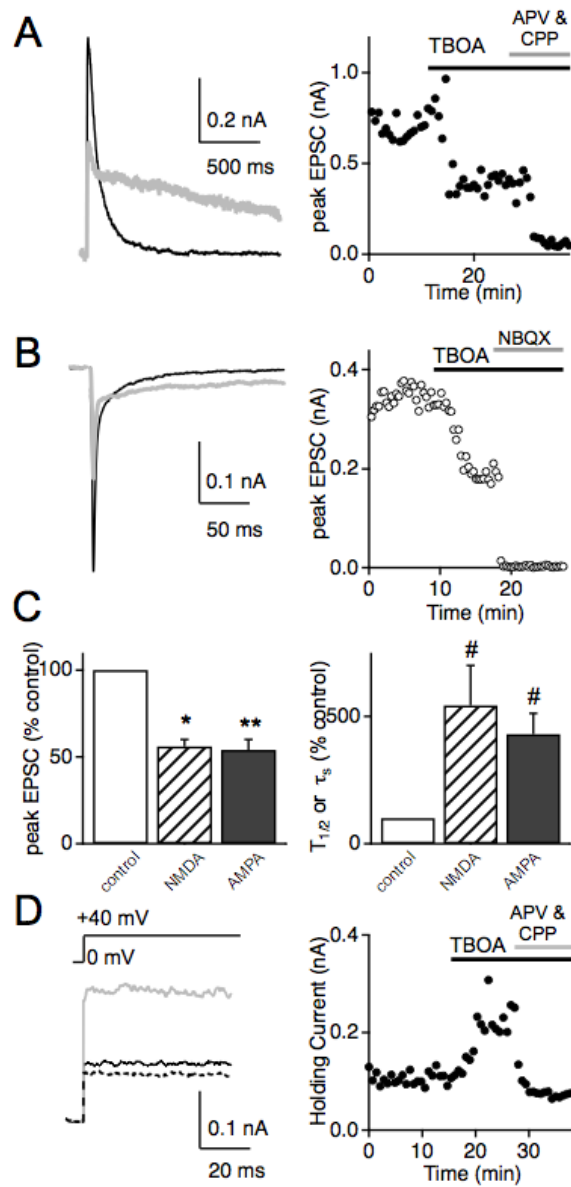
Figure 3.1: Effects of TBOA at the immature retinogeniculate synapse.
Excitatory postsynaptic currents (EPSCs) were measured before and during bath application of 50µM TBOA. Traces from representative experiments are shown for (A, left), NMDAR- (V_h, +40mV) and (B, left) AMPAR-mediated EPSCs (V_h, -70mV); control (black line) TBOA (grey line). Time course of NMDAR- (A, right) AMPAR- (B, right) EPSC amplitudes before and during bath application of 50µM TBOA followed by respective antagonists. (C, left) Summary of the mean normalized amplitudes (± SEM) of both NMDAR- and AMPAR-EPSCs. (C, right) Summary of the effects of TBOA on EPSC decay shown as percentage of control. #, $p < 0.05$. (D) Effects of TBOA on the holding current (I_{hold}) in response to a +40 mV step. Representative traces (left) and time course (right); control (thin line), TBOA (grey line) and NMDAR antagonists (dotted line). Recordings performed at 35±1°C.

current in the presence of TBOA was blocked by NMDAR specific antagonists (Figure 3.1A, right).

We found a similar effect of TBOA on the waveform of the AMPAR EPSC (Figure 3.1B,C). The peak amplitude of the AMPAR EPSC decreased to 54 ± 6% of control (n=5, p=0.001) and the time course of the current also slowed. The decay kinetics of the AMPAR EPSC at immature synapses is well described by a double-exponential relationship (Liu and Chen 2008). In the presence of TBOA, the time constant of the slow component (τ_S) increased to 430 ± 82% of control (n=5, p<0.05) and the current could be completely blocked by AMPAR specific antagonists (Figure 3.1B, right). The average effects of TBOA on the peak EPSC and the decay time courses of both NMDAR and AMPAR currents are compared in Figure 3.1C.

These results demonstrate that glutamate transporters are present at the immature retinogeniculate synapse and that they actively remove glutamate during synaptic transmission. Slowing of the EPSC decay kinetics implies that reduced glutamate clearance results in either extended activation of glutamatergic receptors in the synaptic cleft and/or spillover to receptors further from the release sites. In addition, TBOA increased the relay neuron holding current elicited by a step depolarization from 0 to +40 mV (I_{hold}) to 200 ± 30% of control (n=5, p<0.05). The difference in I_{hold}, with and without TBOA, can be attributed to increased basal activation of NMDARs because it is reversed with bath application of NMDAR antagonists (100μM DL-APV and 20μM(R)-CPP, Figure 3.1D). Since NMDA antagonists do not block all of I_{hold} in control conditions, our results suggest that TBOA exposure increases ambient glutamate concentration by significantly more than 200%.

Biphasic Synaptic Response to Glutamate Transporter Inhibition

While an increase in ambient glutamate or glutamate spillover could explain the slowing of

NMDAR current decay kinetics and the change in I_{hold} in response to bath application of TBOA,

it does not explain the decrease in EPSC peak amplitudes. However, we noticed in some

experiments, such as in Figure 3.1A, that there was often an initial transient increase followed

by a reduction in the peak EPSC. Thus, we asked whether the decrease in peak EPSC was a

secondary effect of elevated glutamate concentrations. To test this possibility, we took

advantage of the fact that the activity of glutamate receptors (both metabotropic and ionotropic)

is more temperature dependent than glutamate diffusion. We reasoned that we might be able to

better appreciate the initial transient increase in NMDAR EPSC peak amplitude by recording at

RT and by sampling more frequently. Figure 3.2A shows that at RT the time course of the peak

EPSC amplitude following inhibition of glutamate transport consisted of two distinct phases.

Immediately following the addition of TBOA, evoked NMDAR currents increased in amplitude

and duration. Over the ensuing 2-5 minutes, however, the current decreased in amplitude, while

maintaining slow decay kinetics. These observations could be explained by a mechanism

wherein an increase in glutamate spillover and/or ambient glutamate concentration leads to a

decrease in neurotransmitter release. Activation of metabotropic glutamate receptors (mGluRs)

has been shown to decrease the probability of release at a number of synapses in the CNS

(Baskys and Malenka 1991; Maki et al. 1994; Min et al. 1998; Oliet et al. 2001; Renden et al.

2005; Scanziani et al. 1997; von Gersdorff et al. 1997). However little is known about the role of

mGluRs at the immature retinogeniculate synapse.

To test for the presence of mGluRs, we examined the effects of TBOA in the presence of an

mGluR antagonist, LY341495 (LY) (Kingston et al. 1998). LY is a very selective antagonist to

group II mGluRs at low concentrations, however, at higher concentrations, (50 µM), it has
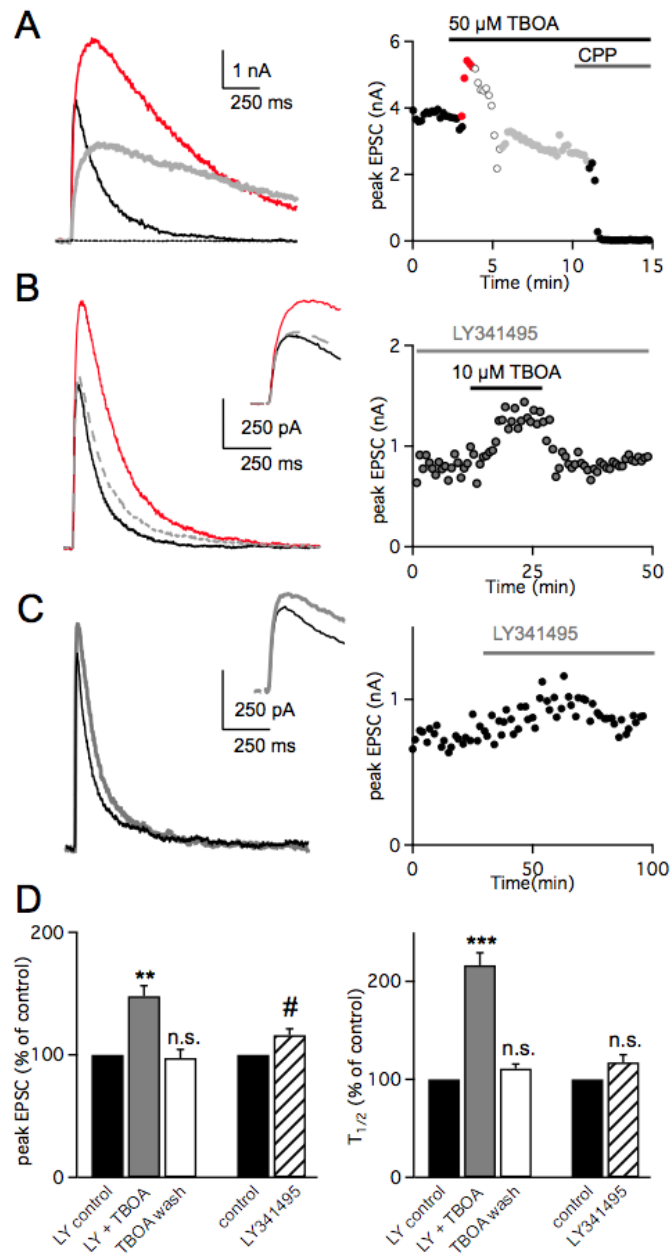
Figure 3.2: Inhibition of group II / III mGluRs prevents TBOA-induced reduction in EPSC amplitude at the immature synapse.
(A) Traces (left) and time course (right) of NMDA-EPSC responses recorded at RT before (black) and during (red: first minute, grey open: minute 2-3, grey filled: minutes 3-5) bath application of 50 μM TBOA followed by NMDAR antagonist, CPP. Stimulation frequency of 0.1 Hz. (B) Representative traces (left) and time course (right) of NMDAR- EPSC responses in the presence of LY341495 (LY, 50μM) before (black line), during (red line) and after (grey dashed line) bath application of 10 μM TBOA. (C) NMDAR-EPSC traces (left) and time course (right) before (black line) and during (grey line) bath application of LY. (D) Summary of data, mean ± SEM. average $T_{1/2}$ (ms): 87 ± 11 in LY vs. 185.4 ± 19.8 in LY and TBOA .#, p<0.05; **, p<0.01; ***, p<0.001. Recordings in (B) and (C) performed at 35±1°C.

44

measureable effects on all mGluR groups (Linden et al. 2009). In the following experiments we used a lower concentration of TBOA, since we found that bath application of 50µM TBOA often led to unstable recordings attributable to excessive changes in holding current. As with 50 µM TBOA, 10 µM TBOA effectively reduced the NMDAR peak EPSC (to 75±5% of control, n=7, p<0.05; data not shown); thus the previously described effect on the peak current is still present even with reduced TBOA concentration. In the presence of 50 µM LY we find that the inhibitory effect of TBOA on EPSC amplitude was prevented. Instead there was a lasting increase in peak EPSC to nearly 150% of control (147±8.6 % of control; n=6, p<0.01; Figure 3.2B,D). Despite the 5-fold reduction in TBOA concentration, we still observed a doubling in NMDAR EPSC $T_{1/2}$ that was reversed with washout of the transporter inhibitor (Figure 3.2B,D). We also find smaller changes in I_{hold} in the presence of 10µM TBOA compared to 50µM, which were reversible (TBOA: 147.8±12.6% of control n=6, p=0.01; Wash: 112.9 ± 17.7% of control n=5, p=0.4; data not shown).

These results suggest that TBOA mediates the reduction in peak EPSC through accumulation of glutamate and subsequent activation of mGluRs. Application of LY alone had a small but significant effect on the NMDAR EPSC amplitude, but not $T_{1/2}$, at baseline stimulation frequencies (peak increased to 116±5% of control, n=6, p<0.05; 0.025 Hz stimulation, Figure 3.2C,D). Our baseline stimulation of the optic tract (0.025 Hz) is at a much lower frequency than the reported mean RGC firing rates of 0.3-0.45 Hz at ages P9-13 in mice (Demas et al. 2003; Torborg and Feller 2005). Thus we interpret these data to indicate that mGluRs can be activated by glutamate spillover and/or ambient glutamate and inhibit neurotransmitter release during physiological levels of RGC activity.

Activation of Group II / III mGluRs regulate neurotransmitter release at the immature retinogeniculate synapse

We next sought to identify the class of mGluRs responsible for the decrease in EPSC amplitude seen with application of TBOA. Our finding that both AMPAR and NMDAR peak currents decreased to a similar extent in the presence of TBOA favors a presynaptic mechanism. Moreover, our experimental conditions were designed to minimize known postsynaptic effects of mGluR signaling (see Methods). Thus we examined the effects of specific mGluR agonists on synaptic strength and the paired pulse response (PPR) to address whether the probability of release was affected. At the retinogeniculate synapse, both pre- and postsynaptic mechanisms have been shown to contribute to PPR (Budisantoso et al. 2012; Chen et al. 2002). To accurately monitor a presynaptic process without contamination of postsynaptic AMPAR desensitization, 50µM cyclothiazide (CTZ) was added to the bath. CTZ prevents desensitization of AMPARs and does not alter release probability at the retinogeniculate synapse (Chen and Regehr 2000). Figure 3.3A-C show the effects of bath application of agonists to different classes of mGluRs on pairs of stimuli separated by an interstimulus interval (ISI) of 50 ms. The time courses of the peak amplitude of the 1st ($EPSC_1$) and 2nd ($EPSC_2$) EPSC are plotted before and during agonist application .The paired-pulse ratio (PPR), calculated as $EPSC_2/EPSC_1$, are shown in the lower panels. Application of group II (APDC) and group III (L-AP4) agonists led to a sustained reduction in $EPSC_1$ (Figure 3.3D). For example, 30 µM APDC inhibited the peak EPSC to 73±4% of control, n=5, p<0.05 and increased PPR to 130±4% (n=5, p<0.01), while 50 µM L-AP4 reduced the current to 68±7% of control, n=6, p<0.05 and increased PPR to 150±9%, (n=6, p<0.05) of control.

The group III class of mGluRs includes mGluR 4, 6,7 and 8, which can all be activated by L-AP4. The EC_{50} or IC_{50} of L-AP4 for mGluR 4, 6 and 8 range from 0.4-1.2 µM
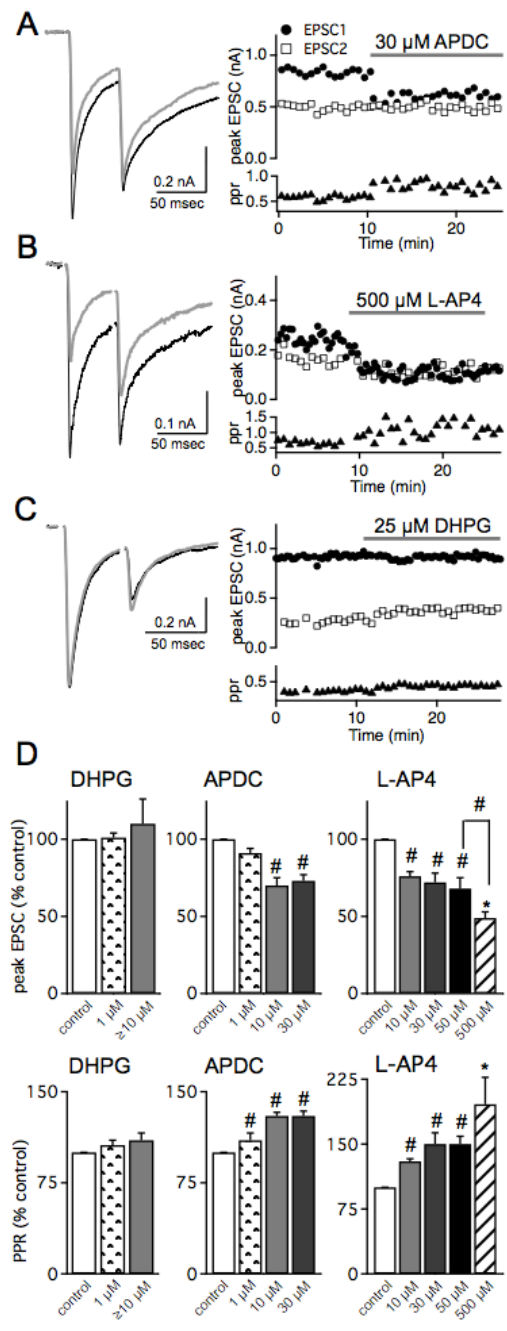
Figure 3.3: mGluR agonists modulate synaptic currents at the immature synapse.
Representative traces (left) and time course (right) of AMPAR-EPSC response to pairs of pulses before (thin line), and during (thick grey line) bath application of the (A) group II mGluR agonist APDC (30μM), (B) group III agonist L-AP4 (500μM) and (C) group I agonist *(S)*-DHPG (25 μM). AMPAR EPSC1 amplitudes (circles), EPSC2 amplitudes (squares) and PPR (triangles). (D) Summary data of peak EPSCs (top) and PPR (bottom) shown as percentage of control in the presence of various concentrations of mGluR agonists. #, $p < 0.05$, * $p < 0.01$. Recordings performed at 25 ± 1°C.

47

(Conn and Pin 1997). However mGluR7 has a lower affinity for the agonist and requires a much higher concentration than 50 µM for full activation (Conn and Pin 1997). Thus we tested the effects of higher concentrations of L-AP4. We found that 500 µM L-AP4 further reduced synaptic strength to 48.9±4% of control (n=5 p=0.01, compared to 50 µM L-AP4: unpaired t-test p<0.05) and increased PPR to 196±31% of control (n=5 p<0.01; Figure 3.3B and D). This data suggests that mGluR7 is also present at the immature retinogeniculate synapse.

In contrast to the group II and III agonists, the group I agonist, DHPG (>10 µM), did not significantly alter the average peak EPSC amplitude (110±16% of control, n=4, p=0.7) or the PPR (110 ± 6%, n=4, p=0.4) (Figure 3.3C and D). The dose-dependent relationship of agonists to the three groups of mGluR are compared in Figure 3.3D. These results demonstrate that agonists for group II and III, but not group I mGluRs lead to a sustained reduction in release probability at the immature retinogeniculate synapse.

The role of glutamate transporters at the mature retinogeniculate synapse

The functional properties of the rodent retinogeniculate synapse remodel dramatically over the first 3-4 postnatal weeks (Chen and Regehr 2000; Hooks and Chen 2006; Jaubert-Miazza et al. 2005). To test whether the role of glutamate transporters also changes over development at this visual synapse, we examined the effects of TBOA in LGN slices prepared from p27-34 mice. Bath application of 10 µM TBOA significantly alters the waveform of the mature NMDAR-EPSC. In contrast to the immature synapse, where we found a decrease in NMDAR-EPSC amplitude without LY (Figure 3.1), TBOA caused a reversible increase in the EPSC amplitude to 163 ± 20.2% of control (n=6, p<0.05; Figure 3.4A). The TBOA-mediated effects on EPSC kinetics and holding current, however, were similar to that of the immature synapse, with a significant and reversible increase in the $T_{1/2}$ (to 185±23.9% of control Figure 3.4A, n=6, p<0.05) and I_{hold} (to 119 ± 3.9% of control, n=6, p <0.01; Figure 3.4C).
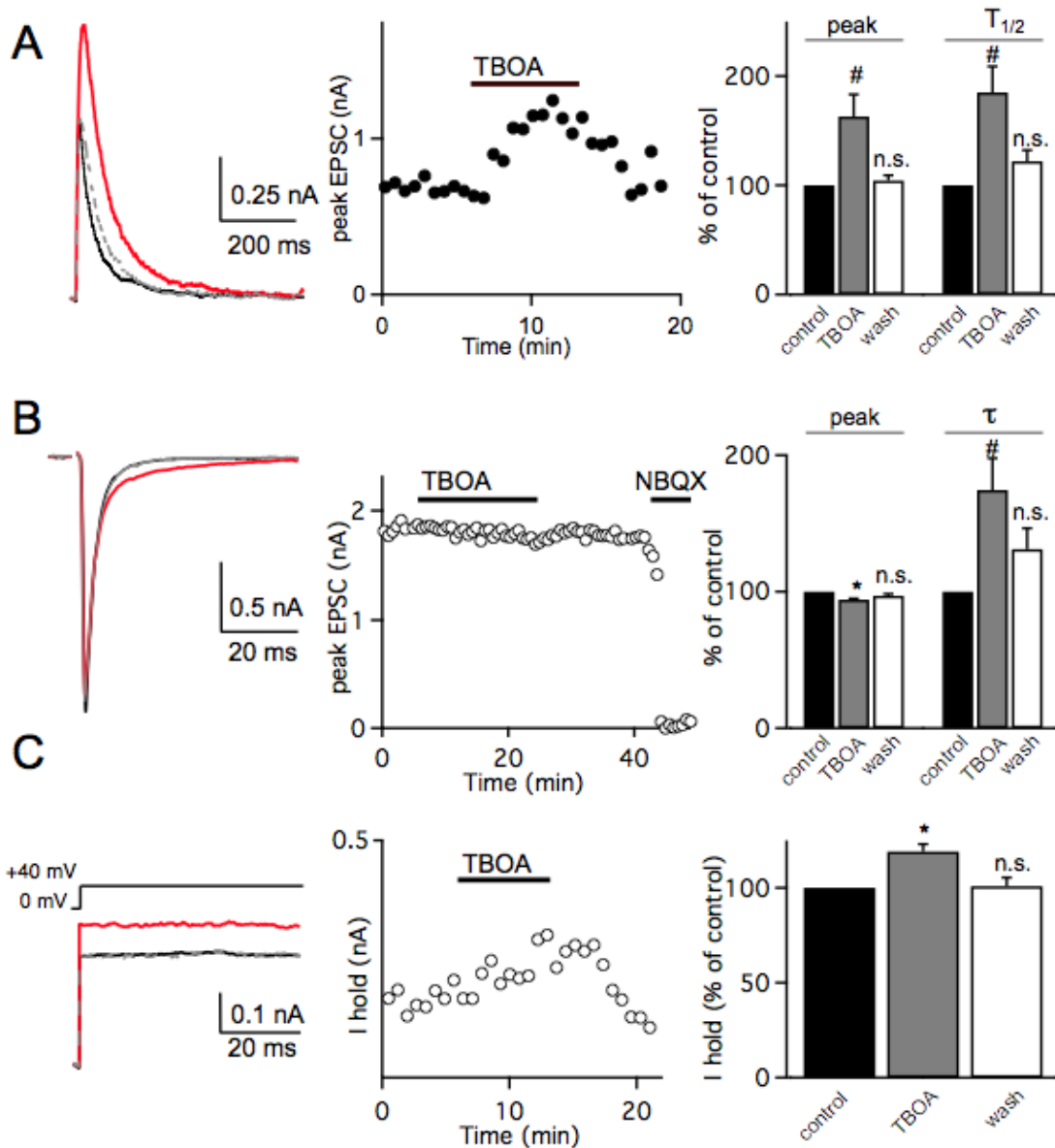
Figure 3.4: Effects of TBOA on EPSCs at the mature retinogeniculate synapse.
Representative traces (A, left) and time course (A, middle) of NMDAR-EPSCs recorded from a mature (p28) relay neuron before (black line) during (red line) and following (dashed grey line) bath application of 10µM TBOA. (A, right) Summary of data plotted as percentage of control; mean ± SEM. (B) Representative traces (left) and time course (middle) of AMPAR EPSCs recorded before (black) during (red line) and following (grey line) application of TBOA followed by receptor antagonist. (B, right) Summary data as percentage of control; mean ± SEM. (C) I_{hold} in response to a +40mV step. Average traces (left) and time course (middle) shown before (black line) during (red line) and following (grey dashed line) the application of TBOA. (C, right) Summary of I_{hold} data shown as percentage of control. Recordings performed at 35±1°C.
# $p<0.05$; * $p<0.01$.

We also find a small but significant decrease in the mature AMPAR-EPSC in the presence of 10µM TBOA (to 94.2 ± 0.8% of control; n=5, p<0.01) and a slowing of the time constant of decay, τ (to 174 ± 23.2% of control, n=5, p<0.05; Figure 3.4B). This reduction in peak amplitude is due to AMPAR desensitization because in the presence of 50µM CTZ, bath application of 10 µM TBOA had no significant effect on peak amplitude (105.5 ± 2.9% of control, n=5, p =0.12, data not shown). However, in the presence of CTZ, EPSC decay kinetics still increased in response to transporter inhibition (τ, 231 ± 3.8% of control, n=5, p<0.05, data not shown). AMPAR desensitization can occur at the mature retinogeniculate synapse as a result of glutamate spillover and/or increased ambient glutamate concentration (Budisantoso et al. 2012; Chen et al. 2002).

Downregulation of mGluRs at the mature retinogeniculate synapse

The difference between the synaptic responses to TBOA at the mature and immature retinogeniculate synapse suggests a reduction over development in the negative feedback loop mediated through mGluRs. To confirm that there is a change in the role of mGluRs at the mature synapse, we tested for the presence of mGluRs using specific agonists as we did for the immature synapse. Figure 3.5A shows that bath application of 50 µM L-AP4 results in a small but persistent decrease in peak AMPAR EPSC (to 84.7 ± 5.6% of control, n=5, p=0.05) where PPR increased to 122.8 ± 5% of control (n=5, p<0.05). This suggests that group III mGluRs are present at the mature synapse. However, increasing the concentration of L-AP4 to 500 µM does not elicit further inhibition, as it did at the immature synapse (see Figure 3.3). This is consistent with a loss of mGluR7 (500 µM L-AP4: $EPSC_1$ to 82.7±3.6% of control, n=6, p<0.05 and PPR to 122.4±9% of control, n=6, p<0.05; but compared to 50 µM L-AP4: $EPSC_1$ unpaired t-test p=0.78; PPR p=0.97; Figure 3.5B and C). A summary of the dose dependence of L-AP4 on the mature AMPAR EPSC and PPR is shown in Figure 3.5B. Thus, while some group III mGluRs
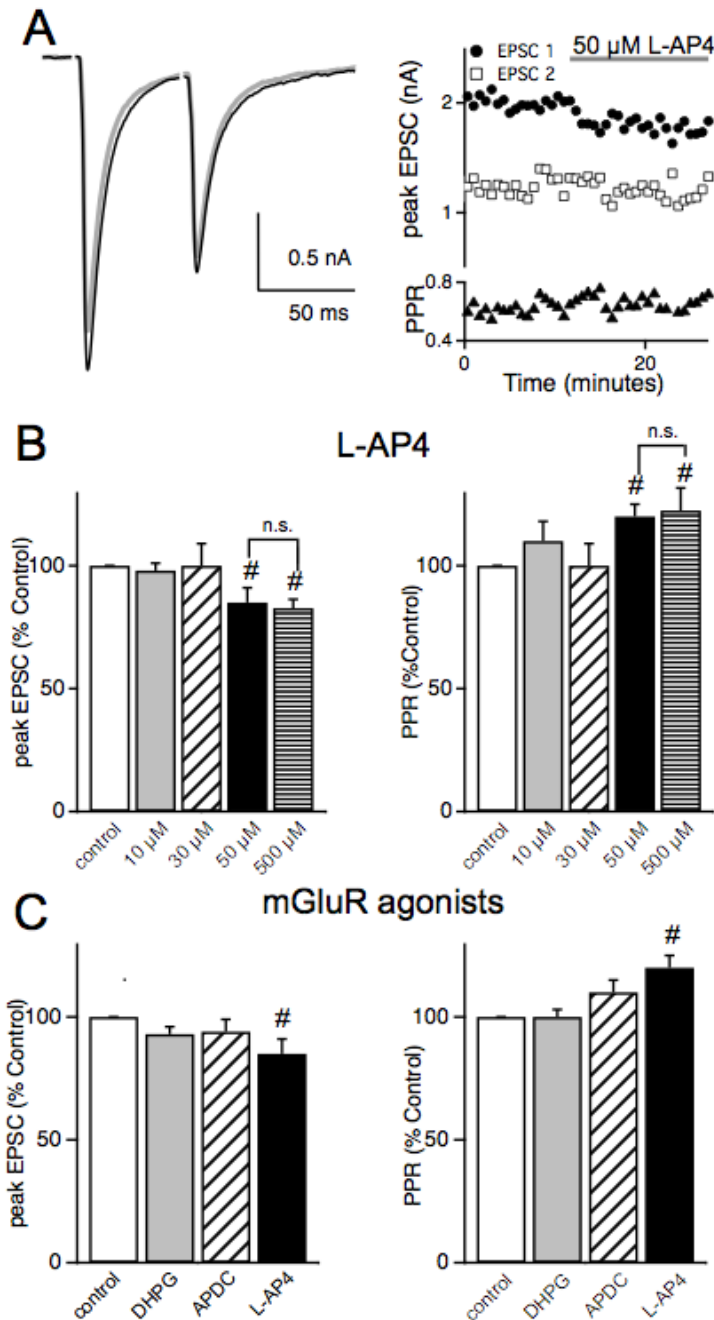
Figure 3.5: Downregulation of mGluRs at the mature retinogeniculate synapse.
Representative traces (A, left) and time course (A, right) of pairs of AMPAR EPSCs before (grey) and during (black) application of 50µM L-AP4. Peak EPSC1 (circles), EPSC2 (squares), and PPR (triangles). (B): Summary data (mean ± SEM) shown as percentage of control in response to three concentrations of L-AP4 (10µM, 30µM, 50µM and 500µM). (C) Summary data for different mGluR agonists. 10µM (S)-DHPG: $EPSC_1$: 93 ± 3% of control, n=6, p=0.16; PPR: 100±3% of control, n=6, p=0.68. 30 µM APDC: 94 ± 5% of control, n=4, p=0.24; PPR: 110±5% of control, n=4, p=0.11. #, p<0.05. Recordings performed at 25±1°C.

remain at the synapse over development, activation of these receptors results in a smaller effect on synaptic strength and release probability in mature synapses when compared to the immature synapses (compare Figures 3.3 and 3.5).

In contrast to group III mGluRs, agonists of group I (10 µM DHPG) and group II (30 µM APDC) did not significantly alter the peak EPSC amplitude or the PPR at the mature retinogeniculate synapse (Figure 3.5C). These results demonstrate that the role of group II mGluRs in mediating release probability is lost over development at the retinogeniculate synapse. Taken together, our data suggest that the mGluR negative feedback mechanism that is present at the immature retinogeniculate synapse is downregulated with age.

Activation of mGluRs during physiologically relevant stimulus trains

Our findings demonstrate that inhibition of glutamate transporter activity can activate a group II/III mGluR-mediated reduction in release probability at the immature synapse. The data also shows that there is activation of mGluRs during basal RGC activity (see Figure 3.2C). We asked how mGluR activation alters the synaptic response during bursts of synchronous RGC activity that have been shown to occur during this developmental period. Action potential firing rates of retinal ganglion cells during bursts in immature mice can increase to greater than 20 Hz (Demas et al. 2003; Kerschensteiner and Wong 2008; Torborg and Feller 2005). Because the AMPAR current is relatively small compared to the NMDAR current early in development, we examined the response of NMDAR currents to trains of optic nerve stimulation. In order to accurately monitor changes in presynaptic neurotransmitter release using NMDAR currents as a reporter, we included the low affinity NMDAR antagonist L-AP5 (1mM) in the bath solution to reduce receptor saturation (Chen et al. 2002). We stimulated the optic tract with trains of 5 stimuli at frequencies of 10 Hz, 20 Hz or 50 Hz. After establishing a stable baseline, 50µM LY was added to the solution. If tonic activation of group II/III mGluRs influence the synaptic response to trains

of stimuli, we would predict that LY would antagonize the binding of glutamate to these receptors, resulting in an increase in the probability of neurotransmitter release.

Indeed, our results are consistent with this prediction. We found a significant increase in the strength of the $EPSC_1$ and a decrease in PPR following relief of mGluR activation (Figure 3.6). $EPSC_1$ amplitude of each train increased to 126 ± 8% of control (n=6, p<0.05). Figure 3.6 (left) shows average traces in response to 5 stimuli at either 10Hz (A), 20 Hz (B) or 50Hz (C) before (black) and during (grey) bath application of 50µM LY. A summary plot of the peak amplitudes of the subsequent EPSCs relative to $EPSC_1$ is shown on the right. The degree of synaptic depression in response to trains of stimuli was enhanced with higher frequencies in control conditions. Bath application of the mGluR antagonist reduced the peak amplitudes of subsequent EPSCs following $EPSC_1$. Synaptic depression was significantly enhanced in the presence of LY (p<<0.002 for all frequencies tested, two-way ANOVA). These results demonstrate that group II/III mGluR are activated during physiological RGC firing patterns and reduce release probability at the immature retinogeniculate synapse.
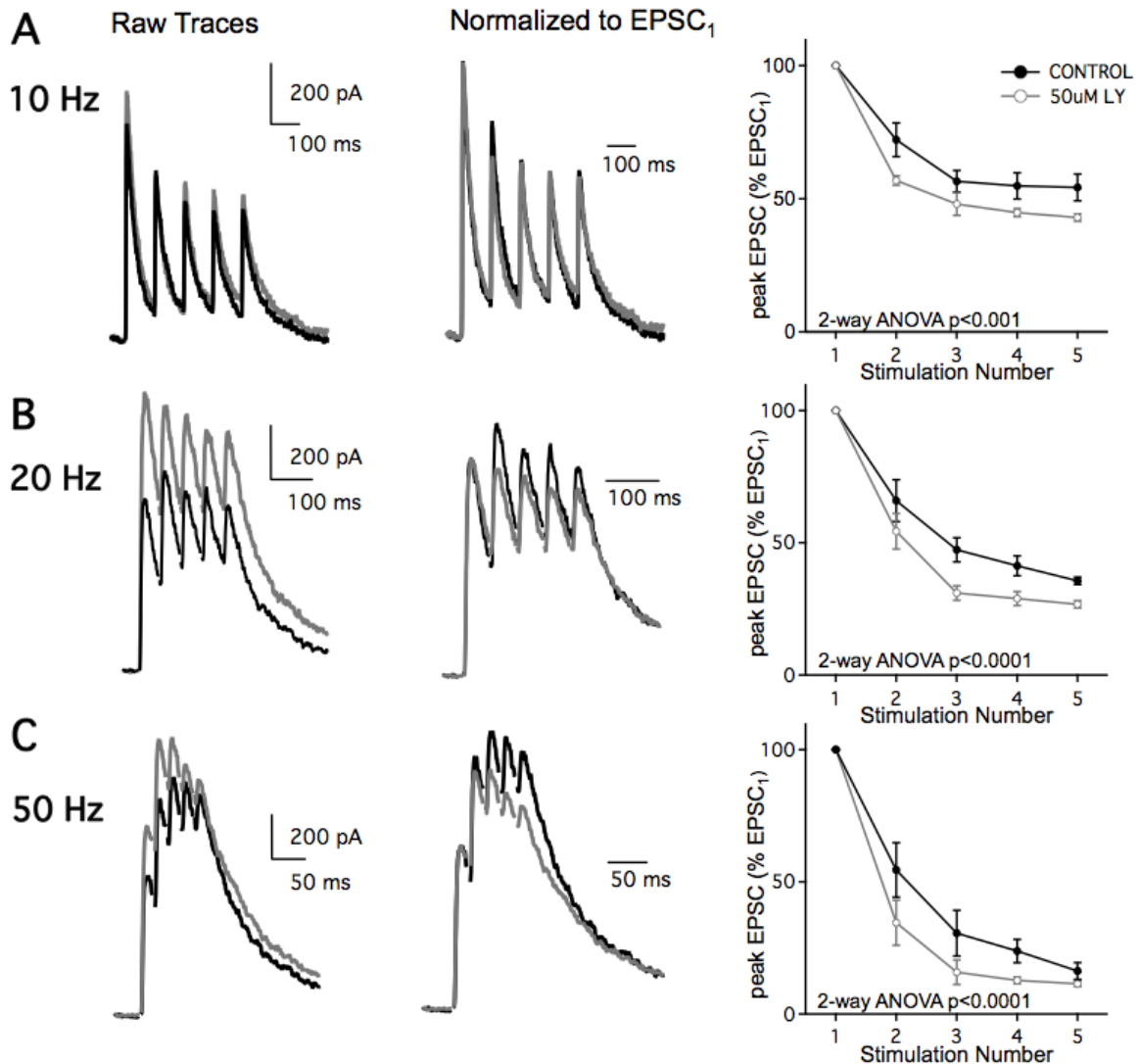
Figure 3.6: mGluRs are activated during physiologically relevant trains.
(Left) Representative traces of NMDAR EPSCs in response to trains of 5 stimuli at 10 Hz (A), 20 Hz (B), and 50 Hz (C) shown before (black) and during (grey) bath application of 50 µM LY. (Middle) NMDAR responses normalized to $EPSC_1$ before (black) and during (grey) application of 50 µM LY. (Right) Summary of the relative changes in EPSC amplitudes during trains of stimuli at frequencies before (black) and during (grey) application of LY, shown as mean ± SEM. Peak amplitudes in a train are normalized to $EPSC_1$. Synaptic depression in response to trains of stimuli is significantly increased in the presence of LY for 10 Hz, 20 Hz and 50 Hz ($p<<0.001$) by two-way ANOVA. Recordings performed at 35±1°C.

DISCUSSION

Developmental regulation of synaptic glutamate concentration

We examined mechanisms regulating glutamate release and clearance at the developing retinogeniculate synapse. First, we show that inhibiting glutamate transporters changes the shape of synaptic currents. This confirms an active role for transporters in removal of glutamate. Second, our experiments unveiled the presence of a negative feedback mechanism present at the immature synapse. When glutamate accumulates, both group II and III mGluRs are activated, resulting in a sustained reduction in neurotransmitter release. Moreover, our results demonstrate that these mGluRs are activated during presynaptic frequencies that mimic immature RGC firing patterns.

The mGluR-mediated negative feedback loop may play an important role during periods of high frequency presynaptic activity. This mechanism could be advantageous early in development to prevent excess glutamate accumulation during correlated bursts of presynaptic activity. The inhibitory network is not fully matured in the LGN until after eye opening (P12-14) (Bickford et al.); thus the activation of group II/III mGluRs may be a major mechanism preventing excessive glutamate accumulation and excitotoxicity. Our data demonstrate that the mGluR-mediated feedback is downregulated at the mature synapse. This suggests that once connections between retina and thalamus have refined and stabilized, an mGluR-type of autoregulation may no longer be needed to control glutamate release.

Glutamate Transporters at the Retinogeniculate Synapse

Glutamate clearance from the synaptic cleft is controlled by diffusion and by its active removal and buffering by transporters. In addition to removing synaptically released glutamate, transporters also maintain extracellular concentrations of the neurotransmitter (Herman and Jahr 2007). Consistent with previous studies (Tzingounis and Wadiche 2007), we show that glutamate transporters maintain ambient levels of extracellular glutamate, shape the synaptic

waveform at the retinogeniculate synapse over development and shield mGluRs from excessive activation at the immature synapse. However, what makes this visual synapse distinct from other CNS synapses is the sensitivity of both NMDAR and AMPAR currents to transporter inhibition.

At both the immature synapse when mGluRs are inhibited, and at the mature synapse, a low concentration of TBOA (10µm) results in a robust increase in the NMDAR EPSC peak and a doubling of the decay kinetics (See Figure 3.2 and 3.4). The degree of increase of the peak current is striking when compared to the SC-CA1 synapse. At this hippocampal connection, TBOA did not alter the amplitude of the NMDAR EPSC at immature ages, and had a small effect at older ages (Christie and Jahr 2006; Diamond 2005; Thomas et al. 2011). Here, at the retinogeniculate synapse, the peak of the NMDAR but not AMPAR EPSC increases in the presence of TBOA. This can be explained by the higher affinity of NMDARs for glutamate and the slower kinetics of the channel when compared to the AMPAR. The increase in NMDAR EPSC peak is likely influenced by the extent of glutamate spillover and the activation of nearby extrasynaptic NMDARs. Moreover, our results also showed a significant increase in AMPAR EPSC decay kinetics throughout development consistent with spillover to neighboring synapses (Budisantoso et al. 2012). In contrast to our study, TBOA does not alter AMPAR kinetics at the SC-CA1 synapse (Christie and Jahr 2006). In addition, 200 µM TBOA has modest or no effects on AMPAR kinetics at the MF-GC synapse in the cerebellum and the calyx of Held, respectively (DiGregorio et al. 2002; Renden et al. 2005). Thus, our findings suggest currents at this visual synapse rely heavily on glutamate transporters to shape the synaptic response. Interestingly, the effects of TBOA on this sensory synapse are similar to the effects seen on the primary afferent synapses in the mature spinal cord (Napier et al. 2012; Nie and Weng 2009).

It is still unclear which glutamate transporters are present at the immature retinogeniculate synapse. Five excitatory amino-acid transporters (EAATs) compose the family of glutamate transporters in the brain. EAAT1, EAAT2, and EAAT3, also known as GLAST, GLT-1 and EAAC1 in the rodent, are expressed throughout the nervous system (Arriza et al. 1997; Danbolt 2001; Fairman et al. 1995; Kanai and Hediger 1992; Pines et al. 1992; Storck et al. 1992). Given the IC_{50}'s of DL-TBOA to GLAST, GLT-1 and EAAC1 (70μM, 6μM and 6μM, respectively) our results showing a dramatic effect of 10uM TBOA suggest that GLT-1 and/or EAAC1 play a role in shaping the synaptic transient at the retinogeniculate synapse (Lebrun et al. 1997; Shimamoto et al. 2000). Our data is consistent with a previous report that localized both GLT-1 and GLAST to nearby glia at the mature synapse (Budisantoso et al. 2012). However, it remains unknown whether there are changes in transporter expression or their subcellular localization over development. It will be interesting in future studies to further investigate the distinct locations and roles of specific glutamate transporter subtypes at the immature synapse.

Autoregulation of Neurotransmitter Release by mGluRs over development

We found that transporters at the immature retinogeniculate synapse prevented excessive glutamate binding to group II/III mGluRs. Consistent with reports from other synapses, activation of these metabotropic receptors reduced synaptic strength and increased PPR (Baskys and Malenka 1991; Conn and Pin 1997; Maki et al. 1994; Min et al. 1998; Oliet et al. 2001; Renden et al. 2005; Scanziani et al. 1997; von Gersdorff et al. 1997). The presence of these receptors was unexpected, as studies in the mature visual thalamus had shown that group II or III mGluRs regulate neurotransmitter release at corticothalamic projections, but not at the retinogeniculate synapse (Alexander and Godwin 2005; 2006; Turner and Salt 1999). However, consistent with these previous studies at the mature synapse, we find that the group II/III mGluRs mediated responses are downregulated with age. Notably, the loss of mGluR function has been described

over development at another sensory synapse, the calyx of Held. At this brainstem synapse, some presynaptic group II/III mGluRs are present in early development and then downregulate with age, athough there is no evidence of presynaptic mGluR7 mediated function at this synapse (Renden et al. 2005). Interestingly, the spiral ganglion neurons in the cochlear hair cells that drive presynaptic input to the Calyx of Held have recently been shown to exhibit wave-like spontaneous activity, with prolonged bursts of spikes reaching 100 Hz, during a pre-hearing developmental period (Tritsch and Bergles 2010; Tritsch et al. 2010). The similarities in the two sensory synapses support the idea that mGluRs play an important role in regulating glutamate release during this period of activity-dependent synapse remodeling.

The rapid effects of group II/III mGluR agonists on release probability suggest that the receptors are located on the presynaptic RGC terminals as opposed to a neighboring cell. To date, no high-resolution immunoelectron microscopy study of the developing LGN has localized mGluRs. However, in another sensory nucleus of the developing thalamus, the ventral posterior nucleus of the somatosensory system, the group II class mGluR2/3 has been localized to 3% of presynaptic axon terminals of asymmetric synapses (Liu et al. 1998). This EM study also noted dense labeling of mGluR2 in glial processes near synapses. Our study cannot completely rule out that mGluR activation in glia could, through an indirect pathway, lead to the reduction of vesicular release at RGC axon terminals. An example of one such indirect pathway involves astrocyte-mediated accumulation of adenosine that binds to presynaptic A1 receptors and reduces release probability (Dittman and Regehr 1996; Pan et al. 1995; Pascual et al. 2005; Scanziani et al. 1992; Zhang and Schmidt 1999). However, we included the A1 receptor blocker DPCPX in all of our experiments. Thus, were astrocytes involved, a substance other than adenosine would be responsible for presynaptic modulation of release. Moreover, mGluR2 expression in astrocytes does not decrease over development in the thalamus (Liu et al. 1998). Thus, we favor a model where mGluRs are transiently expressed in RGC terminals.

Our results demonstrate a dynamic range of mGluR-mediated regulation of glutamate release at the immature retinogeniculate synapse (See Figures 3.1, 3.2 and 3.6). The negative feedback response appears to scale with the degree of glutamate accumulation and spillover. With low frequency stimulation we see a small but significant mGluR-mediated effect, while a substantial decrease in synaptic strength is seen when transporters are inhibited. This could be explained by the subcellular localization of the different mGluRs and by their distinct affinities for glutamate. For example, EM studies in the hippocampus show immunoreactivity for the high-affinity group II mGluR2/3 to axons terminals outside of the synaptic cleft (Shigemoto et al. 1997; Tamaru et al. 2001). In contrast, low-affinity group III mGluR7 (K_d = 1mM glutamate) is found in presynaptic active zones (Brandstatter et al. 1996; Conn and Pin 1997; Shigemoto et al. 1997). Interestingly, it has been shown that mGluR7s are activated during periods of robust presynaptic activity (Pelkey et al. 2005; Pelkey et al. 2007). Thus the varied location and glutamate affinities of different classes of mGluRs could contribute to a diverse repertoire of synaptic responses. Given the dynamic synaptic environment at the immature retinogeniculate synapse, it is possible that activation of mGluRs may play an important role in the process of developmental synaptic refinement.

REFERENCES

Aggelopoulos N, Parnavelas JG, and Edmunds S. Synaptogenesis in the dorsal lateral geniculate nucleus of the rat. *Anat Embryol (Berl)* 180: 243-257, 1989.

Akerman CJ, Smyth D, and Thompson ID. Visual experience before eye-opening and the development of the retinogeniculate pathway. *Neuron* 36: 869-879, 2002.

Alexander GM, and Godwin DW. Presynaptic inhibition of corticothalamic feedback by metabotropic glutamate receptors. *J Neurophysiol* 94: 163-175, 2005.

Alexander GM, and Godwin DW. Unique presynaptic and postsynaptic roles of Group II metabotropic glutamate receptors in the modulation of thalamic network activity. *Neuroscience* 141: 501-513, 2006.

Arriza JL, Eliasof S, Kavanaugh MP, and Amara SG. Excitatory amino acid transporter 5, a retinal glutamate transporter coupled to a chloride conductance. *Proc Natl Acad Sci U S A* 94: 4155-4160, 1997.

Baskys A, and Malenka RC. Agonists at metabotropic glutamate receptors presynaptically inhibit EPSCs in neonatal rat hippocampus. *J Physiol* 444: 687-701, 1991.

Bickford ME, Slusarczyk A, Dilger EK, Krahe TE, Kucuk C, and Guido W. Synaptic development of the mouse dorsal lateral geniculate nucleus. *J Comp Neurol* 518: 622-635, 2010.

Brandstatter JH, Koulen P, Kuhn R, van der Putten H, and Wassle H. Compartmental localization of a metabotropic glutamate receptor (mGluR7): two different active sites at a retinal synapse. *J Neurosci* 16: 4749-4756, 1996.

Budisantoso T, Matsui K, Kamasawa N, Fukazawa Y, and Shigemoto R. Mechanisms underlying signal filtering at a multisynapse contact. *J Neurosci* 32: 2357-2376, 2012.

Cathala L, Holderith NB, Nusser Z, DiGregorio DA, and Cull-Candy SG. Changes in synaptic structure underlie the developmental speeding of AMPA receptor-mediated EPSCs. *Nat Neurosci* 8: 1310-1318, 2005.

Chen C, Blitz DM, and Regehr WG. Contributions of receptor desensitization and saturation to plasticity at the retinogeniculate synapse. *Neuron* 33: 779-788, 2002.

Chen C, and Regehr WG. Developmental remodeling of the retinogeniculate synapse. *Neuron* 28: 955-966, 2000.

Christie JM, and Jahr CE. Multivesicular release at Schaffer collateral-CA1 hippocampal synapses. *J Neurosci* 26: 210-216, 2006.

Conn PJ, and Pin JP. Pharmacology and functions of metabotropic glutamate receptors. *Annu Rev Pharmacol Toxicol* 37: 205-237, 1997.

Danbolt NC. Glutamate uptake. *Prog Neurobiol* 65: 1-105, 2001.

Demas J, Eglen SJ, and Wong RO. Developmental loss of synchronous spontaneous activity in the mouse retina is independent of visual experience. *Journal of Neuroscience* 23: 2851-2860, 2003.

Diamond JS. Deriving the glutamate clearance time course from transporter currents in CA1 hippocampal astrocytes: transmitter uptake gets faster during development. *J Neurosci* 25: 2906-2916, 2005.

Diamond JS, and Jahr CE. Transporters buffer synaptically released glutamate on a submillisecond time scale. *J Neurosci* 17: 4672-4687, 1997.

DiGregorio DA, Nusser Z, and Silver RA. Spillover of glutamate onto synaptic AMPA receptors enhances fast transmission at a cerebellar synapse. *Neuron* 35: 521-533, 2002.

Dittman JS, and Regehr WG. Contributions of calcium-dependent and calcium-independent mechanisms to presynaptic inhibition at a cerebellar synapse. *J Neurosci* 16: 1623-1633, 1996.

Fairman WA, Vandenberg RJ, Arriza JL, Kavanaugh MP, and Amara SG. An excitatory amino-acid transporter with properties of a ligand-gated chloride channel. *Nature* 375: 599-603, 1995.

Herman MA, and Jahr CE. Extracellular glutamate concentration in hippocampal slice. *J Neurosci* 27: 9736-9741, 2007.

Hooks BM, and Chen C. Distinct roles for spontaneous and visual activity in remodeling of the retinogeniculate synapse. *Neuron* 52: 281-291, 2006.

Huttenlocher PR. Development of cortical neuronal activity in the neonatal cat. *Exp Neurol* 17: 247-262, 1967.

Jaubert-Miazza L, Green E, Lo FS, Bui K, Mills J, and Guido W. Structural and functional composition of the developing retinogeniculate pathway in the mouse. *Vis Neurosci* 22: 661-676, 2005.

Kanai Y, and Hediger MA. Primary structure and functional characterization of a high-affinity glutamate transporter. *Nature* 360: 467-471, 1992.

Kerschensteiner D, and Wong RO. A precisely timed asynchronous pattern of ON and OFF retinal ganglion cell activity during propagation of retinal waves. *Neuron* 58: 851-858, 2008.

Kingston AE, Ornstein PL, Wright RA, Johnson BG, Mayne NG, Burnett JP, Belagaje R, Wu S, and Schoepp DD. LY341495 is a nanomolar potent and selective antagonist of group II metabotropic glutamate receptors. *Neuropharmacology* 37: 1-12, 1998.

Krug K, Akerman CJ, and Thompson ID. Responses of neurons in neonatal cortex and thalamus to patterned visual stimulation through the naturally closed lids. *J Neurophysiol* 85: 1436-1443, 2001.

Lebrun B, Sakaitani M, Shimamoto K, Yasuda-Kamatani Y, and Nakajima T. New beta-hydroxyaspartate derivatives are competitive blockers for the bovine glutamate/aspartate transporter. *J Biol Chem* 272: 20336-20339, 1997.

Lieberman AR. Neurons with presynaptic perikarya and presynaptic dendrites in the rat lateral geniculate nucleus. *Brain Res* 59: 35-59, 1973.

Linden AM, Johnson BG, Trokovic N, Korpi ER, and Schoepp DD. Use of MGLUR2 and MGLUR3 knockout mice to explore in vivo receptor specificity of the MGLUR2/3 selective antagonist LY341495. *Neuropharmacology* 57: 172-182, 2009.

Liu X, and Chen C. Different Roles for AMPA and NMDA Receptors in Transmission at the Immature Retinogeniculate Synapse. *J Neurophysiol* 99: 629-643, 2008.

Liu XB, Munoz A, and Jones EG. Changes in subcellular localization of metabotropic glutamate receptor subtypes during postnatal development of mouse thalamus. *J Comp Neurol* 395: 450-465, 1998.

Maki R, Robinson MB, and Dichter MA. The glutamate uptake inhibitor L-trans-pyrrolidine-2,4-dicarboxylate depresses excitatory synaptic transmission via a presynaptic mechanism in cultured hippocampal neurons. *J Neurosci* 14: 6754-6762, 1994.

Min MY, Rusakov DA, and Kullmann DM. Activation of AMPA, kainate, and metabotropic receptors at hippocampal mossy fiber synapses: role of glutamate diffusion. *Neuron* 21: 561-570, 1998.

Mooney R, Penn AA, Gallego R, and Shatz CJ. Thalamic relay of spontaneous retinal activity prior to vision. *Neuron* 17: 863-874, 1996.

Moseley MJ, Bayliss SC, and Fielder AR. Light transmission through the human eyelid: in vivo measurement. *Ophthalmic Physiol Opt* 8: 229-230, 1988.

Napier IA, Mohammadi SA, and Christie MJ. Glutamate transporter dysfunction associated with nerve injury-induced pain in mice. *J Neurophysiol* 107: 649-657, 2012.

Nie H, and Weng HR. Glutamate transporters prevent excessive activation of NMDA receptors and extrasynaptic glutamate spillover in the spinal dorsal horn. *J Neurophysiol* 101: 2041-2051, 2009.

Oliet SH, Piet R, and Poulain DA. Control of glutamate clearance and synaptic efficacy by glial coverage of neurons. *Science* 292: 923-926, 2001.

Pan WJ, Osmanovic SS, and Shefner SA. Characterization of the adenosine A1 receptor-activated potassium current in rat locus ceruleus neurons. *J Pharmacol Exp Ther* 273: 537-544, 1995.

Pascual O, Casper KB, Kubera C, Zhang J, Revilla-Sanchez R, Sul JY, Takano H, Moss SJ, McCarthy K, and Haydon PG. Astrocytic purinergic signaling coordinates synaptic networks. *Science* 310: 113-116, 2005.

Pelkey KA, Lavezzari G, Racca C, Roche KW, and McBain CJ. mGluR7 is a metaplastic switch controlling bidirectional plasticity of feedforward inhibition. *Neuron* 46: 89-102, 2005.

Pelkey KA, Yuan X, Lavezzari G, Roche KW, and McBain CJ. mGluR7 undergoes rapid internalization in response to activation by the allosteric agonist AMN082. *Neuropharmacology* 52: 108-117, 2007.

Pines G, Danbolt NC, Bjoras M, Zhang Y, Bendahan A, Eide L, Koepsell H, Storm-Mathisen J, Seeberg E, and Kanner BI. Cloning and expression of a rat brain L-glutamate transporter. *Nature* 360: 464-467, 1992.

Rafols JA, and Valverde F. The structure of the dorsal lateral geniculate nucleus in the mouse. A Golgi and electron microscopic study. *J Comp Neurol* 150: 303-332, 1973.

Renden R, Taschenberger H, Puente N, Rusakov DA, Duvoisin R, Wang LY, Lehre KP, and von Gersdorff H. Glutamate transporter studies reveal the pruning of metabotropic glutamate receptors and absence of AMPA receptor desensitization at mature calyx of held synapses. *J Neurosci* 25: 8482-8497, 2005.

Scanziani M, Capogna M, Gahwiler BH, and Thompson SM. Presynaptic inhibition of miniature excitatory synaptic currents by baclofen and adenosine in the hippocampus. *Neuron* 9: 919-927, 1992.

Scanziani M, Salin PA, Vogt KE, Malenka RC, and Nicoll RA. Use-dependent increases in glutamate concentration activate presynaptic metabotropic glutamate receptors. *Nature* 385: 630-634, 1997.

Shigemoto R, Kinoshita A, Wada E, Nomura S, Ohishi H, Takada M, Flor PJ, Neki A, Abe T, Nakanishi S, and Mizuno N. Differential presynaptic localization of metabotropic glutamate receptor subtypes in the rat hippocampus. *J Neurosci* 17: 7503-7522, 1997.

Shimamoto K, Shigeri Y, Yasuda-Kamatani Y, Lebrun B, Yumoto N, and Nakajima T. Syntheses of optically pure beta-hydroxyaspartate derivatives as glutamate transporter blockers. *Bioorg Med Chem Lett* 10: 2407-2410, 2000.

Storck T, Schulte S, Hofmann K, and Stoffel W. Structure, expression, and functional analysis of a Na(+)-dependent glutamate/aspartate transporter from rat brain. *Proc Natl Acad Sci U S A* 89: 10955-10959, 1992.

Tamaru Y, Nomura S, Mizuno N, and Shigemoto R. Distribution of metabotropic glutamate receptor mGluR3 in the mouse CNS: differential location relative to pre- and postsynaptic sites. *Neuroscience* 106: 481-503, 2001.

Taschenberger H, Leao RM, Rowland KC, Spirou GA, and von Gersdorff H. Optimizing synaptic architecture and efficiency for high-frequency transmission. *Neuron* 36: 1127-1143, 2002.

Thomas CG, Tian H, and Diamond JS. The relative roles of diffusion and uptake in clearing synaptically released glutamate change during early postnatal development. *J Neurosci* 31: 4743-4754, 2011.

Torborg CL, and Feller MB. Spontaneous patterned retinal activity and the refinement of retinal projections. *Prog Neurobiol* 76: 213-235, 2005.

Torborg CL, Hansen KA, and Feller MB. High frequency, synchronized bursting drives eye-specific segregation of retinogeniculate projections. *Nat Neurosci* 8: 72-78, 2005.

Tritsch NX, and Bergles DE. Developmental regulation of spontaneous activity in the Mammalian cochlea. *J Neurosci* 30: 1539-1550, 2010.

Tritsch NX, Rodriguez-Contreras A, Crins TT, Wang HC, Borst JG, and Bergles DE. Calcium action potentials in hair cells pattern auditory neuron activity before hearing onset. *Nat Neurosci* 13: 1050-1052, 2010.

Turner JP, and Salt TE. Group III metabotropic glutamate receptors control corticothalamic synaptic transmission in the rat thalamus in vitro. *J Physiol* 519 Pt 2: 481-491, 1999.

Tzingounis AV, and Wadiche JI. Glutamate transporters: confining runaway excitation by shaping synaptic transmission. *Nat Rev Neurosci* 8: 935-947, 2007.

von Gersdorff H, Schneggenburger R, Weis S, and Neher E. Presynaptic depression at a calyx synapse: the small contribution of metabotropic glutamate receptors. *J Neurosci* 17: 8137-8146, 1997.

Zhang C, and Schmidt JT. Adenosine A1 and class II metabotropic glutamate receptors mediate shared presynaptic inhibition of retinotectal transmission. *J Neurophysiol* 82: 2947-2955, 1999.

CHAPTER 4:

Prolonged Synaptic Currents Increase Relay Neuron Firing at the Developing

Retinogeniculate Synapse

Prolonged Synaptic Currents Increase Relay Neuron Firing at the Developing Retinogeniculate Synapse

Jessica L. Hauser[§], Xiaojin Liu[§], Elizabeth Y. Litvina and Chinfei Chen*

Department of Neurology, F.M. Kirby Neurobiology Center, Children's Hospital, Boston,
300 Longwood Avenue, Boston, MA 02115
and
Program in Neuroscience, Harvard Medical School,
220 Longwood Avenue, Boston, MA 02115

§ these authors contributed equally to this work

*To whom correspondence should be addressed:
Phone: 617-919-2685, Fax: 617-730-0242
chinfei.chen@childrens.harvard.edu

ABSTRACT

The retinogeniculate synapse, the connection between retinal ganglion cells (RGC) and thalamic relay neurons, undergoes robust changes in connectivity over development. This process of synapse elimination and strengthening of remaining inputs is thought to require synapse specificity. Here we show that glutamate spillover and asynchronous release are prominent features of retinogeniculate synaptic transmission during this period. The immature EPSCs exhibit a slow decay timecourse that is sensitive to low affinity glutamate receptor antagonists and extracellular calcium concentrations, consistent with glutamate spillover. Furthermore, we uncover and characterize a novel, purely spillover-mediated AMPA receptor current from immature relay neurons. The isolation of this current strongly supports the presence of spillover between boutons of different RGCs. In addition, fluorescence measurements of presynaptic calcium transients suggest that prolonged residual calcium contributes to both glutamate spillover and asynchronous release. These data indicate that during development, far more RGCs contribute to relay neuron firing than would be expected based on predictions from anatomy alone.

INTRODUCTION

Even before eye opening, information encoded in retinal activity is relayed to the visual cortex and plays a critical role in the proper formation of retinotopic maps in the visual cortex (Huttenlocher, 1967; Akerman et al., 2002; Kirkby et al., 2013). Remarkably, this information transfer via the retinogeniculate synapse is maintained despite rapidly changing properties of the immature connection (Mooney et al., 1996; Hanganu et al., 2006). Between postnatal day (p)8 and p30, the average strength of a RGC input increases 20-fold, while the number of retinal inputs that innervate a given relay neuron is pruned from many to few (Chen and Regehr, 2000; Jaubert-Miazza et al., 2005). The synaptic mechanisms that allow immature weak retinal inputs to drive relay neuron firing and maintain information transfer are still incompletely understood.

One feature of the immature synapse that has been proposed to aid in the transmission of visual information is the prolonged waveform of the retinogeniculate EPSC (Ramoa and McCormick, 1994; Chen and Regehr, 2000; Hooks and Chen, 2006; Ziburkus and Guido, 2006; Liu and Chen, 2008). The decay time course of both AMPAR and NMDAR EPSCs is slower in the young than the old (Ramoa and Prusky, 1997; Chen and Regehr, 2000; Liu and Chen, 2008). Although receptor subunit changes contribute to part of the developmental acceleration of the EPSC, they cannot account for all of the observed changes in kinetics. Notably, the AMPAR quantal event does not exhibit similar slow decay kinetics to the evoked response, nor does the mEPSC waveform significantly accelerate with age (Liu and Chen, 2008).

These findings suggest that other synaptic mechanisms contribute to the slow time course of the immature EPSC. For example, the slow component could be due to glutamate pooling within the synaptic cleft from impeded diffusion. Alternatively, it could be delayed (asynchronous) release, where the release of additional vesicles persists for up to hundreds of milliseconds following depolarization of the presynaptic terminal (Barrett and Stevens, 1972; Rahamimoff and

Yaari, 1973; Goda and Stevens, 1994; Atluri and Regehr, 1998; Kaeser and Regehr, 2014).

Asynchronous release is driven by presynaptic residual calcium and prolongs the decay time

course of the postsynaptic response, thus enhancing synaptic charge transfer (Zengel and

Magleby, 1981; Zucker and Lara-Estrella, 1983; Vanderkloot and Molgo, 1993; Cummings et al.,

1996). Finally, the slow EPSC decay could be due to glutamate spillover between release sites

located within the same bouton or in neighboring boutons (Trussell et al., 1993; Barbour et al.,

1994; Takahashi et al., 1995; Otis et al., 1996; DiGregorio et al., 2002). At the immature

retinogeniculate synapse, glutamate can spillover to extrasynaptic mGluRs, but whether

glutamate also reaches neighboring release sites is not known (Hauser et al., 2013).

Here, we distinguish between these different explanations for the prolonged current observed at

the immature retinogeniculate synapse. We find that both spillover between synaptic release

sites and asynchronous release contribute to the extended glutamate timecourse. Moreover we

characterize purely spillover-mediated currents from relay neurons indicating that neighboring

RGCs can influence relay neuron firing without making direct contacts onto the cell. This

prolonged glutamate transient is essential for the propagation of retinal activity to the developing

cortex during a dynamic period of robust synaptic maturation and refinement.

METHODS

Slice preparation. All experimental procedures were performed in accordance with federal

guidelines and protocols approved by Boston Children's Hospital. Parasagittal brain slices

containing both the optic tract and the dorsal lateral geniculate nucleus (LGN) were obtained as

previously described (Chen and Regehr, 2000; Liu and Chen, 2008) from p8-34 C57BL/6 mice

(C57BL/6J from Jackson Laboratory, ME or C57BL/6NTac (B6) from Taconic, NY). Briefly, the

brain was quickly removed and immersed into an oxygenated 4°C choline-based cutting solution

containing (in mM): 87 NaCl, 25 $NaHCO_3$, 37.5 choline chloride, 25 glucose, 2.5 KCl, 1.25

NaH$_2$PO$_4$, 7 MgCl$_2$, and 0.5 CaCl$_2$ or 130 Choline chloride, 26 NaHCO$_3$, 1.25 NaH$_2$PO$_4$, 2.5 KCl, 7.0 MgCl$_2$, 0.5 CaCl$_2$ and 25 glucose. Both cutting solutions yielded healthy slices at all ages. The brain tissue was then mounted on the cutting stage of a vibratome (Leica VT1000S) and submerged into oxygenated 4°C cutting solution. Cut 250 µm slices were allowed to recover for 15-20 min at 30°C in the oxygenated cutting solution, and then for another 10-20 min at 30°C in oxygenated artificial cerebral spinal fluid (aCSF) containing (in mM): 125 NaCl, 26 NaHCO$_3$, 1.25 NaH$_2$PO$_4$, 2.5 KCl, 1 MgCl$_2$, 2 CaCl$_2$ and 25 glucose. This aCSF solution was used also for recording.

Electrophysiology. Whole-cell voltage-clamp synaptic recordings from geniculate neurons were obtained using glass pipettes (1-2.0 MΩ) filled with an internal solution consisting of (in mM): 35 CsF, 100 CsCl, 10 EGTA, 10 HEPES, and the L-type calcium channel antagonist, 0.1 methoxyverapamil (Sigma, St. Louis, MO). This solution was designed to minimize the contributions from postsynaptic intrinsic membrane conductances and second messenger systems. In experiments examining AMPAR rectification, 100 µM spermine was included in the internal solution. EPSCs were evoked with stimulus intensities that ranged from 10-150 µA. Series resistance (R$_s$) was <10MΩ (average 5 MΩ), cells were excluded if R$_S$ changed more than 10% during an experiment.

For current clamp experiments, the internal solution contained (in mM): 116 KMeSO$_4$, 6 KCl, 2 NaCl, 20 HEPES, 0.5 EGTA, 4 MgATP, 0.3 NaGTP, 10 Na phosphocreatine, pH 7.25 with KOH. To elicit successful spikes, the amplitude of first EPSC waveform injected were 300 and 1500 pA for immature and mature neurons, respectively (Liu and Chen, 2008). The bath saline solution for all electrophysiological experiments contained the GABA$_A$ receptor antagonist bicuculline (20 µM) or picrotoxin (Sigma, 50µM), and the GABA$_B$ receptor antagonist -N-[1-(S)-3,4-dichlorophenyl)ethyl]amino-2-(S)- hydroxypropyl-P-benzyl-phosphinic acid (CGP55845, 2

70

µM) and the A1 adenosine receptor antagonist 8-Cyclopentyl-1,3-dipropylxanthine (DPCPX, 10µM). 5 µM of 2,3-Dihydro-6-nitro-7-sulphamoyl-benzo(f)quinoxaline (NBQX), 4-(8-Methyl-9*H*-1,3-dioxolo[4,5-*h*][2,3]benzodiazepin-5-yl)-benzenamine dihydrochloride (GYKI 52466, 50µM), 20 to 100 µM 3-((R)-2-Carboxypiperazin-4-yl)-propyl-1-phosphonic acid ((R)-CPP), and (2S-2-amino-2-(1S,2S-2-carboxycycloprop-1-yl)-3-(xanth-9- yl)propanoic acid (LY341495 50µM) was used to block AMPAR, NMDAR, and metabotropic glutamate receptors respectively. All the experiments were performed at $35 \pm 1°C$ unless otherwise indicated.

EGTA-AM experiments were performed as previously described (Atluri and Regehr, 1998; Chen and Regehr, 1999). Briefly, EGTA-acetoxymethyl ester (AM) was dissolved in dimethysulfoxide (DMSO), diluted to a final concentration of 50 µM in aCSF, and continuously bath applied to slices for 15 minutes to allow the chelator to be taken up by all cells in the slice. Excess EGTA-AM was then washed out with aCSF. Measurements of the EPSC or $\Delta F/F$ waveforms for the EGTA-AM condition were obtained 15 minutes after bath washout of EGTA-AM.

Calcium measurements. RGCs were labeled with calcium indicators dyes as previously described (Chen and Regehr, 2003). Briefly, the mouse was placed in an enclosed chamber and isoflurane was delivered via a vaporizer with proper scavenging of fumes. 2-4% isoflurane with a mixture of oxygen was used for induction and 1-3% for maintenance during the procedure. Once properly anesthetized, as tested by foot pad stimulation, a sharp glass electrode (2-5 µm tip diameter) filled with a solution that consisted of a 1:1 mixture of 20% w/v Calcium Green-1 dextran [molecular weight (MW) 3000] and 20% w/v Texas Red dextran (MW 10,000) in 0.1% Triton X-100 was inserted into the retina (Invitrogen, OR). One microliter of the solution was pressure injected into the nasal and temporal regions of the retina (30 psi, 10-15 msec duration; Parker Instruments). 5-10 days after injection, the animal was sacrificed for experiments.

Examination of the slices under 60x objective (Olympus) revealed that retinogeniculate fibers but not postsynaptic cells were labeled.

All fluorescence recordings were performed in the presence of the glutamate receptor antagonists NBQX (5 µM) and CPP (20 µM), bicuculline and CGP55845 (20µm, 2 µm) using a 450-490 excitation/FT510 dichroic/510WB40 emission and 580DF15 excitation/600 dichroic long pass/610 long pass emission filter sets for Calcium Green-1 and Texan Red signals, respectively. Illumination was provided by a 150 W Xenon lamp (Optiquip) and gated with a transistor logic pulse to an electromechanical shutter (Vincent Associates). Collected light from the labeled slice was digitized, and the relative change in fluorescence ($\Delta F/F$) was calculated as described previously (Kreitzer et al., 2000). Calcium measurements were performed at 25°C.

Stock solutions of pharmacological agents were stored at -20°C and diluted according to the final concentrations immediately prior to experiments. Constant bath flow during application of drugs was ensured by a perfusion pump (Gilson, MA). Dead space in the perfusion tubing was reduced to 1 ml, allowing rapid bath exchange of pharmacological agents. All pharmacological agents, including L-(+)-2-Amino-5-phosphonopentanoic acid (L-AP5, 1mM), γ-D-Glutamylgycine (γ-DGG, 1-3mM, 6-Chloro-3,4-dihydro-3-(5-norbornen-2-yl)-2H-1,2,4- benzothiazidiazine-7-sulfonamide-1,1-dioxide (cyclothiazide, CTZ, 50µM), were purchased from Tocris, MO unless otherwise indicated. EGTA, tetra(acetoxymethyl ester) (EGTA, AM), calcium green-1 dextran and Texas Red® 10,000 MW dextran were obtained from Invitrogen (OR).

Data Acquisition and Analysis. Current and voltage-clamp recordings were acquired with a Multiclamp 700A amplifier (Axon Instruments, CA) filtered at 1 kHz and digitized at 10-20 kHz with an ITC-16 interface (Instrutech, NY). Data analysis was performed using Igor software (Wavemetrics, OR), Excel (Microsoft, WA) and Prism (GraphPad Software, Inc.). EPSCs were

analyzed as the average of 5-10 waves. The decay τ of both AMPA and NMDA receptor-mediated EPSCs at immature retinogeniculate synapse were best fitted with a double exponential, $f(x) = y_0 + A_1 e(-x/\tau_{fast}) + A_2 e(-x/\tau_{slow})$ and was quantified as the weighted $\tau = [\tau_{fast} \times A_1/(A_1 + A_2)] + [\tau_{slow} \times A_2/(A_1 + A_2)]$ (Liu and Chen, 2008).

Studies examining short-term synaptic plasticity involved evoking synaptic responses to pairs of retinal input stimuli. Randomized interstimulus intervals ranging from 10-8000 ms were interleaved with a single conditioning pulse as previously described (Chen and Regehr, 2000). For each cell recorded, averages of 3-5 trials were used to measure the paired pulse ratio (EPSC2/EPSC1 X 100) for each ISI.

Spike probability was calculated by summing the number of action potentials that occur over the period following current injection (approximately 10 trials) and dividing the value by number of trials. The criterion for an action potential was a depolarizing change in membrane potential $(dV/dt) \geq 10 Vsec^{-1}$. Synaptic charge (Q) was calculated by integrating the evoked synaptic current. All data are summarized as mean ± SEM, using the two-tailed paired t-test unless otherwise indicated.

RESULTS

Acceleration of the retinogeniculate EPSC waveform over development

Changes in the EPSC waveform over development are evident when comparing the decay kinetics of the AMPAR current of immature (p9-11, red trace) and mature (P26-32, black trace) synapses (Figure 4.1A, left). The synaptic currents, evoked by optic nerve stimulation, were recorded in whole cell voltage clamp mode (V_h=-70mV) and in the presence of the NMDAR selective antagonist, 20 μM (R)-CPP. The immature EPSC waveform exhibited slower decay kinetics when compared to the mature synapse, and this difference persisted even in the
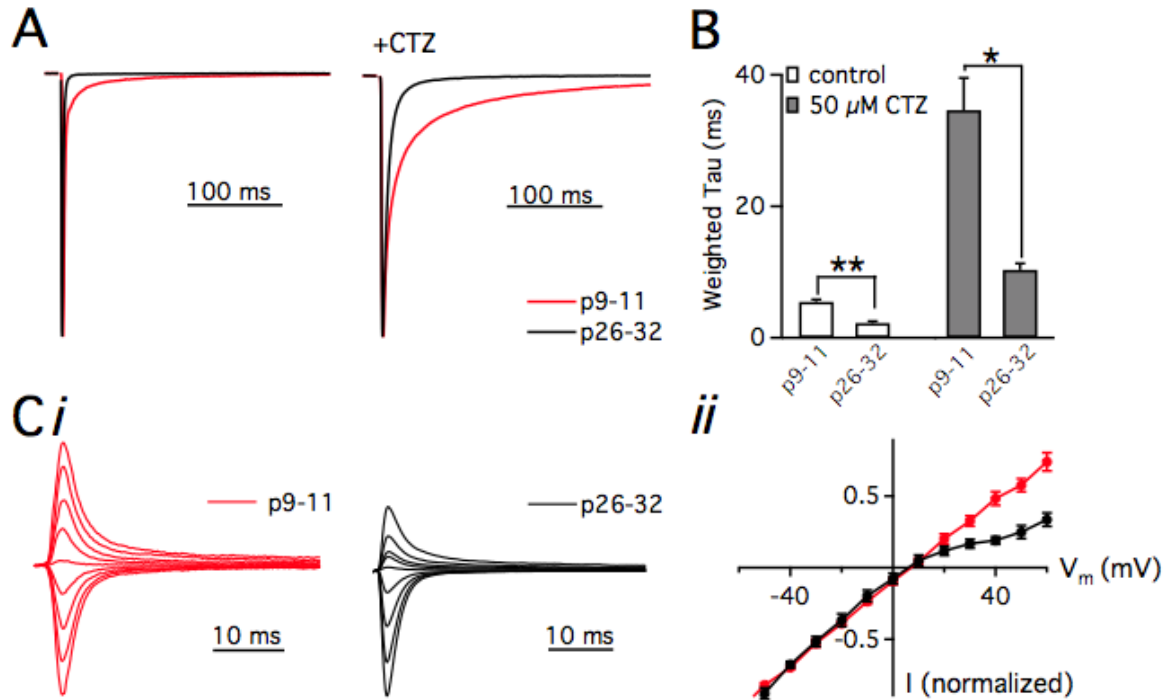
Figure 4.1: Properties of the retinogeniculate AMPAR EPSC change over development
Comparison of the decay time course of the immature (p9-11, red traces) and mature (p26-32, black traces) retinogeniculate AMPAR EPSCs (V_h= -70 mV) in the absence (A, *left*) and presence (A, *right*) of 50µM cyclothiazide (CTZ). Representative traces are averages from 10-15 trials and normalized to the peak. (*B*) Summary graph of the time course of the AMPAR EPSC decay (weighted tau) from the two age groups in control (white) and in CTZ (grey) n=4; (*)p<0.05, (**) p<0.01. Recordings were made in the presence of (R)-CPP to block NMDAR-mediated EPSCs. Bath temperature: 35 ± 1°C. (*C, left*) Representative examples of AMPAR EPSC traces evoked at different holding potentials (-60 to 60 mV in 20mV increments), and (C, *right*) average current-voltage relationship for immature (red, n=5 cells) and mature (black, n=6 cells) synapses. Synaptic currents were recorded with intracellular spermine of p9-11 significantly different from p26-32, p<<0.001, 2-way ANOVA). Recorded at room temperature.

presence of cyclothiazide (50 μM, CTZ), an inhibitor of AMPAR desensitization (Figure 4.1A, right). The AMPAR decay time course, in control and CTZ conditions, could be approximated by a double exponential time constant where the average weighted tau is 2-3 times greater for immature synapses when compared to the mature synapses (Figure 4.1B). Therefore, developmental changes in the AMPAR EPSC waveform cannot be simply explained by differences in receptor desensitization.

Our results involving CTZ suggested that immature EPSC is more sensitive to the inhibitor of desensitization (6.37 ± 0.93 fold increase in weighted tau vs 3.3 ± 0.43 fold), and raised the possibility that the subunit composition of AMPARs may change with age. One means of testing for a change in AMPAR subunit composition is to assess whether the contribution of calcium-permeable AMPAR subunits change with age. In the presence of intracellular polyamines such as spermine, the I-V relationship of Ca^{2+}-permeable AMPARs is known to rectify, whereas that of Ca^{2+}-impermeable AMPARs is linear (Hollmann et al., 1991; Blaschke et al., 1993). Therefore, we compared the AMPAR current-voltage (I-V) relationship of immature to mature synapses using an intracellular recording solution containing 100μM spermine. Figure 4.1C shows increased AMPAR rectification with age. The rectification index, calculated as the peak EPSC current measured at +60 mV/-60 mV, was significantly different at p9-11 when compared to p26-32 (0.74 ± 0.06 vs 0.34 ± 0.05, p<0.01, n=5,6 student t-test). This developmental change in AMPAR composition is opposite that described in hippocampus, but similar to that in another thalamic synapse, the leminscal input onto relay neurons in the somatosensory thalamus (Takeuchi et al., 2012). However, the increased contribution of CP-AMPARs at older ages cannot fully explain the observed change in the EPSC waveform over development. Some calcium permeable AMPAR subunits have been shown to have slower, not faster, decay kinetics (Partin et al., 1996). Moreover, our previous studies showed no significant difference in the quantal waveform of the immature and mature synapses (Liu and Chen, 2008). Taken

together, these data suggest that a change in subunit composition is not responsible for the slow component of the immature AMPAR EPSC.

γ-DGG accelerates the decay of immature AMPAR EPSCs

As postsynaptic mechanisms cannot account for the acceleration of the synaptic waveform, we next asked whether the slow decay of the immature EPSC is influenced by an extended time course of glutamate. For these studies, we took advantage of low affinity glutamate receptor antagonists (Olverman et al., 1988). These agents actively compete with glutamate for binding to receptors and their efficacy of inhibition is dependent on the relative concentration of glutamate. Previous studies have shown that receptors directly across from the site of release experience a peak glutamate concentration much greater than receptors that are located further away from this site (Clements et al., 1992; Diamond, 2001; DiGregorio et al., 2002). We examined the effects of these antagonists on the immature retinogeniculate waveforms.

We recorded isolated AMPAR-mediated currents in the presence of 50μM CTZ and NMDAR antagonists to gain an accurate measurement of the glutamate transient. Bath application of the low affinity AMPAR antagonist, γ-DGG (3mM), reduced the peak AMPAR EPSC amplitude to 51 ± 2.8% of control ($p<0.01$, n=4) and significantly accelerated the decay of the current to 48.8 ± 3.6% of control ($p<0.01$, n=4; weighted tau control: 21.7 ± 3 ms, γ-DGG: 10.6 ± 1.8 ms, Figure 4.2 C). Notably, γ-DGG preferentially inhibited the slow component of the EPSC decay (control vs. γ-DGG: $\tau_{slow=}$ 18.6 ± 3.6 ms vs. 8.4 ± 2 ms n=4, $p=0.01$; τ_{fast} = 3.1 ± 1.2 vs. 2.2 ± 0.4 ms, n=4, $p=0.28$). To ensure the acceleration of the current was not due to voltage-clamp errors, we performed parallel experiments with a low concentration of NBQX (200nM), a high affinity antagonist that dissociates from the receptor slowly. Unlike γ-DGG, NBQX inhibition of AMPAR currents is independent of glutamate concentration. 200 nM NBQX reduced the AMPAR EPSC amplitude to a similar extent as γ-DGG (48.1 ± 5% of control, n=5; p>0.6 NBQX vs. γ-DGG), but
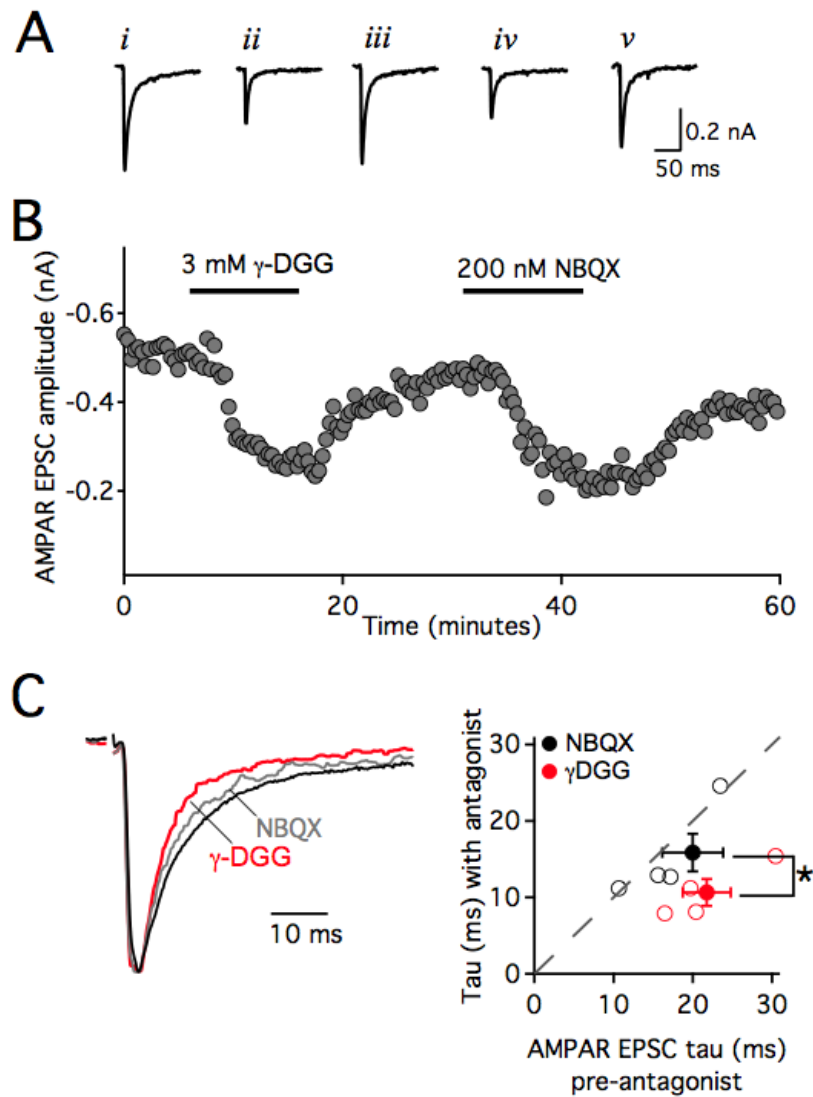
Figure 4.2: γ-DGG accelerates the AMPAR EPSC Tau at the immature synapse
(*A*) AMPAR EPSCs (V_h= -70mV) recorded in the presence of CTZ (50 *μ*M) and NMDAR antagonists (50 *μ*M D-AP5, 20 *μ*M CPP) under control conditions (*i,iii*) and in the presence of 3 mM γ-DGG (*ii*) and 200 nM NBQX (*iv*). Traces are the average of 5-10 consecutive responses and correspond to the peak amplitudes in the time course plotted in (*B*). (*C, left*) Representative normalized AMPAR EPSCs before (black trace) and during (red trace) application of γ-DGG or NBQX (grey trace). (*C, right*) Scatter plot of AMPAR EPSC weighted tau (τ) shown as mean ± SEM (filled circles) before (X axis) and in the presence of antagonist (Y axis) with individual experiments plotted (open circles). γ-DGG (before τ : 21.8 ± 3.0 ms; in antagonist: 10.6 ± 1.8 ms *n*=4) and NBQX (before τ : 20.0 ± 3.8 ms; in antagonist: 15.9 ± 2.5 ms, *n*=5). Bath temperature: 35 ± 1°C. (*) *p*<0.05.

77

the two antagonists differed in their effects on the time course of the decay kinetics. In Figure 4.2 C, the average AMPAR current waveform, normalized to the peak of the EPSC, is shown before and during bath application of γ-DGG (red trace) or NBQX (grey trace). γ-DGG inhibits a greater fraction of the decaying phase of the EPSC, when compared to the peak of the current. In contrast, NBQX did not have a significant effect on the time course of the EPSC (Figure 4.2C, weighted tau=84.1 ± 9.5% of control, n=5, p>0.2, Figure 4.2C; γ-DGG vs. NBQX, p<0.02; γ-DGG also accelerates the decay in 1.5mM $[Ca^{2+}]_o$ Supplemental Figure 7.1). These data suggest that AMPARs that contribute to the tail of the immature EPSC experience a lower peak concentration of glutamate than those receptors open during the peak of the current.

L-AP5 accelerates the decay of the immature retinogeniculate NMDAR EPSC

If the waveform retinogeniculate EPSC does indeed reflect a gradient of peak glutamate concentrations, then we would predict that low affinity antagonists of NMDARs would also accelerate the decay of the EPSC. To test this hypothesis, we compared the effects of bath application of the low affinity NMDAR antagonist L-AP5 (1 mM) to that of low concentration of the high affinity antagonist, R-CPP (1-1.25μM) in a similar approach as our AMPAR experiments. Figure 4.3A,B shows that at these concentrations, both antagonists inhibited the peak amplitude of the NMDAR EPSC to comparable levels (L-AP5 to 34.4 ± 2.3% and CPP to 40.9±4.3% of control, n=7 each, p>0.2). However, the antagonists have distinct effects on the decay of the NMDAR current (Figure 4.3C). On average, L-AP5 significantly accelerated the EPSC decay τ to 65.0 ± 3.3% of control (p<0.01, n=7, Figure 4.3C). R-CPP had a significantly smaller effect on the time course of the EPSC than L-AP5 (CPP decay τ: 82.1 ± 2% of control, n=7, p<0.001; L-AP5 vs. CPP, p<0.01, Figure 4.3C). These data provide further support for the presence of a gradient in peak concentration of glutamate at the immature synapse.
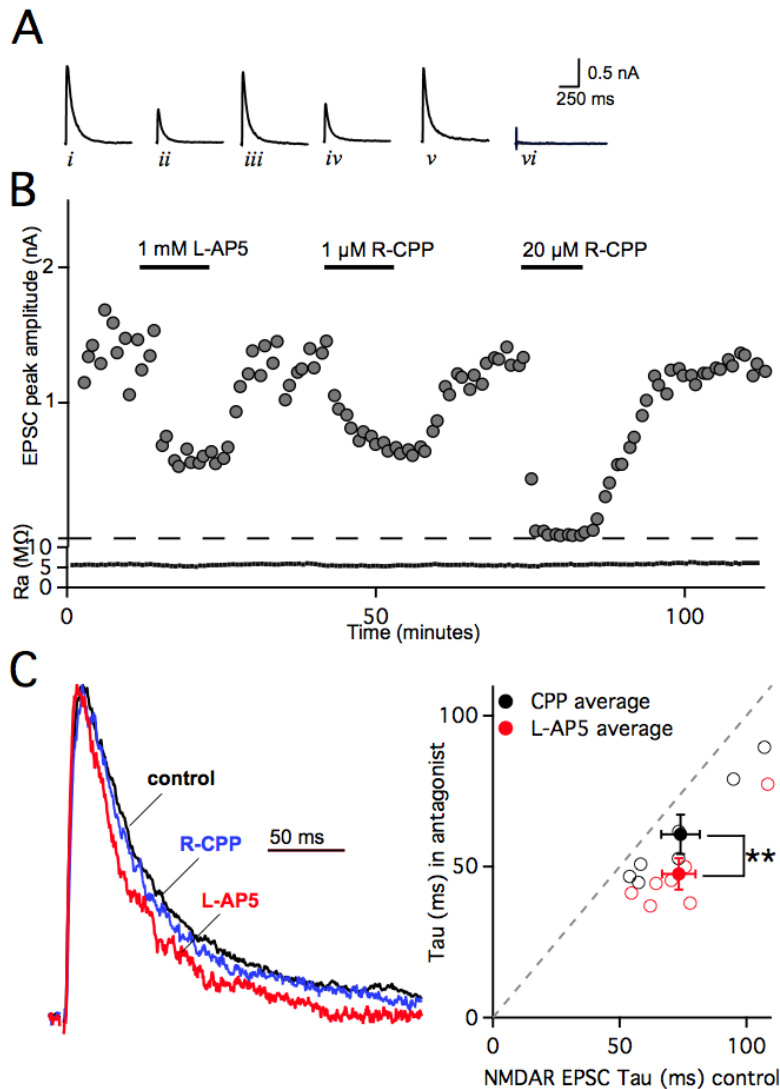
Figure 4.3: L-AP5 accelerates the NMDAR EPSC tau at the immature synapse
(*A*) NMDAR EPSCs (V_h= +40 mV) recorded under control conditions (*i, iii, v*) and in the presence of 1 mM L-AP5 (*ii*), 1 μM (R)-CPP (*iv*) or 20 μM (R)-CPP (*vi*). Traces are the average of 5 consecutive responses and correspond to the amplitudes plotted against time in minutes (*B*). Recordings were performed in the presence of the AMPAR antagonist NBQX (5 μM). Bath temperature: 35 ± 1°C. (*C*) Representative normalized NMDAR EPSCs from before (black trace) and during application of L-AP5 (red trace) or low concentration of (R)-CPP (blue trace). (*C, right*) Scatter plot of NMDAR EPSC weighted tau (τ) before (X axis) and in the presence of antagonist (Y axis). Average values are represented by solid circles shown as mean ± SEM: CPP, black circle- control τ : 74.0 ± 7.7 ms, CPP τ : 60.7± 6.5 ms; L-AP5, red circle, control τ : 73.3 ± 6.6 ms; L-AP5 τ : 47.6± 5.2 ms. Individual experiments are shown as open circles. (**) p=0.01.

79

EPSC Decay Time Course is Dependent on Extracellular Calcium

Compared to NMDARs, AMPARs are much less likely to be located extrasynaptically and have a significantly lower affinity for glutamate (Dingledine et al., 1999; Tarusawa et al., 2009). Therefore, our low affinity AMPAR data suggest that glutamate may diffuse between release sites (aka "spillover") at the immature synapse. If this were true, then the EPSC decay time course could be sensitive to changes in probability of release (P_R)(Trussell et al., 1993; Mennerick and Zorumski, 1995). To alter P_R, we changed the extracellular calcium concentrations (0.5 mM $[Ca^{2+}]_o$ vs. 2.0 mM $[Ca^{2+}]_o$) and compared the normalized AMPAR EPSC waveform (Figure 4.4A). In the presence of 2.0 mM $[Ca^{2+}]_o$ / 1.0 mM $[Mg^{2+}]_o$, the average weighted τ of the AMPAR EPSC decay was 4.1 ± 0.7 ms. Bath exchange to an external solution containing 0.5 mM $[Ca^{2+}]_o$ / 2.5 mM $[Mg^{2+}]_o$ reduced the peak EPSC to 25.4 ± 2.6% of that in 2.0 mM $[Ca^{2+}]_o$/ 1.0 mM $[Mg^{2+}]_o$ (n=5,p<0.001), and significantly accelerated the weighted τ to 1.7 ± 0.2 ms (n=5, p<0.05, Figure 4.4A*iii*). These data provide support for the existence of glutamate spillover at the developing retinogeniculate synapse.

Cyclothiazide relieves Paired Pulse Depression at the immature retinogeniculate synapse

If spillover exists at the immature retinogeniculate synapse, then glutamate released from one site can bind, activate and desensitize receptors at more distant sites. Therefore a population of AMPARs across from a quiescent release site can become desensitized when bound to glutamate released from a neighboring site. AMPAR desensitization that occurs this way would transiently reduce the number of available AMPARs at neighboring quiescent release sites. If glutamate is subsequently released at these neighboring sites within a few miliseconds after the initial release event, the synaptic response will be reduced. At the mature retinogeniculate synapse, postsynaptic AMPAR desensitization is known to contribute to short-term synaptic plasticity because paired-pulse depression is relieved in the presence of CTZ. These observations have been used to describe the presence of glutamate spillover between release

80
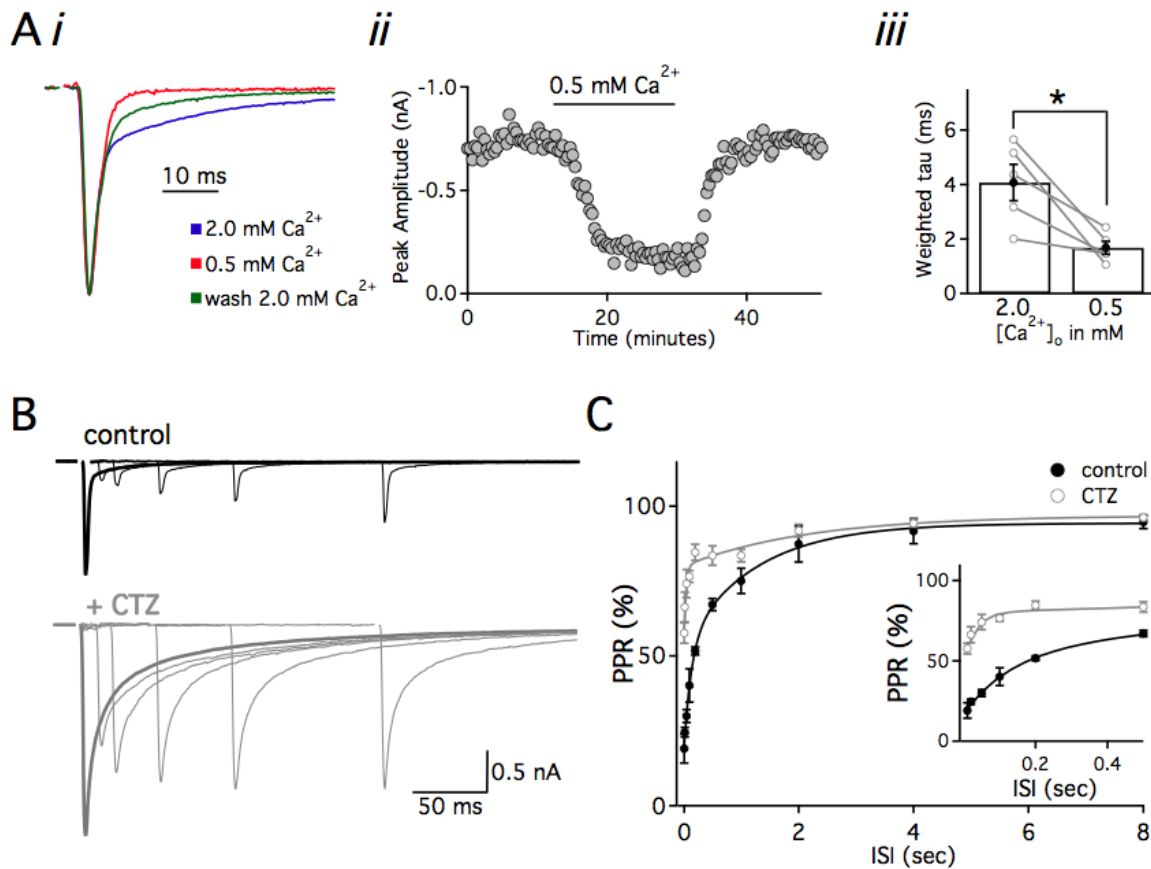
Figure 4.4: Experimental evidence in support of glutamate spillover

(Ai) Overlaid AMPAR EPSC traces normalized to peak amplitude in 2.0 mM (blue and green) and 0.5 mM (red) external Ca^{2+}, recorded at V_h=-70 mV in R-CPP (20 μM) and D-AP5 (50μM) to block NMDAR-mediated EPSCs. To facilitate comparison of decay, normalized EPSCs are aligned by peak amplitude. (ii) Peak amplitude of AMPAR ESPSCs plotted over the time course of an experiment, (iii) Bar graph of AMPAR weighted τ in 2.0 and 0.5 mM external Ca^{2+} (n=5, p<0.05) individual experiments shown in gray. CTZ was not included in the bath solution. (*B*) Superimposed AMPAR EPSC2 traces evoked at different ISIs before (black) and during (grey) bath application of 50 μM CTZ. Traces are the average of 3-5 trials. The EPSC2 waveforms were calculated by subtracting the average single EPSC from the average EPSC response to a pair of stimuli. The single EPSC (EPSC1) waveform is shown in bold. (*C*) The average paired pulse ratio (PPR) calculated as %EPSC2/EPSC1 is plotted against ISIs for control (black; *n=5* cells) and CTZ (grey; *n=5* cells). Error bars indicate SEM, (P<<0.001, 2-way ANOVA). (*Inset*) Initial phase of the recovery from depression is shown on an expanded time scale. Recordings were made in the presence of (R)-CPP (20 μM) to block NMDAR-mediated EPSCs. Bath temperature: 35 ± 1°C. (*) *p*<0.05.

sites at the mature synapse (Chen et al., 2002; Budisantoso et al., 2012). We asked whether short-term depression (STD) in response to pairs of optic tract stimuli is also relieved by CTZ at the immature synapse.

Figure 4.4B shows superimposed traces of the second EPSCs (EPSC2, thin traces) evoked at different interstimulus intervals (ISIs), compared to the first EPSC (EPSC1, bold trace). Bath application of CTZ slowed the AMPAR EPSC decay and increased the paired pulse ratio (PPR, EPSC2/EPSC1, Figure 4.4C). These data are consistent with the findings at the mature synapse and suggest glutamate can diffuse between release sites at the immature retinogeniculate contact (Chen et al., 2002; Budisantoso et al., 2012). However, our results do not distinguish whether the observed glutamate gradient is intra-bouton (within the confines of a single bouton), or inter-bouton (where glutamate escapes from the bouton to spill over to neighboring quiescent sites located in other boutons). In order to differentiate between these possibilities we next examined the glutamate transient of single retinal inputs.

Two populations of single-fiber AMPAR EPSCs

We hypothesized that if release of glutamate from distant release sites contributes to the slow component of the immature EPSC, then we may be able to detect single retinal fiber synaptic responses that are mediated purely by spillover. These currents should have distinctly slower kinetics than conventional synaptic responses. Therefore, we recorded isolated AMPAR-mediated single fiber EPSC in the presence of $50\mu M$ cyclothiazide (CTZ). Single-fiber EPSCs were identified as the synaptic response to minimal stimulation (for details see (Noutel et al., 2011); Figure 4.5A). Figure 4.5B shows two examples of single fiber currents recorded from the same relay neuron. Although the EPSCs were evoked with similar stimulation intensities from two nearby sites in the optic nerve, the activation and decay kinetics were very different. Analysis of 63 single fiber synaptic responses recorded from 50 relay neurons revealed at least
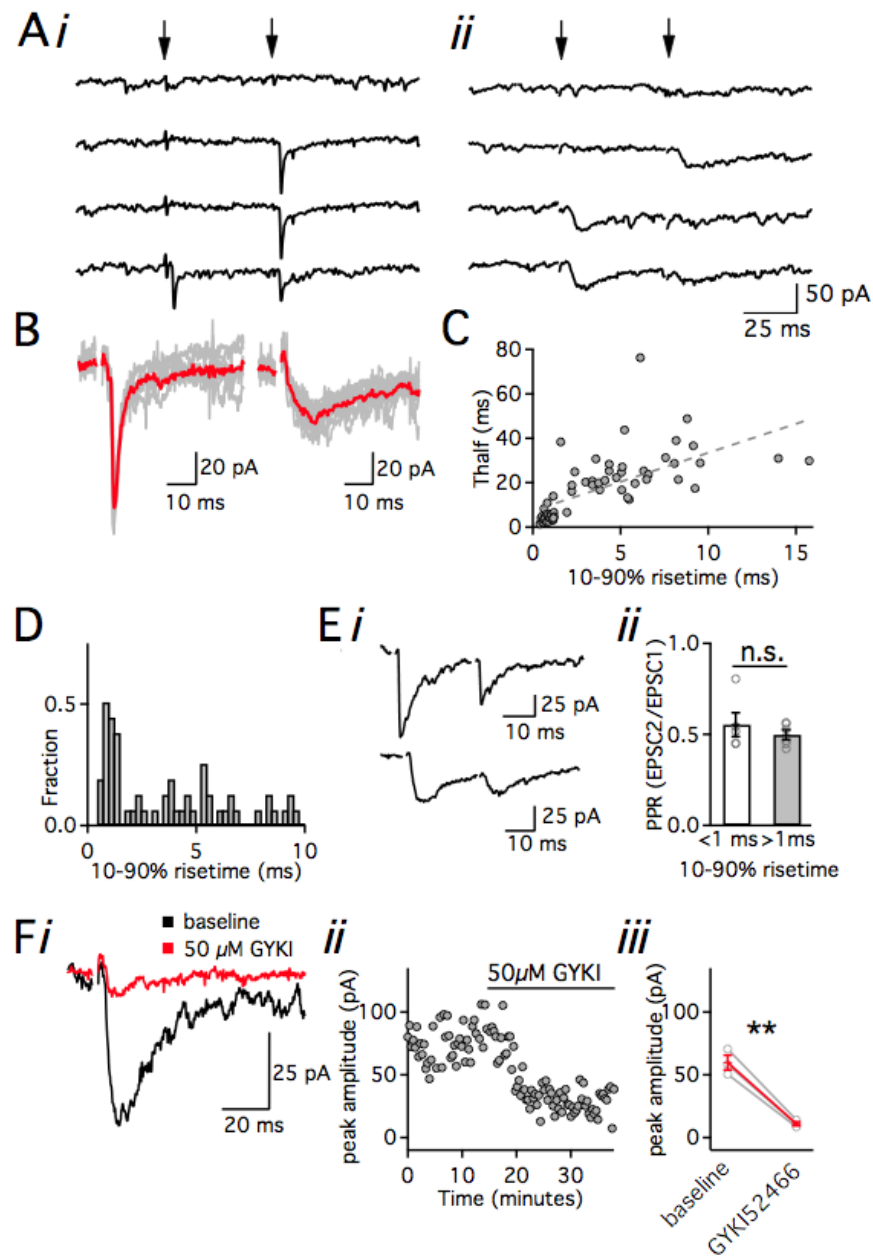
Figure 4.5: Identification of slow and fast-rising single fiber AMPAR EPSCs

(*Ai*) Example of a fast-rise single fiber current. Pairs of stimuli separated by 50 ms (arrowheads indicate the time of stimulus) are increased from sub-threshold until a response emerges from noise (V_h=-70mV). A response on the second, but not first pulse indicates the single fiber response is near-threshold. The same technique is used to identify slow-rising single fiber currents (*ii*). *(B)* Comparison of two types of single fiber AMPAR EPSC responses recorded from the same thalamic relay neuron. The stimulus electrode position in the optic tract differed for the two types of synaptic currents. Overlay of fast- *(left)* and slow-rising *(right)* single fiber currents evoked from 7-10 consecutive trials. The average waveform is shown in red. Currents

Figure 4.5 (Continued)

recorded at V_h= -70 mV in the presence of NMDAR antagonists and CTZ. *(C)* Scatter plot of half decay time versus rise time for all single fibers (n=63), dotted line represents linear regression fit (Pearson correlation coefficient r^2=0.47; p<<0.0001). *(D)* Histogram of the 10-90% rise times of all the observed single-fiber AMPAR EPSCs. *(Ei)* Representative averaged traces showing (paired pulse depression occurs with both fast-rising *(top)* and slow-rising EPSCs *(bottom)*. *(Eii)* Summary graph of average PPR of fast-rise (<1 ms, n=5) and slow-rise (>1 ms, n=5) EPSCs. *(F)* Average traces *(i)* and time course of the peak amplitude *(ii)* of slow-rising EPSC before and during bath application of an AMPAR-specific antagonist 50 µM GYKI52466. *(iii)* Summary plot of the effects of GYKI52466 on the peak amplitude of slow-rising EPSCs (n=3, p<0.01(**)). Bath temperature: 35 ± 1°C.

two types of EPSCs based on their kinetics. In addition to the familiar fast-rise/fast decay single fiber currents, we observed a previously unrecognized population of slow-rising currents with small amplitudes and slow decay kinetics. While the time course of the EPSC decay was highly variable among the single fiber responses, there was a strong correlation between the rise time and decay time of the synaptic current (Figure 4.5C). Fast-rising currents could be distinguished from the slow-rising currents by their 10-90% rise times--a histogram of the rise times shows two distinct peaks, one at 0.67 ms and the other at 5.2 ms (Figure 4.5D n=63 single fiber currents, n=43 mice).

One possible explanation for these slow-rising currents is that they are evoked by inadvertent stimulation of the corticothalamic tract. Relay neurons in the LGN receive excitatory inputs from both retina and cortex, and corticothalamic EPSCs are known innervate the distal dendrites of relay neurons and to exhibit slower kinetics than retinogeniculate currents (Turner and Salt, 1998; Kielland et al., 2006; Jurgens et al., 2012). However, corticothalamic innervation of the LGN is not complete until after eye-opening in mouse (Seabrook et al., 2013), making this explanation less likely. Nevertheless, we tested whether the slow single fiber EPSCs could arise from corticothalamic inputs by taking advantage of the known fact that retinogeniculate and corticothalamic inputs exhibit distinct forms of short-term synaptic plasticity. In response to a pairs of stimulation, retinogeniculate synapses exhibit paired-pulse depression (PPD) because of their high release probability (P_R) while corticothalamic connections display paired-pulse facilitation (PPF) due to their low P_R (Turner and Salt, 1998). We found that in response to pairs of stimulation, the slow-rising EPSC displayed a similar degree of PPD as the fast-rising single fiber EPSCs (Figure 4.5E). These results demonstrate that the slow-rising EPSCs are evoked by stimulating retinal fibers.

We next asked whether the slow-rising single fiber EPSCs were mediated by glutamatergic receptors. We found that bath application of the non-NMDA receptor antagonist NBQX (5uM) completely abolished the slow-rising current (data not shown). However, NBQX inhibits both AMPAR and kainate receptors and the latter are known to give rise to currents with slow kinetics (Bureau et al., 2000). To distinguish between AMPAR and kainate receptors we took advantage of a selective AMPAR antagonist, GYKI 52466 (IC_{50} ~10-20 μM for AMPA and ~450 μM for kainate receptors; (Tarnawa et al., 1989)). Figure 4.5F illustrates the effects of bath application of 50 μM GYKI 52466 on the peak of the slow-rising EPSC. On average, the AMPAR antagonist inhibited the slow-rising current to 18.0 ± 1.0% of control (n=3, p<0.01, Figure 4.5F*iii*). Therefore, the slow-rising retinogeniculate EPSCs result from activation of AMPARs and not other glutamatergic receptors.

The effects of γ-DGG on slow- and fast-rising AMPAR EPSCs

If the slow-rising AMPAR EPSCs represent a population of receptors activated by glutamate spillover from distant release sites, we would predict that the receptors would experience a lower peak concentration of glutamate than that of fast-rising EPSCs. Therefore, we compared the effects of 2 mM γ-DGG on the peak amplitude of the two types of single fiber AMPAR EPSCs. 4.6A and B show representative examples of γ-DGG inhibition of a fast- and slow-rising EPSC, respectively. A plot of the degree of blockade by the low affinity antagonist as a function of all single fiber EPSC rise times showed that synaptic currents with slower rise times were more sensitive to inhibition by γ-DGG than those with faster rise times (Figure 4.6C). We sorted the EPSCs into two groups based on their 10-90% rise times (fast <1.0 ms, slow >1.0 ms) and compared the average block by γ-DGG. The low affinity antagonist blocked a significantly greater percentage of the peak amplitude of the slow-rising currents than of the fast-rising currents (76.2 ± 4.2% vs 35.7 ± 2.7% of baseline, respectively; n=6 for each group, *p*<<0.0001 Figure 4.6C). Therefore, the slow-rising EPSCs experience a lower peak
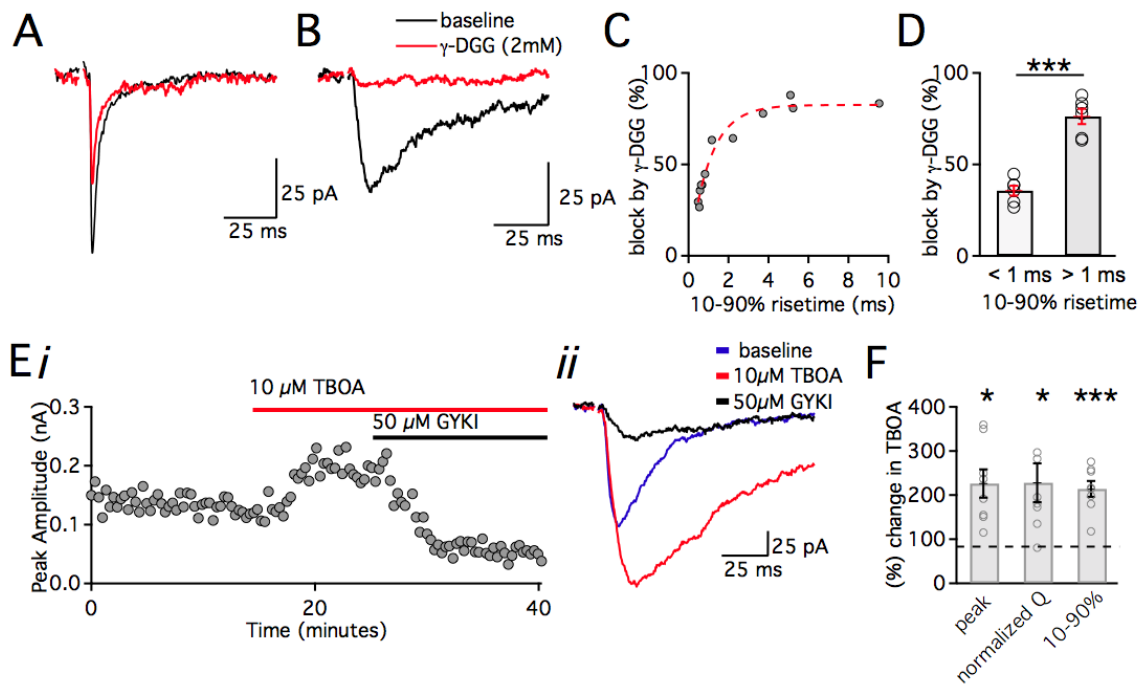
Figure 4.6: AMPA receptors of fast- and slow-rising EPSCs are activated by different glutamate concentrations

The effects of 2 mM γ-DGG *(red)* on fast-rising *(A)* and slow-rising *(B)* AMPAR EPSCs. (C) Plot of the percentage peak amplitude blocked by γ-DGG verses the EPSC rise time (10-90% rise time, ms). The data are fit by an exponential equation (red dotted line). (*D*) Summary graph of the average percent inhibition of the peak amplitude by γ-DGG ('fast' *n*=6; 'slow' *n*=6). (*E,i*) Time course of peak slow-rising AMPAR EPSC before and in the presence of the glutamate transport blocker TBOA (10 μM) followed by the application of 50 μM GYKI52466. *(ii)* Average EPSCs from the same experiment before (blue line), during bath application of TBOA (red line) and in the presence of TBOA+GYKI (black line). Traces are the average of 15-20 trials. (*F*) Summary graph of the effects of TBOA on the slow-rising EPSCs (n=8) quantifying the average change in peak amplitude, rise time and normalized charge transfer. Individual experiments are shown as grey circles. All recordings were performed in the presence of (R)-CPP and D-AP5 to block NMDAR-mediated EPSCs and CTZ to prevent AMPAR desensitization. Bath temperature: 35 ± 1°C. (*)*p*<0.05 (**)*p*<0.01 (***) *p*<0.001.

concentration of glutamate than fast-rising EPSCs, consistent with glutamate diffusing a significant distance after its release. These results suggest the presence of inter-bouton spillover at the immature developing retinogeniculate synapse.

The amplitude of slow-rising AMPAR EPSCs is potentiated by inhibition of glutamate transporters

To further strengthen the argument that the slow-rising EPSC represents a spillover-mediated current, we asked whether it was sensitive to glutamate transporter activity. We reasoned that the degree of inter-bouton glutamate spillover would increase with the inhibition of glutamate uptake. Figure 4.6E illustrates the effects of bath application of 10 μM TBOA on the slow-rising single fiber EPSC (Figure 4.6 E,F). The peak amplitude of the current increased to 226.0 ± 32.2% of control (average peak amplitude control: 76.3 ±15.1 pA to 160.2 ± 27.7 pA in TBOA, n=8, p=0.01). These changes led in an increase in the normalized charge transfer of the EPSC to 214.1± 17.9% of control (n=6, p<0.01, Figure 4.6G). Evidence suggests that the concentration of extrasynaptic glutamate is reduced at physiological temperatures and transporters have been shown to show strong temperature dependence (Wadiche et al., 1995; Asztely et al., 1997; Kullmann and Asztely, 1998). Therefore reducing bath temperature may also increase the amplitude of the slow-rising currents due to inhibiting glutamate transporters. Indeed, slow-rising current amplitude was increased with a reduction in bath temperature (Supplemental Figure 7.2). Therefore, glutamate transporters can regulate the amplitude and time course of the slow-rising EPSCs, consistent with a current driven by a prolonged glutamate transient.

Inhibiting glutamate uptake does not influence the peak amplitude of fast AMPAR EPSCs

Previous studies have shown that purely spillover-mediated AMPAR currents display a robust increase in peak amplitude in the presence of TBOA, whereas direct synaptic contacts do not
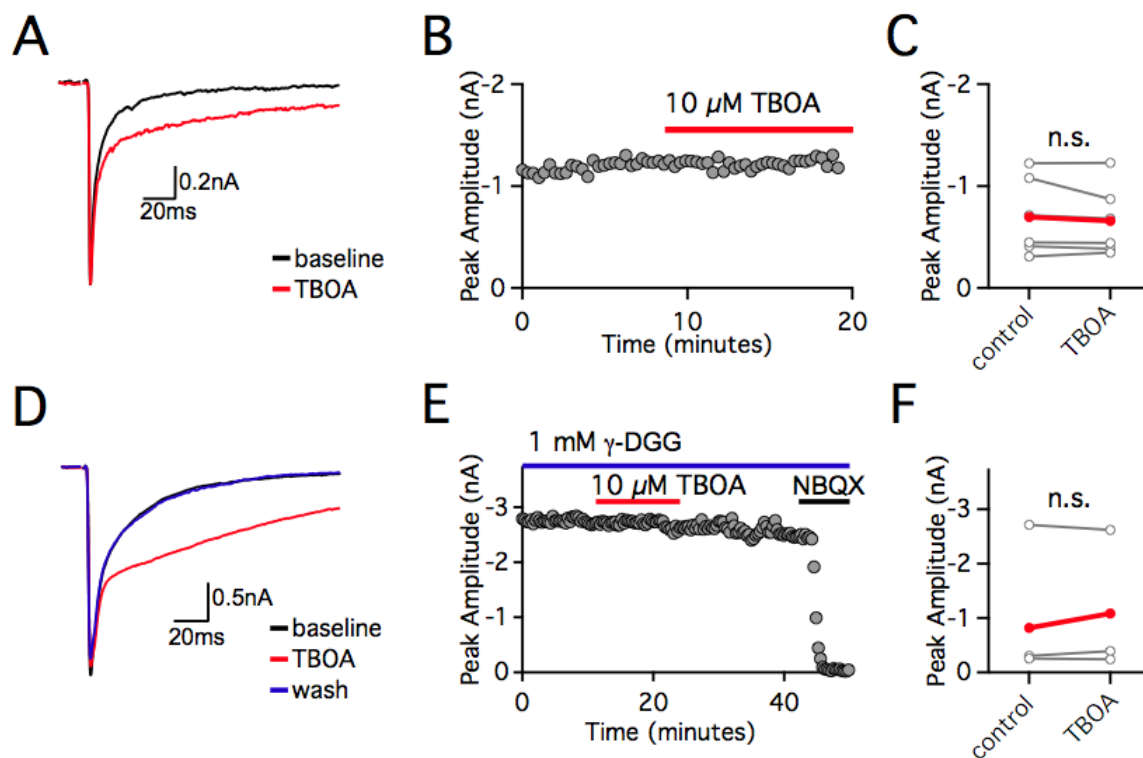
Figure 4.7: Inhibiting glutamate uptake does not influence the peak amplitude of evoked AMPAR EPSCs at the immature synapse

(*A*) Example traces of AMPAR-EPSCs in the presence of 50 μM CTZ and NMDAR antagonists and mGluR antagonist LY341495 (V_h=-70) before (black trace) and during (red trace) bath application of 10 μM TBOA. (*B*) Time course of an experiment showing that bath application of TBOA does not alter the peak amplitude of the AMPAR-EPSC. (*C*) Summary plots show no significant change in the peak amplitude of the AMPAR EPSC during application of TBOA (average: red trace, individual experiments: grey traces, n=6, p>0.3). (*D*) Example traces of AMPAR-EPSCs recorded in the presence of 1mM γ-DGG to prevent receptor saturation, LY341495, CTZ and NMDAR antagonists. Traces are shown before (black) during (red) and after washing out (blue) bath application of 10 μM TBOA. (*E*) Time course of an experiment performed in 1mM γ-DGG, the current is abolished in the presence of 5 μM NBQX. (*F*) Summary plots show no significant change in peak amplitude of the AMPAR EPSC during application of TBOA in the presence of γ-DGG (n=3, p>0.9; average: red trace, individual experiments: grey traces). Bath temperature: 35 ± 1°C.

(Szapiro and Barbour, 2007). We asked whether this was also true at the retinogeniculate synapse. We found that the amplitude of fast-rising AMPAR EPSCs evoked by stimulating multiple retinogeniculate fibers did not change with bath application of 10μM TBOA (peak amplitude: 696.1 ± 154.8 pA to 658.2 ± 140.3 pA in TBOA, n=6 p>0.3; Figure 4.7 A-C). Similar to our previous finding, the decay of the EPSC was prolonged ((Hauser et al., 2013); Figure 4.7A,D).

The absence of an effect of TBOA on the peak AMPAR EPSC could potentially be influenced by receptor saturation. To control for this possibility, we repeated experiments in the presence of the low affinity antagonist γ-DGG (1mM). Even in the presence of γ-DGG the peak amplitudes of the evoked AMPAR EPSCs were unaltered with bath application of TBOA (1090.2 pA to 1083.3 pA in TBOA, n=3 p=0.9; Figure 4.7 D-F). Therefore the decay, but not the peak, of the AMPAR EPSC is influenced by glutamate released from a distant source. These results further support the presence of direct and indirect glutamatergic signaling between retinal ganglion cells and relay neurons in the developing retinogeniculate synapse.

The Effects of EGTA-AM on EPSC waveform over age

Our results strongly suggest that glutamate spillover between boutons contribute to the slow decay of the evoked retinogeniculate EPSC. This would be consistent with our previous findings that retinogeniculate quantal events did not exhibit the slow decay kinetics seen in the EPSCs evoked by suprathreshold stimulation. Previously we proposed that delayed release of glutamate could contribute to the observed differences in the decay of the quantal and evoked EPSC waveform at the immature synapse (Liu and Chen, 2008). In light of our current findings that glutamate spillover contributes to the slow component of the AMPAR EPSC, we asked whether delayed release and spillover co-exist at the immature retinogeniculate synapse.

To test for the presence of delayed release, we used a calcium chelator with a slow binding rate, EGTA. Because of the slow binding rate, EGTA has little effect on the high calcium concentration transient near open calcium channels (local calcium). However, at later time points, after the channels have closed, this high affinity chelator is effective in binding to calcium as it equilibrates within the presynaptic bouton and decays to lower concentrations; this calcium signal is referred to as residual calcium (Ca_{res}). Previous studies at other CNS synapses have demonstrated that introduction of relatively low concentrations of EGTA into presynapticterminals affect residual calcium much more than the local calcium (Borst and Sakmann, 1996). Thus EGTA has been used as a tool to preferentially reduce delayed release over synchronous release (Delaney et al., 1989; Vanderkloot and Molgo, 1993; Cummings et al., 1996; Feller et al., 1996; Ravin et al., 1997; Atluri and Regehr, 1998).

We introduced EGTA into retinal ganglion cell terminals by bath applying the membrane-permeable form of EGTA, EGTA-AM (50 μM) to LGN brain slices (see methods). For voltage-clamp recordings, we used an internal solution that contained 10mM EGTA, therefore any effect of EGTA-AM on the EPSC decay time course could be attributed to alterations in presynaptic calcium. Figure 4.8A shows representative traces of EPSCs recorded at -70 mV in the absence (black trace) and 15 minutes following bath application (red trace) of 50 μM EGTA-AM for young (left) and old (right) synapses. EGTA-AM reduced the peak amplitude of the immature EPSC to 85.1 $\pm$ 3% of control ($p<0.01$, n=8, Figure 4.8A, left). Normalization of the currents to the peak EPSC amplitude before and after exposure to EGTA-AM showed an acceleration of the decay time course of the immature EPSC. The weighted τ of the EPSC decay decreased to 65.1 $\pm$ 5.9% of control in the presence of EGTA-AM ($p<0.05$, n=8, Figure 4.8B,C). Notably, the portion of the immature EPSC most sensitive to the EGTA-AM was the slow component of the EPSC decay time course (Figure 4.8D, red bars, $p<0.05$, n=8, paired t-test). In contrast to the
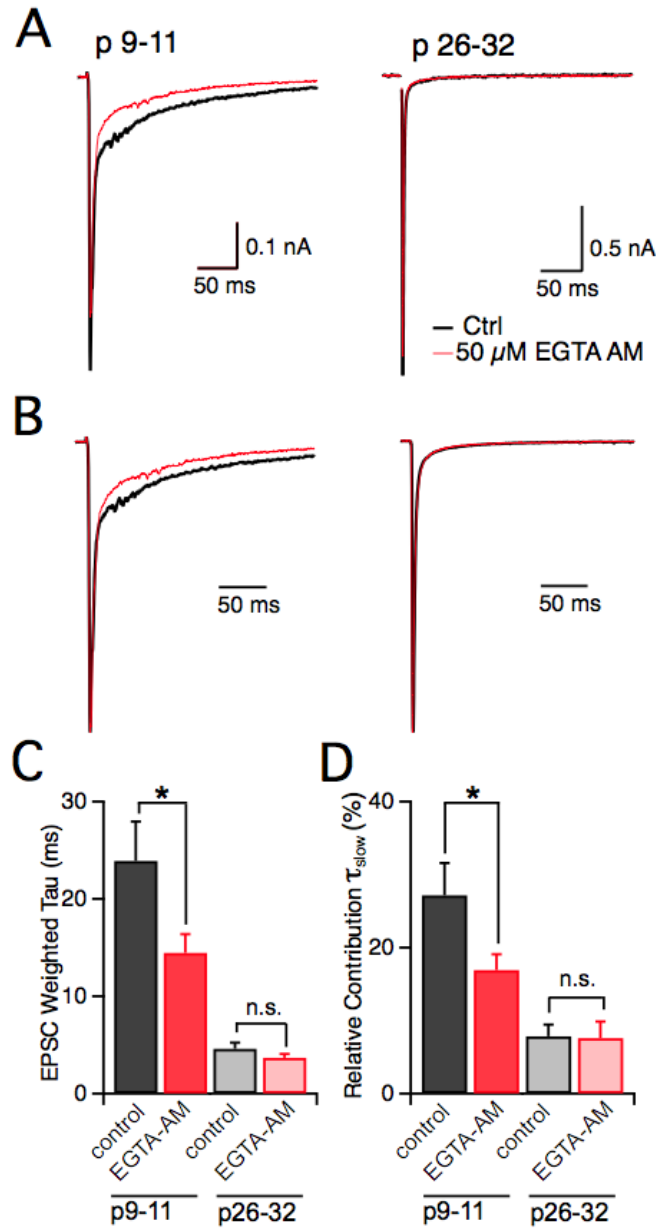
Figure 4.8: EGTA-AM accelerates the decay kinetics of the immature EPSC
(*A*) Representative traces of EPSCs before (black) and 15 minutes after (red) bath application of 50 μM EGTA-AM recorded from immature (*left*) and mature (*right*) synapses. (*B*) Traces from A, normalized to the peak. (*C*) Summary of average weighted τ, before and after bath application of EGTA-AM (for immature: 23.9$\pm$ 4.1 ms to 14.4 $\pm$1.9 ms; *n*=8, *p*<0.09; for mature: 4.6 $\pm$ 0.6 ms to 3.7$\pm$0.4 ms, p>0.09, *n*=6, paired t-test). EPSC decay was fit to a double exponential relationship: y0 +A_1e(-x/ τ_{fast}) + A_2e(-x/ τ_{slow}), and weighted τ = [τ_{fast} X A_1/(A_1 + A_2)] +[τ_{slow} X A_2/(A_1 + A_2)]. (*D*) The relative contribution of τ_{slow} to the weighted τ, [%A_2/(A_1+A_2)], is summarized before (black) and after bath application of EGTA-AM (red). Immature: control, 27.2$\pm$4.4% to EGTA-AM, 16.9$\pm$2.2%, mature: 7.8$\pm$1.6% to 7.6$\pm$2.3% of τ_{total}). (*) *p*<0.05.

immature synapse, EGTA-AM did not significantly alter the peak EPSC amplitude or the decay time course (*p>0.7* n=5-6). These results are consistent with a greater contribution of delayed release to the immature when compared to the mature EPSC.

The Immature Presynaptic Calcium Transient is Sensitive to EGTA

As delayed release is driven by presynaptic residual calcium, we next examined the effect of EGTA-AM on presynaptic residual calcium transient (Zengel and Magleby, 1981; Zucker and Lara-Estrella, 1983; Vanderkloot and Molgo, 1993; Cummings et al., 1996). We introduced calcium green-1 dextran into RGC *in vivo* as previously described (Chen and Regehr, 2003). A mixture of calcium green-1 dextran (K_d=540 nM) and Texas red dextran was introduced into the eyes of anaesthetized mice. Mice were allowed to recover as the dye was taken up by retinal cells. Only axons of RGCs project to the LGN, thus fluorometric calcium measurements obtained from acute LGN slices cut 3-7 days after eye injections represent presynaptic calcium signals from the retinogeniculate synapse. All experiments were performed with inhibitors of $GABA_A$ and $GABA_B$ (bicuculline, CGP55845A) and glutamatergic receptors ((R)-CPP and NBQX) to eliminate both inhibitory and excitatory synaptic transmission.

4. 9 (A,B, *right*) shows the calcium green-1 ΔF/F transient evoked by optic tract stimulation (black trace) and after (grey trace) bath application of EGTA-AM for a p11 and p19 mouse. Under control conditions, the decay time course of ΔF/F at the immature synapse is significantly slower when compared to that at a more mature synapse (p9-11: 349.6 ± 70 ms vs p18-23: 111.7 ± 24 ms, p<0.05, n=4,5 respectively). At the immature synapse, EGTA-AM reduced the peak of the ΔF/F to 60.6±6% of control while the time course of the calcium transient accelerated from 349.6±70 to 24.4±5 ms (to 9.2 ± 4% of baseline) (p<0.05, n=4). In
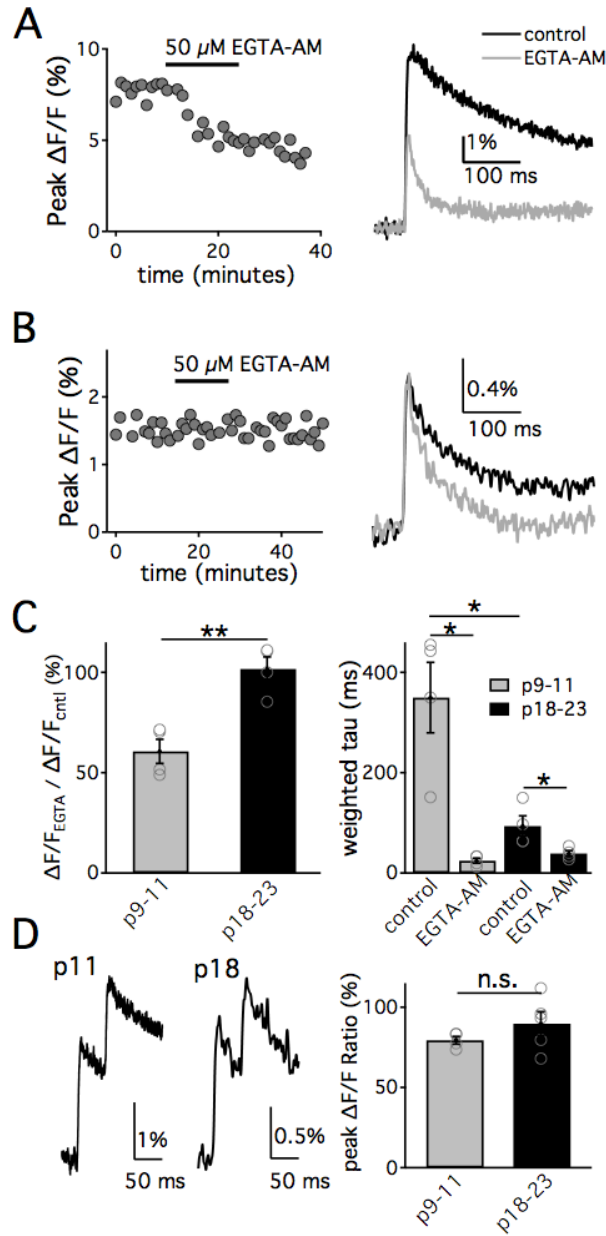
Figure 4.9: The presynaptic calcium transient at the immature synapse is more sensitive to EGTA-AM than that of the mature

Representative time course of peak ΔF/F signal before, during and 15 minutes following application of 50 µM EGTA-AM from P9-11 (*A*, *left*) and P18-23 (*B*, *left*) synapses. (*A, B right*) Representative ΔF/F signals evoked by optic tract stimulation before (black) and 15 minutes after (grey) EGTA-AM application in immature (*A*) and p18-23 (*B*) mice. Traces are the average of 3-5 trials. (*C, left*) Summary of the average change in the peak amplitude (*left*) and weighted tau (*right*) of the ΔF/F in the presence of EGTA-AM relative to baseline in p9-11 (grey) and p18-23 (black). (*D*) Averaged representative traces of ΔF/F signal in response to a pair of optic tract stimuli (ISI = 50 ms) shown for immature (*left*) and p18-23 (*middle)* synapses. (*D, right*) Summary of peak ΔF/F ratio from immature and p18-23 (n=4,5 respectively *p>0.2*) (*) *p<0.05*, (**) *p<0.01*.

contrast, EGTA-AM did not significantly alter the peak of the ΔF/F signal in older synapses

(101.7 ± 6% of baseline; Figure 4.9C). Although the calcium chelator accelerated the decay time

course of the ΔF/F transient at all ages tested, the effects were much less pronounced at older

ages (in mature synapses accelerated decay tau from 93.6 ± 20 ms to 38.8 ± 5.7 ms (n=4,

$p < 0.05$, 43.3 ± 3.5% of baseline).

The slower time course of the presynaptic calcium transient at the immature synapse could be

explained by less dye uptake in young verses in old RGCs, leading to saturation of the calcium

fluorophore. If this were true, one would predict that the response of the presynaptic

fluorescence transient to pairs of stimuli separated by short interpulse intervals would be

different over development. With saturation, fewer fluorophores are available to bind to calcium

after the first stimulus, leading to a reduced second response. To test this possibility, we

compared the ΔF/F signal in response to a pair of optic tract stimuli (ISI=50ms) at two different

age ranges. We found no significant difference in the paired pulse response of peak ΔF/F

signals over development (Figure 4.9D). Therefore, differences in the time course of the

presynaptic calcium transient cannot be attributed to a change in the saturation of the

fluorophore. These data suggest that a prolonged presynaptic Ca^{2+} transient could be

responsible, in part, for the slow EPSC decay at the immature synapse.

EGTA-AM decreases charge transfer in train of optic tract stimulation

Since EGTA-AM inhibits the peak of the Ca transient at the immature synapse, it will likely affect

both synchronous and delayed release (Borst and Sakmann, 1996). As glutamate spillover is

known to decrease with a reduction in release probability, EGTA-AM cannot be used to

distinguish between delayed release and glutamate spillover. However, our results show that

EGTA-AM can accelerate the decay time course of the immature EPSC. Thus it is a useful tool
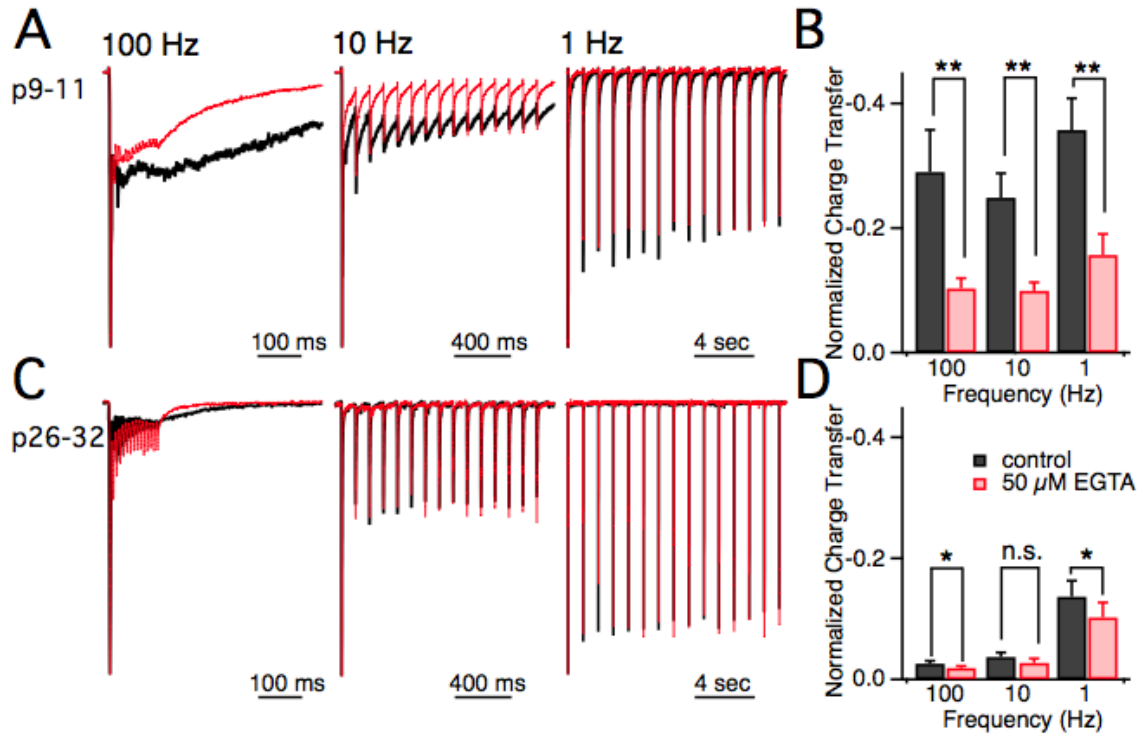
Figure 4.10: The Slow component of the EPSC contributes significantly to the synaptic response to trains of stimuli

Representative EPSCs normalized to the peak of the first EPSC. EPSCs are recorded from immature (*A*) and mature (*C*) synapses in response to trains of 15 stimuli given at 100, 10 and 1 Hz frequencies. Traces are the average of 3-5 trials and are shown before (black) and 15 minutes following bath application of 50 μM EGTA-AM (red). Summary of the normalized charge transfer in response to different stimulus frequencies before (black) and following application of EGTA-AM (red) for immature (*B*) and mature (*D*) synapses. V_h= -70mV. (*) $p<0.05$, (**) $p<0.01$.

for assessing the physiological contributions of the slow component of the EPSC waveform in the developing synapse.

Visual information is encoded in trains of RGC action potentials (Demas et al., 2003; Torborg and Feller, 2005; Kerschensteiner and Wong, 2008). We next asked how bath application of EGTA-AM influences the synaptic response to trains of optic nerve stimuli at different frequencies (Figure 4.10). The synaptic current evoked by trains of optic tract stimuli were compared before and after bath application of 50 µM EGTA-AM. To compare the charge transfer contributed by the slow component of the EPSC waveform, the synaptic response in each condition was normalized to the first EPSC of each train and total charge was calculated. We found that the relative charge transfer was significantly reduced by a 15-min EGTA-AM bath application for the immature synapse (Figure 4.10 A,B $p<0.01$, n=8-10) across all three frequencies tested. In contrast, at the mature synapse, EGTA-AM had a much smaller effect, albeit significant, on relative charge transfer at 100 and 1 Hz ($p<0.05$, n=7) and no effect at 10 Hz ($p>0.2$, n=7, Figure 4.10 C,D). Therefore, the contribution of the slow component of the synaptic waveform to the total synaptic charge transfer in response to trains of stimuli is much greater at immature when compared to mature retinogeniculate synapses.

Prolonged synaptic currents contribute to relay neuron firing

To investigate how the slow decay component of the immature EPSC contributes to the relay of information at the retinogeniculate synapse, we examined how relay neuron spiking changed when the slow component of the current was reduced. The internal solution used for current clamp recordings contains a low concentration of EGTA, unlike that for recording in voltage clamp mode. Because EGTA-AM would be taken up in both the pre- and post-synaptic neurons we could not simply bath apply the calcium chelator while recording relay neuron spikes. An alternative approach to examining the relationship between the slow component of the EPSC
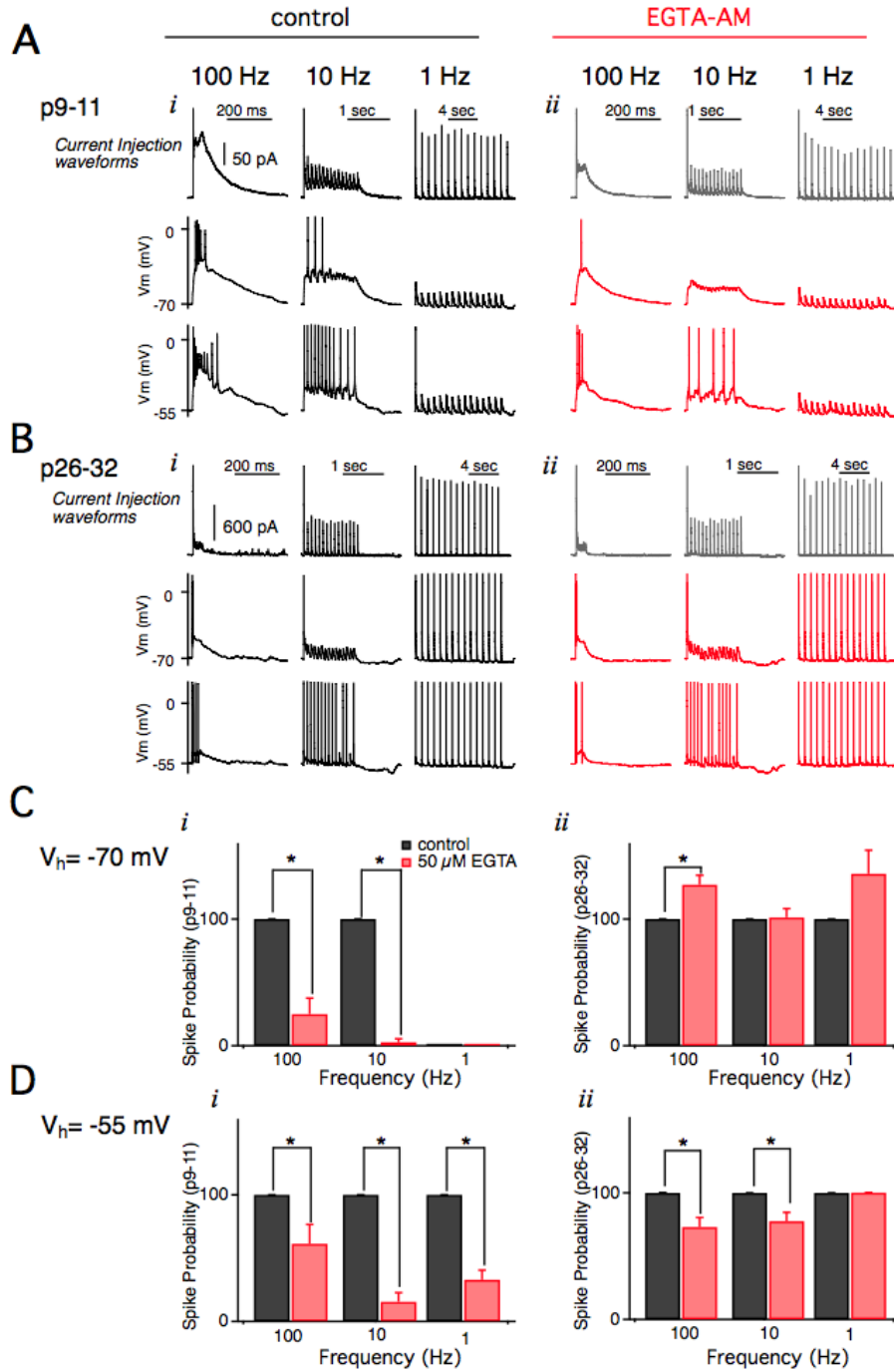
Figure 4.11: Spike pattern of immature relay neurons is influenced by the EPSC decay kinetics

Current clamp recordings of immature (*A*) and mature (*B*) synapses in response to injection of their respective current waveforms. Waveforms were obtained from representative average
Figure legend 4.11 (continued) synaptic responses to 15 stimuli at different frequencies (from left to right: 100, 10 and 1 Hz) before (black traces) and after bath application of 50 μM EGTA-AM (grey traces). Relay neuron spiking was assessed at both V_h of -70 mV (middle panel) and -55 mV (lower panels). (*C, D*) Summary of spike probability following current injection waveform

Figure 4.11 (Continued)

at a holding potential of –70 mV *(C)* and -55 mV   at immature (*left*) and mature (*right*) synapse. Statistical data for 1 Hz for immature neurons are not available because neurons did not fire action potentials in response to 1 Hz stimulation/injected current while holding at -70 mV. (*) *p*<0.05.

and postsynaptic firing is to compare the spike response to the injection of different synaptic current waveforms. For immature and mature mice, representative synaptic responses at different stimulation frequencies obtained from our voltage clamp experiments before and after 50 µM EGTA-AM application (Figure 4.10) were converted into waveforms (Figure 4.11 A and B top panels) and injected into the soma of relay neurons. Waveforms were scaled such that the amplitude of the first EPSC could reliably drive action potential firing (300 and 1500 pA for immature and mature neurons, respectively) at a holding potential of -55 mV in control conditions.

Figure 4.11 A & B show the relay neuron firing response to the injection of current waveforms representing control conditions (left) and after (right) EGTA-AM application for immature and mature synapses. Relay neuron spike probability was analyzed at two holding potentials: one at -70 mV (middle panel) and -55 mV (bottom panel). These two holding potentials were chosen in order to mimic the burst and tonic firing of thalamic relay neurons, respectively. Previous studies have shown that immature relay neurons rest at a more depolarized potential than those of mature neurons, consistent with immature neurons firing predominantly in the tonic mode (Ramoa and McCormick, 1994; MacLeod et al., 1997; Pirchio et al., 1997).

Spike probability of the immature relay neuron was dramatically reduced in response to the EGTA-AM waveforms mimicking the currents evoked by 10 and 100 Hz optic tract stimulation. In contrast, the difference between relay neuron spike probability in response to control and EGTA-AM waveform injections was much smaller at the mature synapse. In the burst mode of firing, the EGTA-AM waveform did not decrease spike probability of mature relay neurons. In fact, there was a significant increase of firing at 100 Hz with EGTA-AM (Figure 4.11C *ii*), suggesting that prolonged synaptic currents in mature relay neurons could depolarize the membrane enough to result in inactivation of Na channels and, in turn, reduced action potential

firing. These data are consistent with a major role for the prolonged component of the EPSC decay in driving relay neuron firing at the immature retinogeniculate synapse.

DISCUSSION

Here we provide evidence that the additional current generated by glutamate spillover and by asynchronous release increases the probability of immature relay neuron firing. The prolonged synaptic current improves the efficiency of RGC transmission to the developing cortex during a period when individual synaptic inputs are weak. By examining single fiber synaptic responses from immature RGC inputs we uncovered a novel, purely spillover-mediated current. Our results suggest that a much larger number of RGCs than those that make direct synaptic contacts influence immature relay neuron spiking—this relay of information is critical for proper wiring of the visual cortex during development.

Asynchronous Release

Given the slow decay of the presynaptic calcium transient at the immature synapse, it is difficult to distinguish contributions of asynchronous release versus spillover to the EPSC waveform. Reducing $[Ca]_o$ will decrease residual calcium (Figure 4.4A; (Chen and Regehr, 2003)). In addition EGTA-AM reduced the amplitude of the $\Delta F/F$ signal and significantly decreased the peak of the immature EPSC (Figure 4.8, 4.9A). At the Calyx of Held, asynchronous release can be clearly separated from spillover using fluctuation analysis (Neher and Sakaba, 2001). However, this approach requires voltage control over the presynaptic bouton, which has not been established at visual synapses. Asychronous release is often shown as the individual quantal events that can be resolved following the synchronous evoked response (Isaacson and Walmsley, 1995; Chen and Regehr, 1999). At the immature retinogeniculate synapse we were unable to reliably isolate such events for several reasons: 1) the peak quantal amplitude at

young ages is small (7 pA); 2) both retinogeniculate and corticothalamic contacts contribute to a relatively high frequency of spontaneous mEPSCs; and 3) spillover leads to extensive AMPAR desensitization that may mask individual single asynchronous events (Chen and Regehr, 2000; Chen et al., 2002; Liu and Chen, 2008). However, we have shown that the immature EPSC decay accelerates in the presence of the slow calcium buffer EGTA-AM. This suggests that release at the immature synapse is sensitive to residual calcium, consistent with asynchronous glutamate release.

Asynchronous release of glutamate has been described at both excitatory and inhibitory synapses in the CNS (Diamond and Jahr, 1995; Isaacson and Walmsley, 1995; Atluri and Regehr, 1998; Lu and Trussell, 2000; Hefft and Jonas, 2005; Hjelmstad, 2006), and has been shown to influence synaptic integration and postsynaptic firing patterns (Iremonger and Bains, 2007; Crowley et al., 2009; Rudolph et al., 2011). We find that the developmental decrease in EPSC time course corresponds to the acceleration of the presynaptic calcium transient. The slow kinetics of the immature transient cannot simply be explained by saturation of the calcium indicator because $\Delta F/F$ response to pairs of stimuli does not change with age (see Figure 4.9).

The substantial developmental acceleration of the calcium transient (τ= ~350 ms vs. ~100 ms) may be due to changes in the concentration and composition of endogenous calcium buffers and/or calcium reuptake mechanisms (Sabatini and Regehr, 1996; Vyleta and Jonas, 2014). Other factors, such as shortening of the presynaptic AP width, changes in presynaptic ion channel expression levels and kinetics or decrease in AP temporal jitter could also contribute to age-dependent acceleration in the presynaptic calcium transient (Wang et al., 1997; Taschenberger and von Gersdorff, 2000).

In our experiments EGTA significantly accelerated the decay and decreased the peak of the EPSC at the immature but not the mature retinogeniculate synapse. At other CNS synapses where the exact concentration of calcium buffer can be controlled, reduction of the peak EPSC amplitude by presynaptic EGTA suggests loose coupling between calcium channels and release machinery (Fedchyshyn and Wang, 2005; Yang et al., 2010; Eggermann et al., 2012; Vyleta and Jonas, 2014). A caveat of using membrane permeable EGTA-AM is that the exact intracellular concentration of the calcium chelator is unknown, thus we cannot assess how components of the release machinery change with age. Despite these limitations, we used EGTA-AM to selectively reduce the prolonged component of the EPSC waveform and investigate its contribution to synaptic transmission.

Glutamate spillover at the immature synapse

We show that excitatory currents at the developing retinogeniculate synapse are by both direct, and spillover-mediated inputs from RGC axons. We provide multiple lines of evidence involving low-affinity antagonists for NMDARs and AMPARs, AMPAR desensitization, manipulations of release probability, and characterization of slow and fast-rising single fiber currents. Taken together, our data strongly suggest that the prolonged decay of the immature EPSC is influenced by spillover of glutamate.

Few central excitatory synapses display such extensive spillover at near physiological temperature and with glutamate transporter activity intact. One example is the mossy fiber to granule cell (GC) synapse in the cerebellar cortex (DiGregorio et al., 2002). Like the retinogeniculate synapse, individual slow rising spillover-mediated AMPAR currents have also been recorded from mature granule cells (DiGregorio et al., 2002; Nielsen et al., 2004). However, the morphology of the two synapses is very different. At the cerebellar synapse, the absence of intervening glia promotes glutamate spillover to non-postsynaptic neurons within a

glomerular glial sheath (DiGregorio et al., 2002). In contrast, glomeruli do not encompass retinogeniculate contacts in the immature LGN (Aggelopoulos et al., 1989; Bickford et al., 2010). The two synapses also respond differently to glutamate transporter inhibition. TBOA did not change the peak amplitude of AMPAR currents at the mossy fiber-GC synapse, whereas, our results show that TBOA potentiated the peak of the slow-rising current at the immature retinogeniculate synapse ((DiGregorio et al., 2002); Figure 4.5). This result suggests that despite the presence of glutamate transporters, there is substantial interaction between retinogeniculate release sites. TBOA's effects on the slow-rising retinogeniculate single fiber currents are more similar to that of the purely spillover-mediated connection between climbing fibers and molecular layer interneurons of the cerebellum (Szapiro and Barbour, 2007; Coddington et al., 2013). Consistent with the studies in the cerebellum, our results suggest that anatomy alone underestimates the influence of presynaptic neurons on postsynaptic firing.

Functional role of a prolonged glutamate transient and synaptic currents

Significant glutamate spillover at the immature synapse is unexpected; the classic view of activity-dependent refinement at the retinogeniculate synapse assumes synapse specificity (Mooney et al., 1993; Butts et al., 2007). It is generally assumed that cross talk between synapses would degrade information signaling in the CNS (Barbour, 2001). This may be the case at synapses in the auditory system, where information is coded in the precise timing of high-frequency transmission (Oertel, 1997). However, in the visual system, relay of information relies heavily on temporal summation of synaptic currents (Sincich et al., 2007; Sincich et al., 2009). Evidence from other central synapses has shown that the consequences of glutamate spillover can be desirable: spillover can increase reliability of synaptic signals, synchronize neural output and influence processing of local circuits (Isaacson, 1999; Arnth-Jensen et al., 2002; DiGregorio et al., 2002; Crowley et al., 2009; Coddington et al., 2013). Therefore,

glutamate spillover at the retinogeniculate connection could ensure reliable transmission of retinal activity to the visual cortex.

There are many potential ways that prolonged synaptic currents could influence activity-dependent synaptic strengthening and weakening. Previously, we demonstrated the presence of high affinity group II/III mGluRs that, when activated, reduce the probability of glutamate release (Hauser et al., 2013). Our studies show that the spillover-mediated component of the EPSC is sensitive to P_R. Therefore, heterosynaptic glutamate spillover and/or differential expression of mGluRs on RGC axon terminals could play a major role in activity-dependent refinement. Notably, the mGluR-mediated response downregulates with age (Hauser et al., 2013).

Alternatively, early in the development of a synaptic circuit, specificity may be less important than establishing connections onto a postsynaptic cell. In this case, spillover could aid in coordinating postsynaptic firing driven by neighboring RGCs. It is feasible that before competition occurs between RGCs innervating the same relay neuron, all synapses strengthen to a level at which each RGC is strong enough to drive relay neuron spiking. The idea that neighboring synapses strengthen and weaken together has been proposed before in other developmental systems. Studies in the hippocampus, as well as the retinotectal synapse in *Xenopus*, have demonstrated that heterosynaptic plasticity exists (Engert and Bonhoeffer, 1999; Tao et al., 2001; Harvey and Svoboda, 2007). At the retinogeniculate synapse, neighboring release sites are more likely to be from the same RGC or from a neighboring RGC (Wong, 1999). A prolonged glutamate transient may help establish and stabilize the initial retinotopy in the developing visual system.

REFERENCES

Aggelopoulos N, Parnavelas JG, Edmunds S (1989) Synaptogenesis in the dorsal lateral geniculate nucleus of the rat. Anatomy and embryology 180:243-257.

Akerman CJ, Smyth D, Thompson ID (2002) Visual experience before eye-opening and the development of the retinogeniculate pathway. Neuron 36:869-879.

Arnth-Jensen N, Jabaudon D, Scanziani M (2002) Cooperation between independent hippocampal synapses is controlled by glutamate uptake. Nature neuroscience 5:325-331.

Asztely F, Erdemli G, Kullmann DM (1997) Extrasynaptic glutamate spillover in the hippocampus: dependence on temperature and the role of active glutamate uptake. Neuron 18:281-293.

Atluri PP, Regehr WG (1998) Delayed release of neurotransmitter from cerebellar granule cells. The Journal of neuroscience : the official journal of the Society for Neuroscience 18:8214-8227.

Barbour B (2001) An evaluation of synapse independence. The Journal of neuroscience : the official journal of the Society for Neuroscience 21:7969-7984.

Barbour B, Keller BU, Llano I, Marty A (1994) Prolonged presence of glutamate during excitatory synaptic transmission to cerebellar Purkinje cells. Neuron 12:1331-1343.

Barrett EF, Stevens CF (1972) The kinetics of transmitter release at the frog neuromuscular junction. The Journal of physiology 227:691-708.

Bickford ME, Slusarczyk A, Dilger EK, Krahe TE, Kucuk C, Guido W (2010) Synaptic development of the mouse dorsal lateral geniculate nucleus. The Journal of comparative neurology 518:622-635.

Blaschke M, Keller BU, Rivosecchi R, Hollmann M, Heinemann S, Konnerth A (1993) A single amino acid determines the subunit-specific spider toxin block of alpha-amino-3-hydroxy-5-methylisoxazole-4-propionate/kainate receptor channels. Proceedings of the National Academy of Sciences of the United States of America 90:6528-6532.

Borst JG, Sakmann B (1996) Calcium influx and transmitter release in a fast CNS synapse. Nature 383:431-434.

Budisantoso T, Matsui K, Kamasawa N, Fukazawa Y, Shigemoto R (2012) Mechanisms underlying signal filtering at a multisynapse contact. The Journal of neuroscience : the official journal of the Society for Neuroscience 32:2357-2376.

Bureau I, Dieudonne S, Coussen F, Mulle C (2000) Kainate receptor-mediated synaptic currents in cerebellar Golgi cells are not shaped by diffusion of glutamate. Proceedings of the National Academy of Sciences of the United States of America 97:6838-6843.

Butts DA, Kanold PO, Shatz CJ (2007) A burst-based "Hebbian" learning rule at retinogeniculate synapses links retinal waves to activity-dependent refinement. PLoS biology 5:e61.

Chen C, Regehr WG (1999) Contributions of residual calcium to fast synaptic transmission. The Journal of neuroscience : the official journal of the Society for Neuroscience 19:6257-6266.

Chen C, Regehr WG (2000) Developmental remodeling of the retinogeniculate synapse. Neuron 28:955-966.

Chen C, Regehr WG (2003) Presynaptic modulation of the retinogeniculate synapse. The Journal of neuroscience : the official journal of the Society for Neuroscience 23:3130-3135.

Chen C, Blitz DM, Regehr WG (2002) Contributions of receptor desensitization and saturation to plasticity at the retinogeniculate synapse. Neuron 33:779-788.

Clements JD, Lester RA, Tong G, Jahr CE, Westbrook GL (1992) The time course of glutamate in the synaptic cleft. Science 258:1498-1501.

Coddington LT, Rudolph S, Vande Lune P, Overstreet-Wadiche L, Wadiche JI (2013) Spillover-mediated feedforward inhibition functionally segregates interneuron activity. Neuron 78:1050-1062.

Crowley JJ, Fioravante D, Regehr WG (2009) Dynamics of fast and slow inhibition from cerebellar golgi cells allow flexible control of synaptic integration. Neuron 63:843-853.

Cummings DD, Wilcox KS, Dichter MA (1996) Calcium-dependent paired-pulse facilitation of miniature EPSC frequency accompanies depression of EPSCs at hippocampal synapses in culture. The Journal of neuroscience : the official journal of the Society for Neuroscience 16:5312-5323.

Delaney KR, Zucker RS, Tank DW (1989) Calcium in motor nerve terminals associated with posttetanic potentiation. The Journal of neuroscience : the official journal of the Society for Neuroscience 9:3558-3567.

Demas J, Eglen SJ, Wong RO (2003) Developmental loss of synchronous spontaneous activity in the mouse retina is independent of visual experience. The Journal of neuroscience : the official journal of the Society for Neuroscience 23:2851-2860.

Diamond JS (2001) Neuronal glutamate transporters limit activation of NMDA receptors by neurotransmitter spillover on CA1 pyramidal cells. The Journal of neuroscience : the official journal of the Society for Neuroscience 21:8328-8338.

Diamond JS, Jahr CE (1995) Asynchronous release of synaptic vesicles determines the time course of the AMPA receptor-mediated EPSC. Neuron 15:1097-1107.

DiGregorio DA, Nusser Z, Silver RA (2002) Spillover of glutamate onto synaptic AMPA receptors enhances fast transmission at a cerebellar synapse. Neuron 35:521-533.

Dingledine R, Borges K, Bowie D, Traynelis SF (1999) The glutamate receptor ion channels. Pharmacological reviews 51:7-61.

Eggermann E, Bucurenciu I, Goswami SP, Jonas P (2012) Nanodomain coupling between Ca(2)(+) channels and sensors of exocytosis at fast mammalian synapses. Nature reviews Neuroscience 13:7-21.

Engert F, Bonhoeffer T (1999) Dendritic spine changes associated with hippocampal long-term synaptic plasticity. Nature 399:66-70.

Fedchyshyn MJ, Wang LY (2005) Developmental transformation of the release modality at the calyx of Held synapse. The Journal of neuroscience : the official journal of the Society for Neuroscience 25:4131-4140.

Feller MB, Delaney KR, Tank DW (1996) Presynaptic calcium dynamics at the frog retinotectal synapse. Journal of neurophysiology 76:381-400.

Goda Y, Stevens CF (1994) Two components of transmitter release at a central synapse. Proceedings of the National Academy of Sciences of the United States of America 91:12942-12946.

Hanganu IL, Ben-Ari Y, Khazipov R (2006) Retinal waves trigger spindle bursts in the neonatal rat visual cortex. The Journal of neuroscience : the official journal of the Society for Neuroscience 26:6728-6736.

Harvey CD, Svoboda K (2007) Locally dynamic synaptic learning rules in pyramidal neuron dendrites. Nature 450:1195-1200.

Hauser JL, Edson EB, Hooks BM, Chen C (2013) Metabotropic glutamate receptors and glutamate transporters shape transmission at the developing retinogeniculate synapse. Journal of neurophysiology 109:113-123.

Hefft S, Jonas P (2005) Asynchronous GABA release generates long-lasting inhibition at a hippocampal interneuron-principal neuron synapse. Nature neuroscience 8:1319-1328.

Hjelmstad GO (2006) Interactions between asynchronous release and short-term plasticity in the nucleus accumbens slice. Journal of neurophysiology 95:2020-2023.

Hollmann M, Hartley M, Heinemann S (1991) Ca2+ permeability of KA-AMPA--gated glutamate receptor channels depends on subunit composition. Science 252:851-853.

Hooks BM, Chen C (2006) Distinct roles for spontaneous and visual activity in remodeling of the retinogeniculate synapse. Neuron 52:281-291.

Huttenlocher PR (1967) Development of cortical neuronal activity in the neonatal cat. Experimental neurology 17:247-262.

Iremonger KJ, Bains JS (2007) Integration of asynchronously released quanta prolongs the postsynaptic spike window. The Journal of neuroscience : the official journal of the Society for Neuroscience 27:6684-6691.

Isaacson JS (1999) Glutamate spillover mediates excitatory transmission in the rat olfactory bulb. Neuron 23:377-384.

Isaacson JS, Walmsley B (1995) Counting quanta: direct measurements of transmitter release at a central synapse. Neuron 15:875-884.

Jaubert-Miazza L, Green E, Lo FS, Bui K, Mills J, Guido W (2005) Structural and functional composition of the developing retinogeniculate pathway in the mouse. Visual neuroscience 22:661-676.

Jurgens CW, Bell KA, McQuiston AR, Guido W (2012) Optogenetic stimulation of the corticothalamic pathway affects relay cells and GABAergic neurons differently in the mouse visual thalamus. PloS one 7:e45717.

Kaeser PS, Regehr WG (2014) Molecular mechanisms for synchronous, asynchronous, and spontaneous neurotransmitter release. Annual review of physiology 76:333-363.

Kerschensteiner D, Wong RO (2008) A precisely timed asynchronous pattern of ON and OFF retinal ganglion cell activity during propagation of retinal waves. Neuron 58:851-858.

Kielland A, Erisir A, Walaas SI, Heggelund P (2006) Synapsin utilization differs among functional classes of synapses on thalamocortical cells. The Journal of neuroscience : the official journal of the Society for Neuroscience 26:5786-5793.

Kirkby LA, Sack GS, Firl A, Feller MB (2013) A role for correlated spontaneous activity in the assembly of neural circuits. Neuron 80:1129-1144.

Kreitzer AC, Gee KR, Archer EA, Regehr WG (2000) Monitoring presynaptic calcium dynamics in projection fibers by in vivo loading of a novel calcium indicator. Neuron 27:25-32.

Kullmann DM, Asztely F (1998) Extrasynaptic glutamate spillover in the hippocampus: evidence and implications. Trends in neurosciences 21:8-14.

Liu X, Chen C (2008) Different roles for AMPA and NMDA receptors in transmission at the immature retinogeniculate synapse. Journal of neurophysiology 99:629-643.

Lu T, Trussell LO (2000) Inhibitory transmission mediated by asynchronous transmitter release. Neuron 26:683-694.

MacLeod N, Turner C, Edgar J (1997) Properties of developing lateral geniculate neurones in the mouse. International journal of developmental neuroscience : the official journal of the International Society for Developmental Neuroscience 15:205-224.

Mennerick S, Zorumski CF (1995) Presynaptic influence on the time course of fast excitatory synaptic currents in cultured hippocampal cells. The Journal of neuroscience : the official journal of the Society for Neuroscience 15:3178-3192.

Mooney R, Madison DV, Shatz CJ (1993) Enhancement of transmission at the developing retinogeniculate synapse. Neuron 10:815-825.

Mooney R, Penn AA, Gallego R, Shatz CJ (1996) Thalamic relay of spontaneous retinal activity prior to vision. Neuron 17:863-874.

Neher E, Sakaba T (2001) Estimating transmitter release rates from postsynaptic current fluctuations. The Journal of neuroscience : the official journal of the Society for Neuroscience 21:9638-9654.

Nielsen TA, DiGregorio DA, Silver RA (2004) Modulation of glutamate mobility reveals the mechanism underlying slow-rising AMPAR EPSCs and the diffusion coefficient in the synaptic cleft. Neuron 42:757-771.

Noutel J, Hong YK, Leu B, Kang E, Chen C (2011) Experience-dependent retinogeniculate synapse remodeling is abnormal in MeCP2-deficient mice. Neuron 70:35-42.

Oertel D (1997) Encoding of timing in the brain stem auditory nuclei of vertebrates. Neuron 19:959-962.

Olverman HJ, Jones AW, Watkins JC (1988) [3H]D-2-amino-5-phosphonopentanoate as a ligand for N-methyl-D-aspartate receptors in the mammalian central nervous system. Neuroscience 26:1-15.

Otis TS, Wu YC, Trussell LO (1996) Delayed clearance of transmitter and the role of glutamate transporters at synapses with multiple release sites. The Journal of neuroscience : the official journal of the Society for Neuroscience 16:1634-1644.

Partin KM, Fleck MW, Mayer ML (1996) AMPA receptor flip/flop mutants affecting deactivation, desensitization, and modulation by cyclothiazide, aniracetam, and thiocyanate. The Journal of neuroscience : the official journal of the Society for Neuroscience 16:6634-6647.

Pirchio M, Turner JP, Williams SR, Asprodini E, Crunelli V (1997) Postnatal development of membrane properties and delta oscillations in thalamocortical neurons of the cat dorsal lateral geniculate nucleus. The Journal of neuroscience : the official journal of the Society for Neuroscience 17:5428-5444.

Rahamimoff R, Yaari Y (1973) Delayed release of transmitter at the frog neuromuscular junction. The Journal of physiology 228:241-257.

Ramoa AS, McCormick DA (1994) Developmental changes in electrophysiological properties of LGNd neurons during reorganization of retinogeniculate connections. The Journal of neuroscience : the official journal of the Society for Neuroscience 14:2089-2097.

Ramoa AS, Prusky G (1997) Retinal activity regulates developmental switches in functional properties and ifenprodil sensitivity of NMDA receptors in the lateral geniculate nucleus. Brain research Developmental brain research 101:165-175.

Ravin R, Spira ME, Parnas H, Parnas I (1997) Simultaneous measurement of intracellular Ca2+ and asynchronous transmitter release from the same crayfish bouton. The Journal of physiology 501 (Pt 2):251-262.

Rudolph S, Overstreet-Wadiche L, Wadiche JI (2011) Desynchronization of multivesicular release enhances Purkinje cell output. Neuron 70:991-1004.

Sabatini BL, Regehr WG (1996) Timing of neurotransmission at fast synapses in the mammalian brain. Nature 384:170-172.

Seabrook TA, El-Danaf RN, Krahe TE, Fox MA, Guido W (2013) Retinal input regulates the timing of corticogeniculate innervation. The Journal of neuroscience : the official journal of the Society for Neuroscience 33:10085-10097.

Sincich LC, Horton JC, Sharpee TO (2009) Preserving information in neural transmission. The Journal of neuroscience : the official journal of the Society for Neuroscience 29:6207-6216.

Sincich LC, Adams DL, Economides JR, Horton JC (2007) Transmission of spike trains at the retinogeniculate synapse. The Journal of neuroscience : the official journal of the Society for Neuroscience 27:2683-2692.

Szapiro G, Barbour B (2007) Multiple climbing fibers signal to molecular layer interneurons exclusively via glutamate spillover. Nature neuroscience 10:735-742.

Takahashi M, Kovalchuk Y, Attwell D (1995) Pre- and postsynaptic determinants of EPSC waveform at cerebellar climbing fiber and parallel fiber to Purkinje cell synapses. The Journal of neuroscience : the official journal of the Society for Neuroscience 15:5693-5702.

Takeuchi Y, Yamasaki M, Nagumo Y, Imoto K, Watanabe M, Miyata M (2012) Rewiring of afferent fibers in the somatosensory thalamus of mice caused by peripheral sensory nerve transection. The Journal of neuroscience : the official journal of the Society for Neuroscience 32:6917-6930.

Tao HW, Zhang LI, Engert F, Poo M (2001) Emergence of input specificity of ltp during development of retinotectal connections in vivo. Neuron 31:569-580.

Tarnawa I, Farkas S, Berzsenyi P, Pataki A, Andrasi F (1989) Electrophysiological studies with a 2,3-benzodiazepine muscle relaxant: GYKI 52466. European journal of pharmacology 167:193-199.

Tarusawa E, Matsui K, Budisantoso T, Molnar E, Watanabe M, Matsui M, Fukazawa Y, Shigemoto R (2009) Input-specific intrasynaptic arrangements of ionotropic glutamate receptors and their impact on postsynaptic responses. The Journal of neuroscience : the official journal of the Society for Neuroscience 29:12896-12908.

Taschenberger H, von Gersdorff H (2000) Fine-tuning an auditory synapse for speed and fidelity: developmental changes in presynaptic waveform, EPSC kinetics, and synaptic plasticity. The Journal of neuroscience : the official journal of the Society for Neuroscience 20:9162-9173.

Torborg CL, Feller MB (2005) Spontaneous patterned retinal activity and the refinement of retinal projections. Progress in neurobiology 76:213-235.

Trussell LO, Zhang S, Raman IM (1993) Desensitization of AMPA receptors upon multiquantal neurotransmitter release. Neuron 10:1185-1196.

Turner JP, Salt TE (1998) Characterization of sensory and corticothalamic excitatory inputs to rat thalamocortical neurones in vitro. The Journal of physiology 510 (Pt 3):829-843.

Vanderkloot W, Molgo J (1993) Facilitation and Delayed Release at About 0-Degrees-C at the Frog Neuromuscular-Junction - Effects of Calcium Chelators, Calcium-Transport Inhibitors, and Okadaic Acid. Journal of neurophysiology 69:717-729.

Vyleta NP, Jonas P (2014) Loose coupling between Ca2+ channels and release sensors at a plastic hippocampal synapse. Science 343:665-670.

Wadiche JI, Arriza JL, Amara SG, Kavanaugh MP (1995) Kinetics of a human glutamate transporter. Neuron 14:1019-1027.

Wang GY, Ratto G, Bisti S, Chalupa LM (1997) Functional development of intrinsic properties in ganglion cells of the mammalian retina. Journal of neurophysiology 78:2895-2903.

Wong RO (1999) Retinal waves and visual system development. Annual review of neuroscience 22:29-47.

Yang YM, Fedchyshyn MJ, Grande G, Aitoubah J, Tsang CW, Xie H, Ackerley CA, Trimble WS, Wang LY (2010) Septins regulate developmental switching from microdomain to nanodomain coupling of Ca(2+) influx to neurotransmitter release at a central synapse. Neuron 67:100-115.

Zengel JE, Magleby KL (1981) Changes in miniature endplate potential frequency during repetitive nerve stimulation in the presence of Ca2+, Ba2+, and Sr2+ at the frog neuromuscular junction. The Journal of general physiology 77:503-529.

Ziburkus J, Guido W (2006) Loss of binocular responses and reduced retinal convergence during the period of retinogeniculate axon segregation. Journal of neurophysiology 96:2775-2784.

Zucker RS, Lara-Estrella LO (1983) Post-tetanic decay of evoked and spontaneous transmitter release and a residual-calcium model of synaptic facilitation at crayfish neuromuscular junctions. The Journal of general physiology 81:355-372.

Page intentionally left blank

CHAPTER 5:

Glutamate Transporters at the Retinogeniculate Synapse

ABSTRACT

The retinogeniculate synapse, the connection between retinal ganglion cells (RGCs) and thalamic relay neurons in the lateral geniculate nucleus (LGN), undergoes robust synaptic remodeling in the first few postnatal weeks. During this dynamic period, several mechanisms influence the shape and strength of excitatory transmission: changes in postsynaptic receptor composition, activation of metabotropic glutamate receptors (mGluRs), asynchronous release of glutamate, and glutamate spillover between different RGC terminals. The ionotropic receptors that contribute to immature synaptic currents experience a gradient in peak glutamate concentrations. However, the extent to which glutamate transporters, and which specific transporters, contribute to this gradient are not known. Moreover, whether receptors that mediate transmission at the mature synapse also experience a gradient in peak glutamate concentrations has not yet been addressed. In this study, we provide evidence that glutamate transporters are responsible for establishing a detectable gradient of peak glutamate concentrations at the immature, but not mature, retinogeniculate synapse. In addition, we found that the glutamate transporter GLT-1 is expressed in both astrocytes and excitatory synaptic terminals in the developing LGN. While GLT-1 is predominantly expressed in astrocytes in the CNS, it is also found in some presynaptic terminals in the hippocampus and striatum. Glial GLT-1 subserves the majority of glutamate removal, leaving the functional role of presynaptic GLT-1 still unclear. We attempted to address the functional role of presynaptic GLT-1 using a mouse in which GLT-1 was genetically removed from neurons. However, we were unable to identify a functional role at the retinogeniculate synapse. Our preliminary studies suggest that neuronal GLT-1 does not shield activation of nearby mGluRs, and that the majority of synaptic glutamate is removed from the developing retinogeniculate synapse by non-neuronal GLT-1 glutamate transporters.

INTRODUCTION

Glutamate transporters are a family of five membrane-bound proteins that actively move glutamate from the extracellular milieu to the inside of the cell. In addition to maintaining low concentrations of extracellular glutamate, they recover the majority of synaptically released glutamate and prevent glutamate excitotoxicity (Tzingounis and Wadiche, 2007). The slow transport of glutamate from the extracellular space into neurons and glia originally led to the assumption that the dominant role of glutamate transporters is to maintain low ambient glutamate. However, the location, density and different properties of the transporters have also implicated them in synaptic transmission. Transporters have been shown to prevent glutamate spillover between synapses, shield the activation of extrasynaptic receptors, and shape the timecourse of synaptic currents (Tzingounis and Wadiche, 2007). Of the five excitatory amino-acid transporters (EAAT1-5), the most abundant glutamate transporter is GLT-1, also known as EAAT2, and it is responsible for the majority of glutamate uptake in the brain (Danbolt et al., 1992; Haugeto et al., 1996; Danbolt, 2001). While GLT-1 is predominantly expressed in astrocytes of the brain, it has also been observed in presynaptic terminals in the hippocampus and striatum, although the functional role of presynaptic GLT-1 is unknown (Chen et al., 2004).

We found that GLT-1 is expressed at the retinogeniculate synapse. Using immuno–electron microscopy, GLT-1 was observed in both astrocytes and excitatory presynaptic terminals in the developing LGN. Our previous studies, performed at the immature retinogeniculate synapse using the non-selective competitive inhibitor DL-threo-β-benzyloxyaspartate (TBOA), showed that glutamate transporters shape the time course of excitatory transmission and shield excessive activation of extrasynaptic metabotropic glutamate receptors (mGluRs) (Hauser et al., 2013). Moreover, the ionotropic receptors that mediate immature synaptic currents experience a gradient of glutamate concentrations. The extent to which glutamate transporters, and which glutamate transporters, contributes to this gradient is unknown.

In this preliminary study, we investigated whether glutamate transporters contribute to the gradient of peak glutamate concentration at the immature and mature retinogeniculate contacts. In addition, we sought to address to what extent neuronal GLT-1 contributes to the overall activity of transporters at the immature retinogeniculate synapse. Using a mouse in which GLT-1 is selectively removed from neurons, we performed experiments to address whether neuronal GLT-1 shields the activation of mGluRs or shapes excitatory currents at the immature synapse. Our results suggest that neuronal GLT-1 does not play a major role in synaptic transmission at the developing retinogeniculate synapse.

RESULTS

Glutamate transporters establish a gradient of glutamate concentration at the immature retinogeniculate synapse

Previous studies performed at the developing retinogeniculate synapse have shown that the NMDARs present on immature relay neurons in the LGN experience a gradient of peak glutamate concentrations following stimulation of the optic tract (Hauser et al., 2014). To determine whether glutamate transporters are responsible for establishing the gradient in glutamate concentration and limiting the activation of extrasynaptic NMDARs, we designed an experiment that combined the use of low-affinity antagonists and an inhibitor of glutamate transporters. If the NMDAR EPSC wave form reflects a gradient of peak glutamate concentrations dependent on the active removal or buffering of glutamate by glutamate transporters, then this would predict that a gradient would be much more difficult to detect when transporters are inhibited. Therefore, we hypothesized that the low-affinity antagonist to NMDARs L-AP5 would have a smaller effect on the timecourse of the EPSC in the presence of the non-transportable inhibitor of glutamate transporters TBOA.

In this set of experiments, L-AP5 (1mM) was bath applied either in the presence or absence of TBOA (10μM) (Figure 5.1A). 1 mM-LAP5 reduced the EPSC peak amplitude to a similar extent either alone or in the presence of TBOA (L-AP5 alone: amplitude, 47.7 ± 2.2% of baseline; L-AP5 and TBOA: amplitude, 53.5 ± 4.6% of baseline; n=9, 8, p=0.29; Figure 5.1 C*i*). This suggests that the peak concentration of glutamate in the cleft is not significantly different when glutamate transport is inhibited. In the presence of TBOA alone, the decay of the NMDAR ESPC was significantly prolonged, similar to previous studies (T_{half}: 239.2 ± 4.6% of baseline, n=8, p<0.05; (Hauser et al., 2013)). Also, in agreement with previous studies, bath application of L-AP5 alone significantly accelerated the decay of the NMDAR EPSC (to 71.1 ± 2.7% of baseline, n=9 p<0.001; (Hauser et al., 2014)). However, in the presence of TBOA, L-AP5 no longer accelerated the decay of the NDMAR EPSC (TBOA plus L-AP5: 100.7 ± 5.6% of baseline in TBOA, n=8, p=0.9; Figure 5.1 C*ii*). Moreover, the effects of L-AP5 on the decay of the NMDAR EPSC in the absence and presence of TBOA were significantly different from each other (n=9, 8; p<0.001, Figure 5.1 Cii). These results indicate that inhibiting glutamate transporters increases the activation of the NMDARs that, under normal conditions, experience a lower peak concentration of glutamate than those receptors that contribute to the peak of the NMDAR EPSC. Furthermore, they indicate a role for glutamate transporters in establishing a gradient of peak glutamate concentration at the immature synapse.
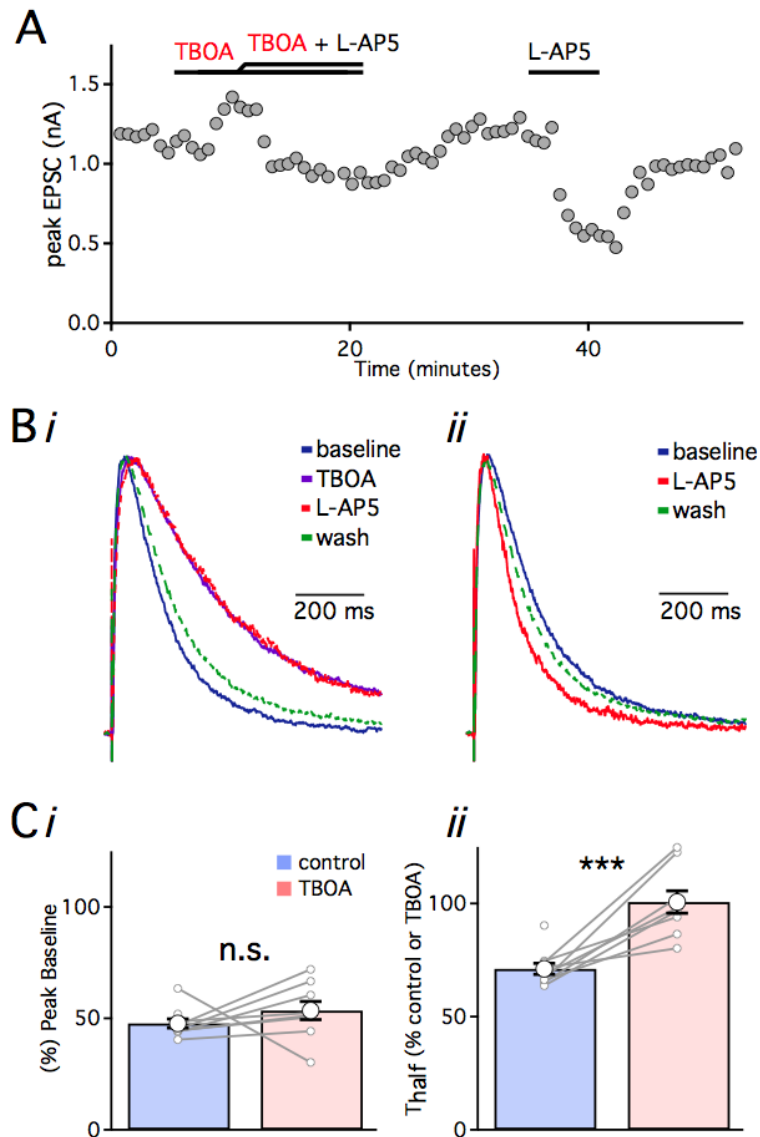
Figure 5.1: In the presence of TBOA, L-AP5 no longer accelerates the decay of the NMDAR EPSC at the immature retinogeniculate synapse

(A) Time course of an experiment demonstrating one sequence of experimental drug application. (B) Overlay of representative NMDAR EPSCs normalized to peak amplitude from before (blue trace), during application of 1 mM L-AP5 (red trace) and washout of L-AP5 (green), in (Bi) the L-AP5 is applied in the presence of 10 μM TBOA (purple trace) recorded from p8-11 mice. (C) Summary bar graphs of the effect of L-AP5 on the peak amplitude (i) and T_{half} (ii) in control conditions (n=9) and in the presence of TBOA (n=8). Recordings were made in the presence of NBQX (5 μM) to block AMPAR-mediated EPSCs. Bath temperature: 35 ± 1°C. (***) $p<0.001$.

The absence of a clearly detectable glutamate gradient at the mature retinogeniculate synapse

Several features of the retinogeniculate synapse mature during the first few postnatal weeks, including the elimination of synaptic contacts and the strengthening of remaining contacts (Chen and Regehr, 2000; Jaubert-Miazza et al., 2005). At the immature synapse, the low-affinity antagonist to NMDARs, L-AP5, significantly accelerates the decay of the EPSC compared to control suggesting that NMDARs at the immature synapse experience a detectable concentration gradient of peak glutamate. This gradient can also include glutamate released from neighboring RGCs that do not directly contact the immature relay neuron (Hauser et al., 2014). The number of direct inputs onto a mature relay neuron is far fewer and the strength much greater than those onto an immature neuron (Chen and Regehr, 2000). To address whether NMDARs at mature contacts also experience a difference in peak concentrations of glutamate, we bath applied L-AP5 to acute retinogeniculate slices prepared from mature (p27-34) mice. If the waveform at the mature retinogeniculate contact includes NMDARs activated by a range of peak glutamate concentrations, then we would predict L-AP5 would accelerate the EPSC decay.

In the presence of L-AP5, the peak of the NMDAR EPSC was significantly reduced to $54.3 \pm 2.8\%$ of baseline (1091.7 ± 141.96 pA to 601.68 ± 97.14 pA in 1 mM L-AP5; n=9, p<<0.0001; Figure 5.2 Bi). This reduction is similar to that found at the immature synapse (Figure 5.1 Ci), this suggests that the peak cleft concentration of glutamate does not significantly change over development (p8-11:$47.7 \pm 2.2\%$ of baseline; p27-34: $54.0 \pm 2.8\%$ of baseline n=9,9 p=0.1). To ensure that any potential differences in the decay of the current were not due to voltage-clamp errors, we performed parallel experiments with a low concentration of CPP. Bath application of the high affinity antagonist CPP ($1\mu M$) significantly reduced the peak of the NDMAR EPSC to $62.5 \pm 3.76\%$ of baseline (1104.53 ± 229.86 pA to 710.66 ± 175.58 pA in 1uM CPP; n=7,
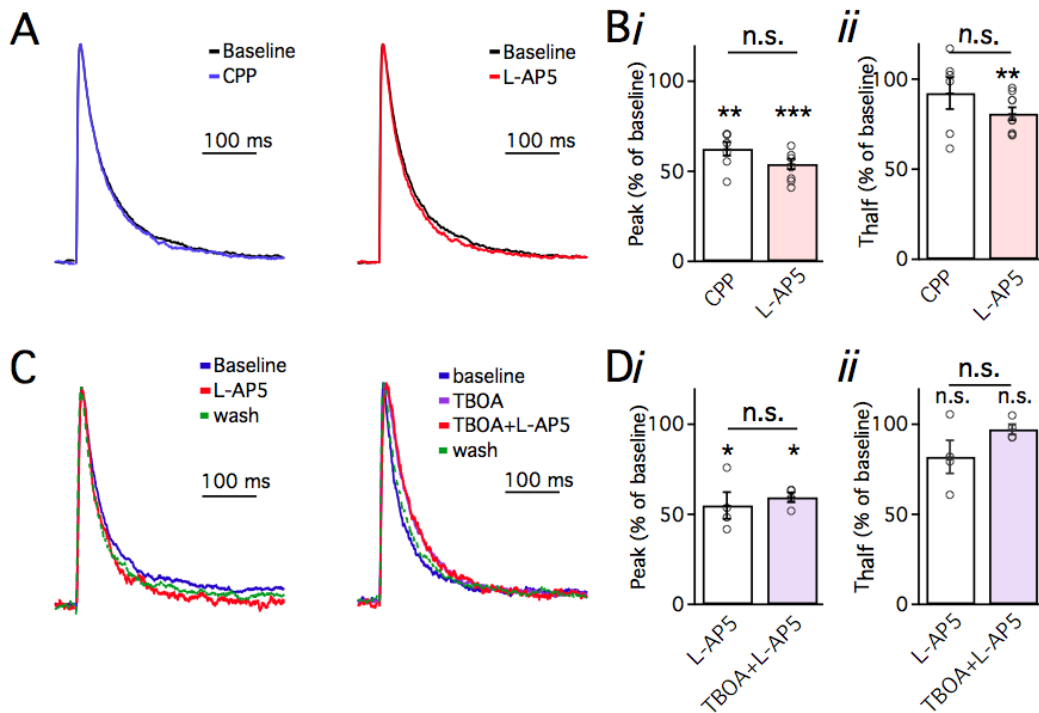
Figure 5.2: L-AP5 does not significantly alter the decay of the mature NMDAR EPSC
(A) Overlay of representative NMDAR EPSCs normalized to peak amplitude from before (black trace) and during application of CPP (blue trace, left) or L-AP5 (red trace, right) (B) Bar graph summary of the effects of CPP (n=7) and L-AP5 (n=9) on peak amplitude (i) and T_{half} (ii) recorded from p27-34 mice. (C) Overlay of representative NMDAR EPSCs normalized to peak amplitude from before (blue trace), during application of L-AP5 (red trace) and following washout of L-AP5 (green dotted trace). In C *left,* L-AP5 is applied in the presence of 10µM TBOA. (D) Bar graph summary of the effects of 1mM L-AP5 on peak amplitude (i) and T_{half} (ii) of the NMDAR EPSC either in control conditions (white bars, n=4) or in the presence of TBOA (purple bars, n=4). Individual experiments are shown as grey circles.
(*) *p*<0.05*;* (**) *p*<0.01; (****) *p*<<0.0001. Bath temperature: 35 ± 1°C.

p<0.01; Figure 5.2 B*i*). The extent to which the two antagonists inhibited the peak of the

NMDAR EPSC was not significantly different (n=9, 7 p=0.097). In the presence of L-AP5, the

T_{half} of the NMDA EPSC significantly accelerated from baseline (47.9 ± 3.8 ms to 38.0 ± 2.6 ms

in L-AP5; n=9, p<0.01), whereas the T_{half} was not significantly accelerated in the presence of

CPP (44.8 ± 7.1 ms to 38.12 ± 2.6 ms in CPP; n=7, p=0.02). However, in contrast to our

findings at the immature synapse, the effects of L-AP5 and CPP on the decay of the NMDAR

EPSC were did not reach significance (L-AP5: 80.8 ± 3.54% of baseline; CPP: 92.21 ± 8.87%

of baseline; n=9,7, p =0.21, Figure 5.2 B*ii*). This suggests that the acceleration of the NMDAR EPSC seen in the presence of the low-affinity antagonist was largely influenced by changes in voltage clamp and not due to the presence of a clearly detectable gradient of peak glutamate concentrations.

Glutamate transporters are present and actively shape the waveform at both mature and immature retinogeniculate contacts (Hauser et al., 2013). Given that a detectable gradient of peak glutamate concentration was not obviously detected at the mature synapses, we next asked whether additional extrasynaptic NMDARs could contribute to the synaptic waveform when transporters are inhibited. If this hypothesis were true, then we would predict that a low-affinity antagonist might have a more substantial effect on the EPSC decay with glutamate transporters inhibited than under control conditions.

We bath applied L-AP5 (1mM) to retinogeniculate slices in the absence and presence of TBOA (10µM). In both conditions, L-AP5 significantly reduced the peak of the NMDAR EPSC to a similar extent (L-AP5 alone: amplitude 590.1 ± 48.8 pA to 321.4 ± 41.2 pA; n=4 p=0.01; L-AP5 and TBOA: amplitude 555.1 ± 154.7 pA to 327.3 ± 88.3 pA in 1mM L-AP5; n=4, p<0.05; L-AP5 alone: 54.9 ± 7.4% of baseline; L-AP5 with TBOA: 59.4 ± 2.7 % of baseline, n=4, p>0.5; Figure 5.2 Di). However, no significant difference between the decay of the EPSC in the two conditions was observed (L-AP5 alone: T_{half} 81.9 ± 9% of baseline vs. L-AP5 with TBOA: T_{half} 97.1 ± 3% of TBOA baseline, n=4 p>0.2; Figure 5.2 D*ii*). These data suggest that while there may be a gradient of peak glutamate concentrations at the mature synapse, the differences are much more difficult to detect than at the immature synapse.

Low-affinity antagonists do not alter sodium-dependent glutamate uptake

One potential pharmacological caveat that may occur when combining low-affinity antagonists with the glutamate transport inhibitor TBOA is that the low-affinity antagonists may also inhibit glutamate transporters. Antagonists of glutamate transporters and ionotropic glutamate receptors are based on their ability to compete with glutamate binding; one could imagine overlap in their ability to inhibit their targets. In order to address this concern, glutamate uptake was measured in cultured cells using a technique previously described (for detailed methods see Chapter 2 and (Petr et al., 2013a)), and the amount of sodium-dependent glutamate uptake was compared between conditions (Figure 5.3).

No significant effects were found between the no treatment control condition and various concentrations of the low-affinity NMDAR antagonist L-AP5 (100 µM: 91.2 ± 9.5% of control; 300 µM: 96.6 ± 10.9% of control; and 1.0 mM: 94.9 ± 11.1% of control; n=3). In addition, no significant differences were observed between control and various concentrations of the low-affinity AMPAR antagonist γ-DGG (100 µM: 90.4 ± 10% of control; 300 µM: 95.3 ± 11.7% of control; and 1.0 mM: 90.0 ± 11.4% of control; n=3). The glutamate transport inhibitor TBOA (30µM) significantly reduced glutamate uptake to 9.8 ± 0.5% of control (n=3). These results confirm that low-affinity antagonists to NMDARs (L-AP5) and AMPARs (γ-DGG) do not alter sodium-dependent glutamate uptake through glutamate transporters.
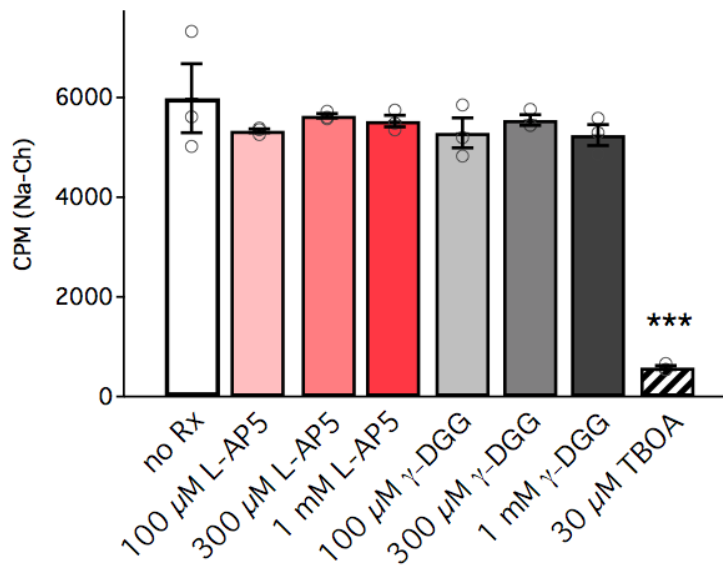
Figure 5.3: Na$^+$- dependent glutamate uptake is not inhibited by low-affinity antagonists to NMDA and AMPA receptors

Sodium dependent glutamate uptake was measured in absence and presence of varying concentrations of NMDAR (L-AP5) and AMPAR (γ-DGG) low-affinity antagonists. In the presence of the low-affinity antagonists, no significant differences were detected in the amount of Na$^+$- dependent uptake. In contrast, 30 μM TBOA significantly inhibited uptake. Error bars indicate SEM. Data is pooled data from 3 experiments. (***) $p<0.001$

The glutamate transporter GLT-1 is expressed in axon terminals and astrocytes in the immature LGN

Previous studies have shown that the glutamate transporter GLT-1 is predominantly expressed in astrocytes of the CNS, and its expression level increases with age (Furuta et al., 1997; Danbolt, 2001). GLT-1 has also been found in axon terminals of the hippocampus and striatum (Chen et al., 2004; Furness et al., 2008; Petr et al., 2013b). To investigate whether GLT-1 is expressed in the LGN early in development, electron microscopy was performed on sections from littermates: one p8 wildtype and one p8 complete KO of GLT-1 (Tanaka et al., 1997).

The presence of GLT-1 in glia and glutamatergic axon terminals at p8 was observed using a monoclonal antibody directed against the C-terminus of GLT-1a (1:10,000 provided by Dr. Jeffrey Rothstein). Figure 5.4 shows example micrographs depicting GLT-1 labeled in astrocytes (Figure 5.4 A) and presynaptic glutamatergic membranes (Figure 5.4 B) in wildtype p8 LGN. In KO tissue, immunolabeling is drastically reduced, although not completely eliminated (Figure 5.4 C). Interestingly, very few astrocytes were found in GLT-1 KO LGN. The micrograph in Figure 5.4 D shows an example of a nicely-developed excitatory synapse surrounded by large unoccupied extracellular space. This could imply that in the absence of GLT-1, there is a reduction in the number of astrocytes or slower astrocytic development compared to wildtype.

A total of 129 micrographs from WT LGN and 51 micrographs from KO LGN were analyzed for labeling of synapses and astrocytes (Figure 5.4E,F). A total of 89 astrocytes were found in WT; 21 of these were unlabeled, 5 were lightly labeled, and 63 were intensely labeled (24, 6 and 71% respectively). In contrast, a total of 39 astrocytes were identified in KO LGN and none of these astrocytes showed labeling for GLT-1. Using the same micrographs, 71 excitatory synapses were identified from WT LGN and 42 from GLT-1 KO LGN. Of the 71 asymmetric synapses found in WT LGN, 24 displayed intense labeling of GLT-1 in presynaptic terminals (34%), 18 were lightly labeled (25%), and 29 did not have any labeling (41%). Of the 42 synapses identified in the GLT-1 KO LGN, 5 were intensely labeled (12%), 3 were lightly labeled (7%), and 34 were unlabeled (81%). While some background labeling was seen in the complete KO of GLT-1 (Figure 5.4D), there was a significant reduction of labeled compared to WT. Future studies using a greater dilution of primary antibody (1:30,000) may reduce the background labeling of presynaptic terminals.

126
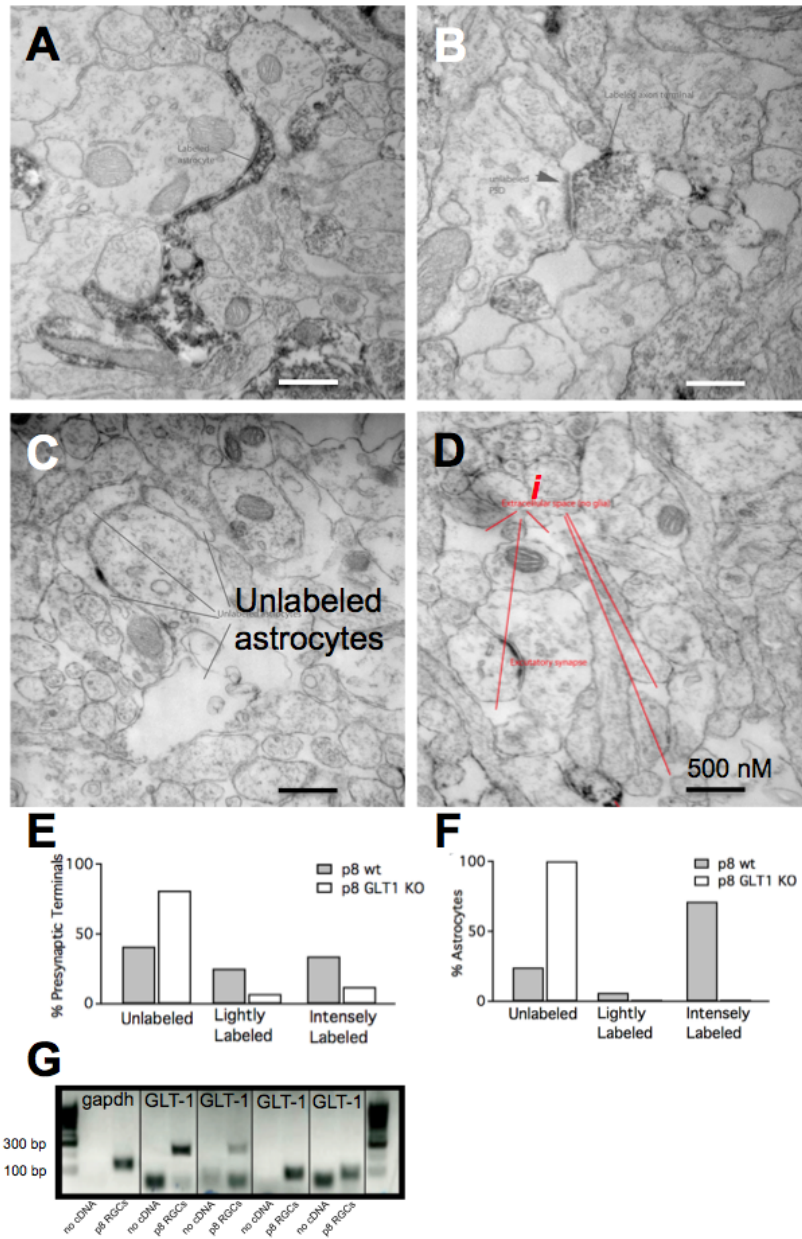
Figure 5.4: GLT-1 is expressed in the developing LGN and p8 RGCs
Electron micrographs (EM) of p8 LGN immunolabled using a monoclonal anti-GLT-1a antibody directed against the C-terminus of GLT-1a. GLT-1 expression in astrocytes (A) and in a subpopulation of axon terminals forming asymmetric synapses (B). Reduced labeling of GLT-1 is seen in the complete knockout of GLT-1 (C). Panel D shows the absence of astrocytes and extensive extracellular space (*i*) in the complete GLT-1 KO. Quantitative description of electron micrographs comparing percentage of total presynaptic terminals (E) or astrocytes (F) unlabeled, lightly labeled and intensely labeled between p8 wild-type and GLT-1 null littermates. (G) PCR using primers designed against GLT-1 and GAPDH in RGCs acutely isolated from P8 mice using immunopanning. Sizes of bands correlated with predicted sizes: 270, 259, 100 and 84 bp. Scale bar=500nM

At early developmental time points, excitatory synaptic terminals of retinogeniculate and cortical origin cannot be differentiated based on morphology (Bickford et al., 2010). Starting around age p14, retinal terminals are found with round vesicles, large profiles, and pale mitochondria (RLP) (Aggelopoulos et al., 1989). In contrast, excitatory terminals from cortex have round vesicles, small profiles and dark mitochondria (RSD profiles). Therefore, we cannot conclude whether the excitatory terminals labeled in the p8 LGN are corticothalamic or retinogeniculate. However, we next addressed whether we could detect GLT-1 mRNA in immature RGCs. We performed PCR on cDNA isolated from p8 RGCs (generous gift of Allison Bialas and Beth Stevens (Bialas and Stevens, 2013)) using primers designed to recognize all 3 mRNA variants of GLT-1 (for detailed methods see Chapter 2). Using these primers, we were able to see bands at all of the predicted sizes (Figure 5.3 G). This suggests that GLT-1 mRNA is present in p8 RGCs. Future studies using co-labeling of the presynaptic vesicular glutamate transporter (VGluT2) and GLT-1 would further confirm the presence of GLT-1 in presynaptic retinogeniculate and not corticothalamic terminals because axonal projections from the cortex express VGluT1.

Comparing properties of the retinogeniculate synapse between neuronal KOs of GLT-1 and control littermates

We generated conditional GLT-1 knockouts to investigate a possible role for the neuronal GLT-1 at the retinogeniculate synapse. GLT-1$^{flx/flx}$ mice were crossed to mice that express Cre recombinase under the neuronal-specific Synapsin promoter (Synapsin/Cre) to knockout GLT-1 only in neurons, leaving glial GLT-1 expression intact (GLT-1 nKO mice, for details see Chapter 2). While the relative concentration of GLT-1 in axon terminals is much lower than that found in surrounding glia, the proximity of GLT-1 to the synaptic cleft suggests it may have a functional role in synaptic transmission.
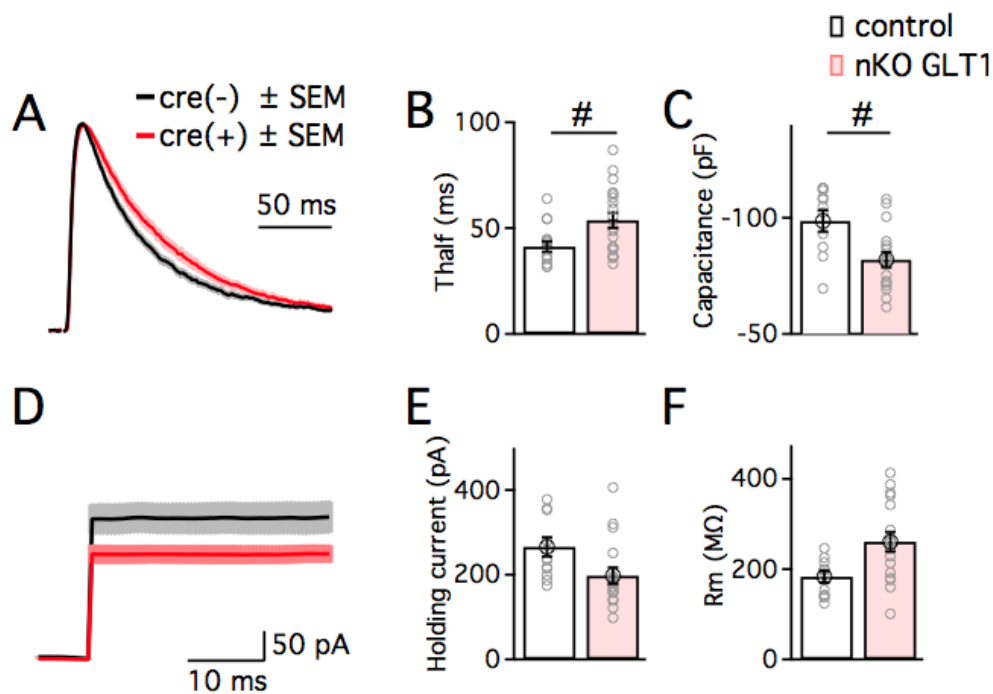
Figure 5.5: Differences between neuronal KOs of GLT-1 and control littermates
Average time course of normalized NMDAR EPSCs (A) and holding current in response to a +40mV step (D) recorded from GLT-1$^{flx/flx}$SynapsinCre$^+$ (nKO) and GLT-1$^{flx/flx}$SynapsinCre$^-$ (control) littermates ages p9-11. Graphs of the T_{half} of normalized NMDAR EPSCs (*B*) relay neuron capacitance (C) baseline holding currents (*E*), and membrane resistances (F) from nKO and control littermates (n=20,12). Individual data points are shown as grey circles. (#)p<0.05. Bath temperature: 35 ± 1°C.

In wildtype mice the presence of the glutamate transport inhibitor TBOA significantly prolongs the decay of the NMDAR EPSC at the retinogeniculate synapse (Hauser et al., 2013; Hauser et al., 2014). We hypothesized that if neuronal GLT-1 were contributing to removal or buffering of synaptic glutamate, then we would expect to see differences between the two genotypes in the shape of the baseline NMDAR EPSC waveform. While no significant differences were found in the peak currents, ages, stimulus intensities, or access in p8-11 mice that were either Cre(+) (GLT-1 nKO) versus their Cre(-) littermates recorded from the two groups (all experiments were performed blind to genotype), the T_{half} of the NMDAR EPSC in nKOs was significantly slower than control littermates (Cre(-):41.3 ± 2.4 ms v. nKO: 53.7 ± 3.6 ms, n=12, 20 p<0.05, unpaired

t-test. Figure 5.5 A,B). In addition to the differences in the recorded NMDAR EPSC waveforms, relay neurons of the GLT-1 nKO were found to have a smaller capacitance than control neurons (control: 95.6 ± 5.1 pF and nKO 82.9 ± 3.1 pF; n=12, 20; p<0.05 unpaired t-test; Figure 5.5 C).

While no other significant differences were found in the baseline currents recorded from the two genotypes, some trends were noted. The relay neurons from the nKO had slightly higher membrane resistances than control (control: 219.3 ± 38 MΩ; nKO: 254.0 ± 20.66 MΩ, n=12, 20; p=0.083, Mann-Whitney, Figure 5.5 F). In addition, we found that in the nKO, the holding current (I_{hold}) in response to a +40-mV step was less than that found in control littermates (control: 248.3 ± 38.0 pA; nKO: 199.8 ± 17.9 pA; n=12, 20; p=0.077, Mann-Whitney, Figure 5.5 D). If a portion of the I_{hold} includes current contributions from the basal activation of NMDARs, baseline I_{hold} differences could reflect a difference in the concentration of ambient glutamate. To test whether the I_{hold} could indicate tonic low-level activation of NMDARs by ambient glutamate, we performed experiments on wildtype mice and looked at the effects of a high concentration of the high-affinity antagonist (20 μM CPP) on the holding current.

Bath application of CPP on acute slices prepared from control, wildtype mice, resulted in a significant decrease the average size of the I_{hold} following a +40mV- step (baseline I_{hold}: 118.2 ± 9.3 pA to 67.8 ± 3.3 pA in CPP; n=4, p<0.01, Figure 5.6). On average, 50.4 ± 6.2 pA of the I_{hold} is sensitive to CPP (42.2 ± 1.9%). These data suggest that the trend toward a difference in the I_{hold} between genotypes may indicate differences in extracellular glutamate concentration.
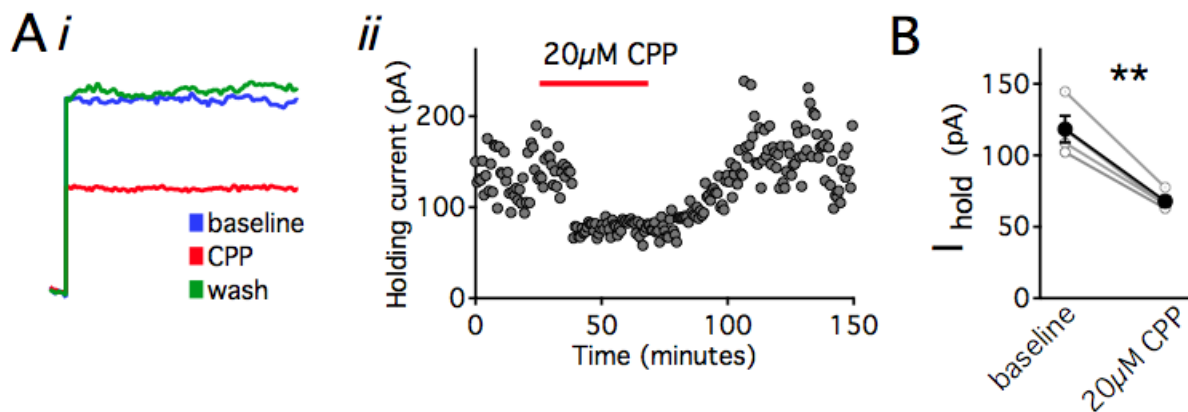
Figure 5.6: NMDARs contribute Holding currents following a +40mV step
I_{hold} in response to a +40mV step recorded from p10-11 mice. Average traces (Ai) and time course (Aii) are shown before (blue trace) during (red trace) and following (green trace) application of 20 μM (R)-CPP. (B) Summary of multiple experiments showing the contribution of CPP-sensitive current; average and SEM shown in black, individual experiments shown in grey (n=4, p<0.01). (**)p<0.01. Bath temperature: 35 ± 1°C.

No striking differences in baseline mGluR occupancy between genotypes

Early in development, glutamate transporters shield the excessive activation of presynaptic mGluRs (Hauser et al., 2013). If neuronal GLT-1 normally prevents glutamate from reaching, binding, and activating presynaptic mGluRs, then if we inhibit the mGluR response in the neuronal knockout of GLT-1, we would expect the peak of the NMDAR EPSC to increase to a greater extent than control littermates. We measured the NMDAR EPSC before and during bath application of LY and found that, similar to previous reports, the peak of the control was significantly increased (698.3 ± 93.5 pA to 798.3 ± 95 pA in LY341495, n=8, p<0.01). Addition of LY to the bath also led to an increase in the peak amplitude of the nKO, although this difference did not reach significance (717.5 ± 141.3 pA to 850.5 ± 161.9 pA in LY, n=6, p=0.088; Figure 5.7B). No significant difference was found when comparing the percentage increase in peak amplitude between the two genotypes (control in LY: 116.3 ± 4.2% of baseline; nKO in LY: 120 ± 9.3% of baseline; n=8,6; p=0.73). These results do not support the hypothesis that neuronal

GLT-1 shields presynaptic mGluRs from glutamate activation, rather, there appears to be no

significant difference between genotypes and the baseline occupancy of mGluRs.
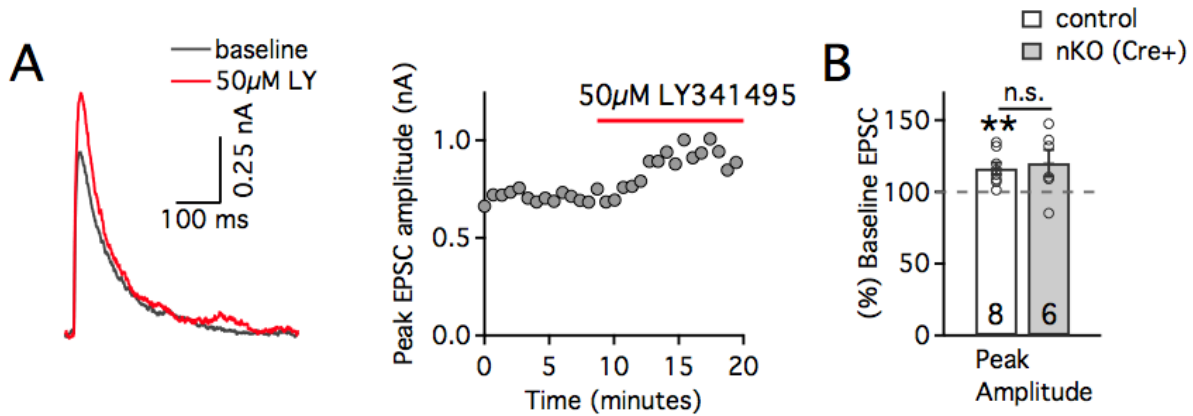

Figure 5.7: Inhibition of group II/III metabotropic glutamate receptors (mGluRs) in nKO of GLT-1 and control littermates
Example averaged NMDAR EPSC traces (A, left) and timecourse (A, right) before (black line) and during (red line) bath application of 50µM LY341495. Example recording are from a p10 GLT-1 nKO mouse. (B) Summary bar graphs showing the effects of LY on NMDAR EPSC peak amplitude percentage of baseline in control (white) and GLT-1 nKO (grey) mice (n=8,6). Individual parameters shown as grey circles. (**)$p < 0.01$. Bath temperature: 35 ± 1°C

Neuronal GLT-1 is not the major glutamate transporter responsible for removing synaptically released glutamate

Glutamate transporters shape the EPSC waveform at the immature retinogeniculate synapse

(Hauser et al., 2013). When transport is inhibited, the peak of the NMDAR- EPSC increases

(when the mGluR response is inhibited with 50 µM LY341495) and the decay of the EPSC is

significantly prolonged. If a significant portion of this response were due to the inhibition of

neuronal GLT-1, then we might expect a significantly reduced response to TBOA in the nKO of

GLT-1. We recorded isolated NMDAR EPSCs (V_h=+40mV) in the presence of LY to prevent

mGluR activation and compared the responses of GLT-1 nKO to transporter inhibition.

In the presence of TBOA, the peak current significantly increased in both genotypes (control: 741.1 ± 84.6 pA to 1000.8 ± 133.3 pA in TBOA n=8, p<0.01; nKO: 915.5 ± 128.2 pA to 1552.3 ± 282 pA in TBOA n=8, p<0.05, Figure 5.8A, B*i*). In addition, the T_{half} of the NMDAR EPSC was also significantly prolonged in both genotypes, in agreement with previous studies (control: n=8, p<0.001; nKO: n=8, p<<0.0001; Figure 5.8 B*ii*). However, these changes in the synaptic waveform were similar in both the GLT-1 nKO and their littermate controls (Figure 5.8 B*iii*). These results suggest that neuronal GLT-1 does not play a major role in shaping the NMDAR EPSC waveform at the immature retinogeniculate synapse.
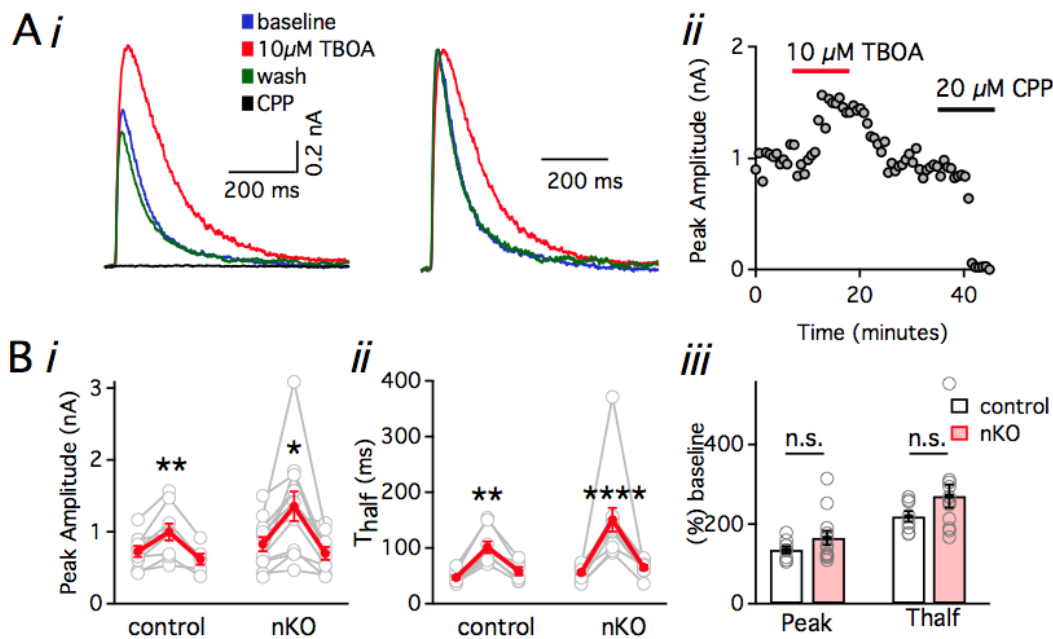
Figure 5.8: Inhibition of glutamate transporters in nKO of GLT-1 and control littermates
(A) Representative NMDAR EPSC averaged traces (i) recorded before (blue), during application of 10µM TBOA (red), following washout of TBOA (green), and in the presence of 20µM CPP. (Ai, *right*) NMDAR EPSC traces normalized to peak amplitude. (Aii) Example time course of an experiment plotting NMDASR EPSC peak amplitude under control conditions or in the presence of TBOA or CPP. (B) Summary data comparing the response of Cre (-) control and Cre(+) GLT-1 nKO NMDAR EPSC peak amplitude (i), T_{half} (ii) before, during and following TBOA application. (B*iii*) Summary bar graphs showing the percentage change from baseline in peak and T_{half} in the presence of TBOA. Cre(-), control (n=9), Cre(+) GLT-1 nKO (n=12).
Bath temperature: 35 ± 1°C.

Differences between nKO of GLT-1 and control littermates are not due to the presence of Cre protein

The minor differences seen between the GLT-1 nKO and their littermate controls may be due to the absence of GLT-1 from neurons expressing Synapsin. However, because of the way the animals were generated (GLT-1$^{flx/flx}$ crossed with GLT-1$^{flx/flx}$SynapsinCre$^{+/-}$), another possibility is that the presence of Cre protein in synapsin expressing cells could also explain the differences. Although not widely addressed in the literature, the presence of Cre protein has been shown to cause developmental delays in other areas of the nervous system. To control for this possibility, we compared Synapsin/Cre positive and Cre negative littermates and looked for differences in synaptic waveforms and passive properties of relay neurons.

No significant differences between the two genotypes were found in the shape of the NMDAR EPSC (n= 8,14, p>0.7; Figure 5.9) or the holding current in response to a +40mV step (n=8, 14, p>0.7). In addition, no differences were found in the relay neuron capacitance or membrane resistance between the two genotypes (Cm: n=8,14 p>0.7 and Rm: n=8,14, p>0.7). Also, no differences were found in the baseline occupancy of mGluRs (n =6, 9; p>0.3). Inhibition of glutamate transport with 10µM TBOA had similar effects on NMDAR currents recorded from the two genotypes (Peak amplitude control, nKO n=7,9, p>0.3; T$_{half}$: n=7, 9; p>0.55 unpaired t-test). These results indicate that differences between the GLT-1 nKO mice and their littermate controls are unlikely to be due to the presence of Cre protein.
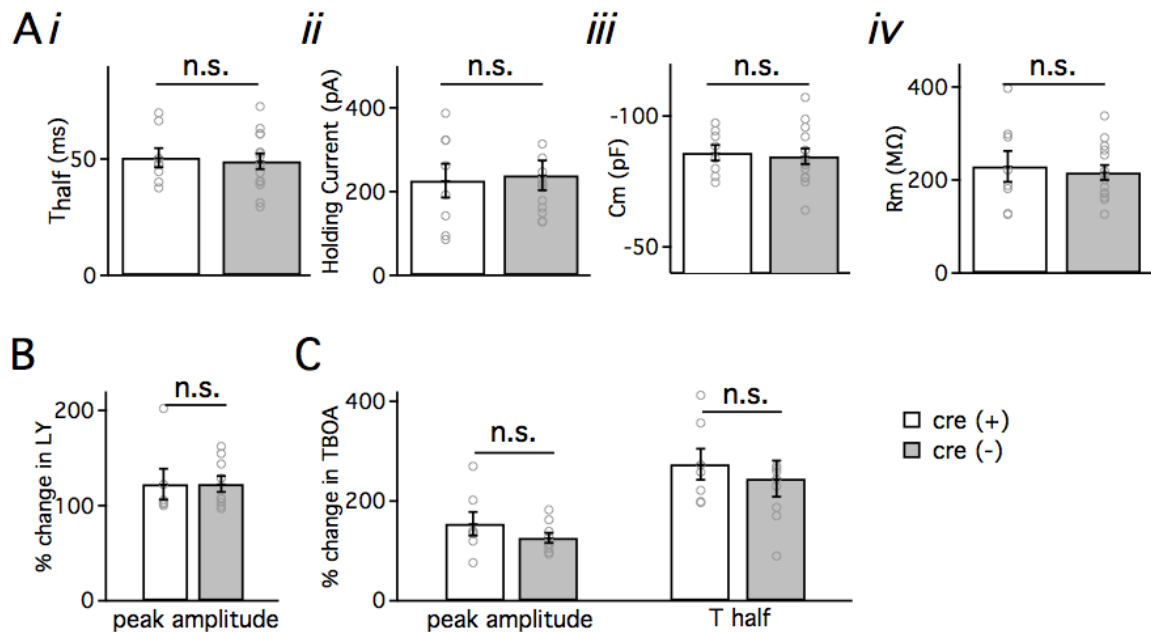
Figure 5.9: Control experiments for the presence of CRE protein
Summary bar graphs comparing Synapsin/Cre negative (Cre(-), white bars) and Synapsin/Cre positive (Cre(+), grey bars) littermates. (Ai) T_{half} of the normalized NMDAR EPSC. (Aii) Baseline holding currents following a +40mV step. (Aiii) Cell capacitance. (Aiv) Membrane resistance (Cre(-) n=8; Cre(+) n=14). (B) Summary bar graphs comparing the effects of 50µM LY341495 (Cre(-) n= 6 and Cre(+) n= 9). (C) Effects of 10µM TBOA on NMDAR peak amplitude and T_{half} shown as percentage of baseline (Cre(-) n= 7 and Cre(+) n= 9). Individual experiments are shown as grey circles. (n.s.) not significant, all *p* values >0.7. Bath temperature for all experiments: 35 ± 1°C.

GLT-1 nKO and littermate controls have similar peak concentrations of synaptic glutamate

At the immature retinogeniculate synapse, the NMDARs that contribute to the EPSC waveform are activated by a gradient of peak glutamate concentrations. This gradient is dependent on intact glutamate transporter uptake (see Figure 5.1). If neuronal GLT-1 plays a role in establishing the gradient, then we would predict that the low-affinity antagonist to NMDARs would not accelerate the NMDAR EPSC waveform. To test this hypothesis, we measured the effect of L-AP5 on isolated NMDAR currents in GLT-1 nKO mice. In the presence of 1mM L-AP5, the peak amplitude of the NMDAR EPSC was significantly reduced to 30.7 ± 5.5% of

baseline (780.8 ± 84.1 pA to 242.2 ± 51 pA in L-AP5; n=6, p<0.001, Figure 5.10). Moreover, the decay of the NMDAR ESPC was significantly accelerated to 68.4 ± 4% of baseline (62.7 ± 4.7 ms to 43.6 ± 5.7 ms in L-AP5; n=6, p<0.001). These results are consistent with our previous findings at wildtype immature retinogeniculate synapses.

To control for potential voltage-clamp errors, experiments were performed in parallel using a low concentration of the high affinity NMDAR antagonist CPP. CPP decreased the peak NMDAR current to a similar extent as L-AP5 (CPP: 34.5 ± 3.9% of baseline v L-AP5: 30.7 ± 5.5% of baseline; n=8,6 p>0.5; Figure 5.10 B). However, the effects of the two antagonists significantly differed on their influence on the decay kinetics of the NMDAR EPSC (CPP: 94.2 ± 10% of baseline v. L-AP5 68.4 ± 4% of baseline n=8,6, p<0.05). These results are also consistent with those previously describing this synapse, and indicate that neuronal GLT-1 does not play a major role in establishing the gradient of peak glutamate concentrations experienced by NMDARs at the immature synapse.

Another analysis that allows for the comparison of glutamate concentrations between genotypes is to compare the effects of the low-affinity antagonist directly between GLT-1 nKO and littermate controls. If the peak concentration of glutamate reached in the synaptic cleft is greater in the absence of neuronal GLT-1, then we would expect for the low-affinity antagonist to have a smaller effect on the peak of the NMDAR EPSC when compared to controls. However, L-AP5 did not have a significantly different effect in reducing the peak NMDAR amplitude between the two genotypes (Peak amplitude: Cre(-) 44.95 ± 4.9% of baseline in L-AP5 v. Cre(+) 30.7 ± 5.5% of baseline in L-AP5, n=5, 6; p=0.09). Moreover, the antagonist accelerated the NMDAR EPSC decay to a similar extent (Cre(-) : 78.4 ± 4.8 % of baseline in L-AP5 v. Cre(+): 68.4 ± 4.0% of baseline in L-AP5, n=5,6; p=0.15; Figure 5.10 C). These results further suggest a minor role of neuronal GLT-1 in shaping synaptic currents at the immature retinogeniculate synapse.

136
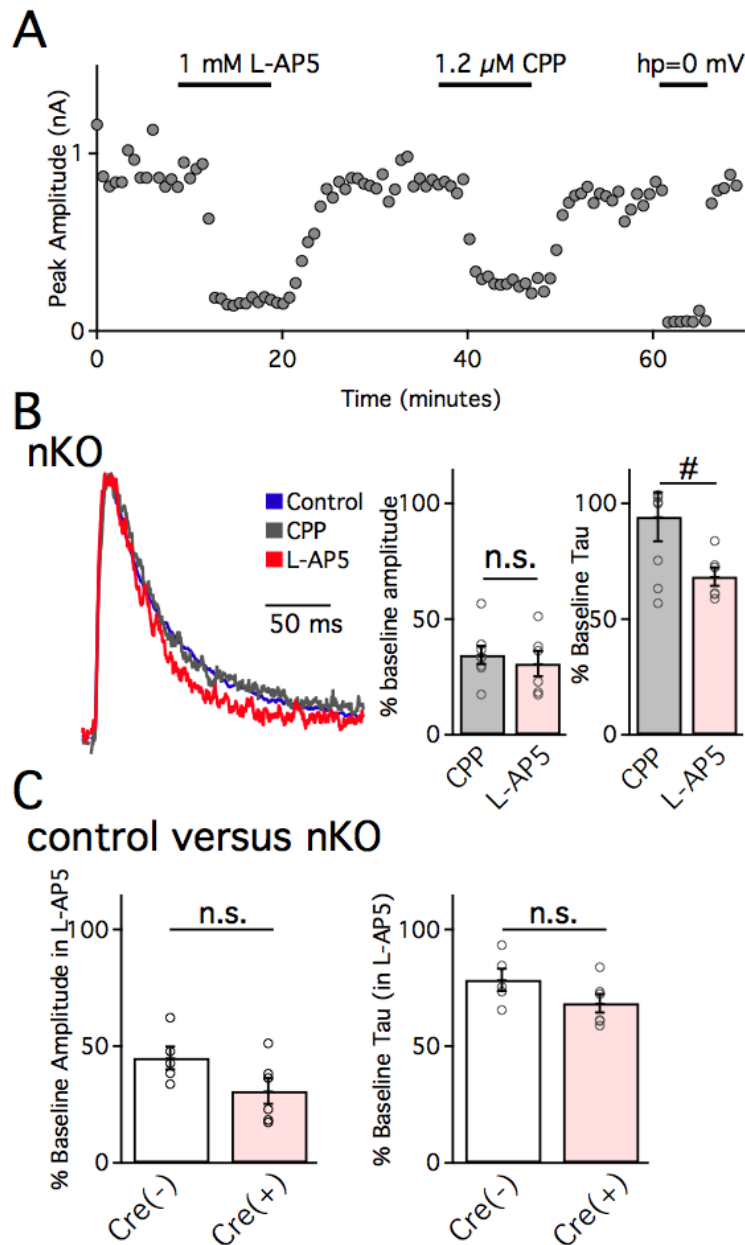
Figure 5.10: L-AP5 significantly accelerates the NMDAR EPSC in nKO of GLT-1
(A) Example time course of an experiment plotting NMDAR EPSC (V_h= +40 mV) peak amplitudes under control conditions or in the presence of 1mM L-AP5, 1.2 μM CPP or at V_h=0 mV. (B) Representative normalized NMDAR EPSCs recorded from GLT-1 nKO from baseline (blue trace) and during application of L-AP5 (red trace) or low concentration of (R)-CPP (grey trace). (B, *right*) Summary bar graphs showing CPP and L-AP5 effects on peak amplitude and tau shown as percentage of baseline (n=8,6). (C) Summary bar graphs comparing the effects of 1mM L-AP5 on Cre(-) (n=5) and Cre(+) (n=6) GLT-1 nKOs on peak amplitude (left) and NMDAR EPSC decay (right). (#)p<0.05; Bath temperature for all experiments: 35 ± 1°C.

DISCUSSION

Glutamate transporters in the brain serve roles beyond maintaining the low ambient levels of glutamate needed to establish a suitable signal-to-noise ratio (Tzingounis and Wadiche, 2007). When ambient glutamate levels are excessively high, neuronal death can occur through a process of excitotoxicity (Choi, 1988; Meldrum and Garthwaite, 1990; Lipton and Rosenberg, 1994). Aside from this primary function, glutamate transporters have also been shown to influence synaptic transmission (Tzingounis and Wadiche, 2007). In this study, we provide evidence that glutamate transporters contribute to the gradient of peak glutamate concentrations experienced by NMDARs at the immature, but not mature, retinogeniculate synapse. We also tested the hypothesis that the unique position of the neuronal glutamate transporter, GLT-1, in presynaptic terminals may play a functional role in determining the strength and shape of synaptic transmission at the immature synapse. Our data suggest that neuronal GLT-1 is not the major glutamate transporter responsible for shaping synaptic transmission early in development, and its function in presynaptic terminals remains unclear. Further studies will be needed to determine the role of neuronal GLT-1.

Glutamate spillover at the retinogeniculate synapse over development

The geometry of a synapse can either promote or inhibit the extent of glutamate spillover (Sykova and Nicholson, 2008). For example, at synaptic connections where there are multiple release sites in close proximity and a high probability of release, neurotransmitter is more likely to accumulate and activate extrasynaptic receptors. At the mature retinogeniculate connection, diffusion of glutamate is largely restricted to two dimensions because of the large contact size of each RGC bouton and an average of 27 release sites per bouton (Budisantoso et al., 2012). In some cases, glia form glomeruli around aggregates of presynaptic terminals, which further limit glutamate diffusion (Rafols and Valverde, 1973; Aggelopoulos et al., 1989; Budisantoso et al., 2012). Physiological data suggests there are fewer release sites per RGC axon in the young

LGN, although it's likely that there is more than one release site per immature bouton (Chen and Regehr, 2000). Our EM studies at the immature retinogeniculate synapse are consistent with those in the literature, where some astrocytes are present but do not fully encapsulate synaptic terminals (Aggelopoulos et al., 1989; Bickford et al., 2010). Since glutamate spillover occurs throughout development, this could mean that there are distinct differences in the type of spillover.

The low-affinity antagonists to NMDARs at the retinogeniculate synapse at two developmental timepoints had similar effects on the peak currents, suggesting that the peak glutamate concentration in the cleft does not significantly change with development. In contrast to the immature synapse, application of L-AP5 to the mature synapse did not accelerate the decay of the NMDAR current, implying that the ionotropic receptors experience a more uniform concentration of glutamate. This is in contrast with published experimental and modeling studies showing that AMPAR desensitization occurs from intersynaptic glutamate diffusion and spillover (Chen et al., 2002; Budisantoso et al., 2012). One reason for this discrepancy is that our studies relied on currents generated by high-affinity NMDARs and, therefore, may not be sensitive enough to detect a gradient in peak glutamate concentration at the mature synapse. In addition, we recorded currents generated by the stimulation of multiple RGC axons. Performing similar experiments on single fiber currents may also be more sensitive and potentially reduce the extent of voltage clamp error at later ages. Despite these caveats, studies at the mature synapse only indicate that glutamate can diffuse between RGC terminals that make direct contacts onto the same relay neuron. Purely spillover-mediated currents can be isolated from the immature synapse, but have not been found at the mature contact (unpublished observations). These data suggest that although glutamate spillover may occur throughout development, glutamate is able to diffuse far greater distances in the immature LGN.

Developmental changes in glutamate clearance at other central synapses

Developmental changes in glutamate clearance have also been studied at a number of other CNS synapses. At the hippocampal CA3-CA1 Schaffer collateral synapse, changes in both neuropil structure and glutamate uptake influence the timecourse of synaptically released glutamate during development (Thomas et al., 2011). Specifically, early in development, glutamate clearance is dominated by diffusion due to vast extracellular space. Later, following upregulation in transporter expression and consolidation of the neuropil, transporters play a more dominant role in glutamate clearance (Thomas et al., 2011). At the large glutamatergic synapse of the auditory system, the Calyx of Held, postsynaptic AMPAR desensitization due to glutamate spillover influences short-term plasticity prior to the onset of hearing, but then disappears in older animals (Neher and Sakaba, 2001; Joshi and Wang, 2002; Taschenberger et al., 2002; Renden et al., 2005; Taschenberger et al., 2005). At another synapse, the rat hypothalamic supraoptic nucleus, glutamate clearance is modulated by hormonal control of glial coverage (Oliet et al., 2001). Excitatory transmission is influenced by the synaptic micro-environment, including neuropil structure, glial coverage, transporter location, and expression. All of these factors can vary depending on the brain region, developmental stage, and physiological state of the body.

The glutamate transporter GLT1 in excitatory synaptic terminals

Our EM and PCR data suggest that GLT-1 is expressed in excitatory retinogeniculate synaptic terminals in the developing LGN, though further evidence is needed to confirm its presence in retinogeniculate terminals, specifically, co-labeling of GLT-1 and the RGC terminal-specific vesicular glutamate transporter, VGlut2. The function of GLT-1 in excitatory synaptic terminals has been a subject of debate (Tzingounis and Wadiche, 2007). If the glutamate transporter is present in presynaptic terminals, what function could it serve, considering it has a relatively low expression compared to astrocytes? In the hippocampus, the postsynaptic glutamate

transporter EAAC1 has been shown to buffer synaptically released glutamate, prevent activation of extrasynaptic NMDARs, and influence synaptic plasticity (Diamond, 2001; Scimemi et al., 2009).

We observed minor differences in the shape of the NMDAR EPSC in the neuronal knockout of GLT-1. The prolonged current seen in the nKO could imply that glutamate removal is impeded in the absence of neuronal GLT-1. Conversely, the absence of GLT-1 in neurons may lead to a developmental delay. The trend toward a larger input resistance and a decreased cell capacitance in the nKO relay neurons are consistent with developmental delay (Ramoa and McCormick, 1994). A major caveat of using the Synapsin/Cre mouse is that GLT-1 will be removed from all pre- and postsynaptic neurons that express Synapsin I. A more targeted approach that removes GLT-1 only from RGCs would address problems of specificity. This could be accomplished by injecting AAV2-Cre into the eyes of GLT-1$^{flox/flox}$ mice to target RGCs (Malik et al., 2005; Shevtsova et al., 2005). Also, not all presynaptic terminals in the LGN showed GLT-1 immunoreactivity. The currents in these present studies were generated by stimulating multiple retinogeniculate fibers at low frequency (0.025 Hz) and, therefore, may have masked a more subtle synaptic phenotype. Perhaps using a single-fiber approach or stimulating at more natural frequencies (similar to (Hauser et al., 2013) in the future would reveal differences between GLT-1 nKO and controls. The lack of a more striking phenotype could also be attributed to compensatory upregulation of GLT-1 or other glutamate transporters in nearby astrocytes. To address this concern, future studies using in situ hybridization or immunoreactivity could be used to examine the expression of GLT-1, GLAST or EAAT3 in LGNs of GLT-1 nKOs and control littermates.

Recorded hippocampal NMDAR-mediated currents from the complete knockout of GLT-1 show significantly less inhibition by L-AP5 than wild-type slices, implying that the peak concentration

of synaptic glutamate is greater in the complete absence of GLT-1 (Tanaka et al., 1997). In contrast, our studies using the low-affinity antagonists on currents from GLT-1 nKOs suggest that the glutamate transient is not significantly altered from controls.

In Purkinje cells of the cerebellum, the perisynaptic postsynaptic glutamate transporter EAAT4 prevents the activation of postsynaptic group I mGluRs and thus influences the extent of synaptic depression (Brasnjo and Otis, 2001; Wadiche and Jahr, 2005; Tsai et al., 2012). Given the location of the presynaptic GLT-1, we hypothesized that the transporter may shield the excessive activation of presynaptic group II/III mGluRs present at the immature synapse (Hauser et al., 2013). However, we failed to observe any significant differences between GLT-1 nKO and control littermates to the group II/III antagonist. An example of a presynaptic glutamatetransporter that influences synaptic transmission is found in rod bipolar cells of the retina (Palmer et al., 2003; Hasegawa et al., 2006). The transporter, EAAT5 regulates synaptic transmission by hyperpolarizing presynaptic terminals due to its large anion current (Veruki et al., 2006); however, only EAAT4 and EAAT5 have been shown to display prominent anion currents making it is unlikely GLT-1 serves a similar role in retinogeniculate presynaptic terminals (Sarantis et al., 1988; Fairman et al., 1995; Arriza et al., 1997; Danbolt et al., 1998; Dehnes et al., 1998).

Lastly, inhibiting glutamate transporters with the non-selective competitive inhibitor TBOA produced similar changes in synaptic currents in both GLT-1 nKO and littermate controls. These data suggest that neuronal GLT-1 is not the major transporter responsible for removing glutamate early in development. Thus, a functional role for neuronal GLT-1 in synaptic transmission at the retinogeniculate contact remains elusive. One potential function of neuronal GLT-1 could be to maintain the presynaptic pool of glutamate (Danbolt, 2001). Perhaps future

studies that use the neuronal GLT-1 knockout may help to elucidate whether GLT-1 significantly

shapes synaptic transmission or has a role in other neuronal processes.

REFERENCES

Aggelopoulos N, Parnavelas JG, Edmunds S (1989) Synaptogenesis in the dorsal lateral geniculate nucleus of the rat. Anatomy and embryology 180:243-257.

Arriza JL, Eliasof S, Kavanaugh MP, Amara SG (1997) Excitatory amino acid transporter 5, a retinal glutamate transporter coupled to a chloride conductance. Proceedings of the National Academy of Sciences of the United States of America 94:4155-4160.

Bialas AR, Stevens B (2013) TGF-beta signaling regulates neuronal C1q expression and developmental synaptic refinement. Nature neuroscience 16:1773-1782.

Bickford ME, Slusarczyk A, Dilger EK, Krahe TE, Kucuk C, Guido W (2010) Synaptic development of the mouse dorsal lateral geniculate nucleus. The Journal of comparative neurology 518:622-635.

Brasnjo G, Otis TS (2001) Neuronal glutamate transporters control activation of postsynaptic metabotropic glutamate receptors and influence cerebellar long-term depression. Neuron 31:607-616.

Budisantoso T, Matsui K, Kamasawa N, Fukazawa Y, Shigemoto R (2012) Mechanisms underlying signal filtering at a multisynapse contact. The Journal of neuroscience : the official journal of the Society for Neuroscience 32:2357-2376.

Chen C, Regehr WG (2000) Developmental remodeling of the retinogeniculate synapse. Neuron 28:955-966.

Chen C, Blitz DM, Regehr WG (2002) Contributions of receptor desensitization and saturation to plasticity at the retinogeniculate synapse. Neuron 33:779-788.

Chen W, Mahadomrongkul V, Berger UV, Bassan M, DeSilva T, Tanaka K, Irwin N, Aoki C, Rosenberg PA (2004) The glutamate transporter GLT1a is expressed in excitatory axon terminals of mature hippocampal neurons. The Journal of neuroscience : the official journal of the Society for Neuroscience 24:1136-1148.

Choi DW (1988) Glutamate neurotoxicity and diseases of the nervous system. Neuron 1:623-634.

Danbolt NC (2001) Glutamate uptake. Progress in neurobiology 65:1-105.

Danbolt NC, Storm-Mathisen J, Kanner BI (1992) An [Na+ + K+]coupled L-glutamate transporter purified from rat brain is located in glial cell processes. Neuroscience 51:295-310.

Danbolt NC, Chaudhry FA, Dehnes Y, Lehre KP, Levy LM, Ullensvang K, Storm-Mathisen J (1998) Properties and localization of glutamate transporters. Progress in brain research 116:23-43.

Dehnes Y, Chaudhry FA, Ullensvang K, Lehre KP, Storm-Mathisen J, Danbolt NC (1998) The glutamate transporter EAAT4 in rat cerebellar Purkinje cells: a glutamate-gated chloride channel concentrated near the synapse in parts of the dendritic membrane facing

astroglia. The Journal of neuroscience : the official journal of the Society for Neuroscience 18:3606-3619.

Diamond JS (2001) Neuronal glutamate transporters limit activation of NMDA receptors by neurotransmitter spillover on CA1 pyramidal cells. The Journal of neuroscience : the official journal of the Society for Neuroscience 21:8328-8338.

Fairman WA, Vandenberg RJ, Arriza JL, Kavanaugh MP, Amara SG (1995) An excitatory amino-acid transporter with properties of a ligand-gated chloride channel. Nature 375:599-603.

Furness DN, Dehnes Y, Akhtar AQ, Rossi DJ, Hamann M, Grutle NJ, Gundersen V, Holmseth S, Lehre KP, Ullensvang K, Wojewodzic M, Zhou Y, Attwell D, Danbolt NC (2008) A quantitative assessment of glutamate uptake into hippocampal synaptic terminals and astrocytes: new insights into a neuronal role for excitatory amino acid transporter 2 (EAAT2). Neuroscience 157:80-94.

Furuta A, Rothstein JD, Martin LJ (1997) Glutamate transporter protein subtypes are expressed differentially during rat CNS development. The Journal of neuroscience : the official journal of the Society for Neuroscience 17:8363-8375.

Hasegawa J, Obara T, Tanaka K, Tachibana M (2006) High-density presynaptic transporters are required for glutamate removal from the first visual synapse. Neuron 50:63-74.

Haugeto O, Ullensvang K, Levy LM, Chaudhry FA, Honore T, Nielsen M, Lehre KP, Danbolt NC (1996) Brain glutamate transporter proteins form homomultimers. The Journal of biological chemistry 271:27715-27722.

Hauser JL, Edson EB, Hooks BM, Chen C (2013) Metabotropic glutamate receptors and glutamate transporters shape transmission at the developing retinogeniculate synapse. Journal of neurophysiology 109:113-123.

Hauser JL, Liu X, Litvina EY, Chen C (2014) Prolonged Synaptic Currents Increase Relay Neuron Firing at the Developing Retinogeniculate Synapse. Journal of neurophysiology.

Jaubert-Miazza L, Green E, Lo FS, Bui K, Mills J, Guido W (2005) Structural and functional composition of the developing retinogeniculate pathway in the mouse. Visual neuroscience 22:661-676.

Joshi I, Wang LY (2002) Developmental profiles of glutamate receptors and synaptic transmission at a single synapse in the mouse auditory brainstem. The Journal of physiology 540:861-873.

Lipton SA, Rosenberg PA (1994) Excitatory amino acids as a final common pathway for neurologic disorders. The New England journal of medicine 330:613-622.

Malik JM, Shevtsova Z, Bahr M, Kugler S (2005) Long-term in vivo inhibition of CNS neurodegeneration by Bcl-XL gene transfer. Molecular therapy : the journal of the American Society of Gene Therapy 11:373-381.

Meldrum B, Garthwaite J (1990) Excitatory amino acid neurotoxicity and neurodegenerative disease. Trends in pharmacological sciences 11:379-387.

Neher E, Sakaba T (2001) Estimating transmitter release rates from postsynaptic current fluctuations. The Journal of neuroscience : the official journal of the Society for Neuroscience 21:9638-9654.

Oliet SH, Piet R, Poulain DA (2001) Control of glutamate clearance and synaptic efficacy by glial coverage of neurons. Science 292:923-926.

Palmer MJ, Taschenberger H, Hull C, Tremere L, von Gersdorff H (2003) Synaptic activation of presynaptic glutamate transporter currents in nerve terminals. The Journal of neuroscience : the official journal of the Society for Neuroscience 23:4831-4841.

Petr GT, Schultheis LA, Hussey KC, Sun Y, Dubinsky JM, Aoki C, Rosenberg PA (2013a) Decreased expression of GLT-1 in the R6/2 model of Huntington's disease does not worsen disease progression. The European journal of neuroscience 38:2477-2490.

Petr GT, Bakradze E, Frederick NM, Wang J, Armsen W, Aizenman E, Rosenberg PA (2013b) Glutamate transporter expression and function in a striatal neuronal model of Huntington's disease. Neurochemistry international 62:973-981.

Rafols JA, Valverde F (1973) The structure of the dorsal lateral geniculate nucleus in the mouse. A Golgi and electron microscopic study. The Journal of comparative neurology 150:303-332.

Ramoa AS, McCormick DA (1994) Developmental changes in electrophysiological properties of LGNd neurons during reorganization of retinogeniculate connections. The Journal of neuroscience : the official journal of the Society for Neuroscience 14:2089-2097.

Renden R, Taschenberger H, Puente N, Rusakov DA, Duvoisin R, Wang LY, Lehre KP, von Gersdorff H (2005) Glutamate transporter studies reveal the pruning of metabotropic glutamate receptors and absence of AMPA receptor desensitization at mature calyx of held synapses. The Journal of neuroscience : the official journal of the Society for Neuroscience 25:8482-8497.

Sarantis M, Everett K, Attwell D (1988) A presynaptic action of glutamate at the cone output synapse. Nature 332:451-453.

Scimemi A, Tian H, Diamond JS (2009) Neuronal transporters regulate glutamate clearance, NMDA receptor activation, and synaptic plasticity in the hippocampus. The Journal of neuroscience : the official journal of the Society for Neuroscience 29:14581-14595.

Shevtsova Z, Malik JM, Michel U, Bahr M, Kugler S (2005) Promoters and serotypes: targeting of adeno-associated virus vectors for gene transfer in the rat central nervous system in vitro and in vivo. Experimental physiology 90:53-59.

Sykova E, Nicholson C (2008) Diffusion in brain extracellular space. Physiological reviews 88:1277-1340.

Tanaka K, Watase K, Manabe T, Yamada K, Watanabe M, Takahashi K, Iwama H, Nishikawa T, Ichihara N, Kikuchi T, Okuyama S, Kawashima N, Hori S, Takimoto M, Wada K (1997) Epilepsy and exacerbation of brain injury in mice lacking the glutamate transporter GLT-1. Science 276:1699-1702.

Taschenberger H, Scheuss V, Neher E (2005) Release kinetics, quantal parameters and their modulation during short-term depression at a developing synapse in the rat CNS. The Journal of physiology 568:513-537.

Taschenberger H, Leao RM, Rowland KC, Spirou GA, von Gersdorff H (2002) Optimizing synaptic architecture and efficiency for high-frequency transmission. Neuron 36:1127-1143.

Thomas CG, Tian H, Diamond JS (2011) The relative roles of diffusion and uptake in clearing synaptically released glutamate change during early postnatal development. The Journal of neuroscience : the official journal of the Society for Neuroscience 31:4743-4754.

Tsai MC, Tanaka K, Overstreet-Wadiche L, Wadiche JI (2012) Neuronal glutamate transporters regulate glial excitatory transmission. The Journal of neuroscience : the official journal of the Society for Neuroscience 32:1528-1535.

Tzingounis AV, Wadiche JI (2007) Glutamate transporters: confining runaway excitation by shaping synaptic transmission. Nature reviews Neuroscience 8:935-947.

Veruki ML, Morkve SH, Hartveit E (2006) Activation of a presynaptic glutamate transporter regulates synaptic transmission through electrical signaling. Nature neuroscience 9:1388-1396.

Wadiche JI, Jahr CE (2005) Patterned expression of Purkinje cell glutamate transporters controls synaptic plasticity. Nature neuroscience 8:1329-1334.

Page intentionally left blank.

CHAPTER 6:

Conclusions

Conclusions

A hallmark of mammalian circuit development is the refinement of initially coarse and imprecise connections through activity-dependent processes (Hong and Chen, 2011). The mechanisms that drive proper circuit refinement have been a subject of great interest (Blaschke et al., 1993; Huberman, 2007). Generally, it is assumed that patterned spontaneous activity drives the proper wiring of circuits using learning rules first described by D.O.Hebb (Hebb, 1949; Kandel et al., 2000; Butts, 2002). Hebbian plasticity rules state that the repetitive stimulation of a postsynaptic cell by a presynaptic input causes long-term strengthening of that synaptic connection (long-term potentiation, or LTP; (Malenka and Nicoll, 1999)). Conversely, weak synaptic inputs not correlated with postsynaptic activity, continue to weaken (long-term depression, LTD; (Katz and Shatz, 1996)). LTP is thought to sculpt remarkable synaptic specificity, in that only those synapses that are activated become strengthened, while neighboring synapses are unchanged (Matsuzaki et al., 2004).

In this dissertation I have described a number of mechanisms that influence excitatory transmission at the developing retinogeniculate synapse. It is quite clear that synaptically released glutamate is able to escape the synaptic cleft and exert its actions on several types of extrasynaptic metabotropic and ionotropic glutamate receptors. These findings are not entirely consistent with the notion of synaptic specificity, as interpreted within a strict Hebbian framework. Therefore, the rules governing the proper wiring of the retinogeniculate synapse are likely richer than previously thought.

How might proper synaptic refinement at the retinogeniculate synapse occur in the absence of synapse specificity?

Refinement of this contact could be influenced by small differences in the expression patterns of mGluRs. One could imagine that some RGC terminals may express higher densities of these receptors and through heterosynaptic activation of neighboring mGluRs undergo a reduction in synaptic strength. This is consistent with our findings that the response to mGluRs diminishes with age (Hauser et al., 2013). It would be interesting to look at whether synaptic refinement occurs properly in mGluR2/3 knockout mice (Linden et al., 2005).

Additionally, it is possible that glutamate spillover could accomplish strengthening of synapses without compromising synaptic specificity, an idea suggested by Jeff Diamond (Diamond, 2002; Scimemi et al., 2009) that may apply to the developing LGN. The total charge transfer is integrated across many synapses onto a single relay neuron. At the immature retinogeniculate synapse the strength of individual synaptic inputs is extremely weak early in development. However, we've shown that prolonged synaptic currents increase the probability of relay neuron spiking (Hauser et al., 2014). These prolonged currents are influenced by glutamate spillover, asynchronous release, and the expression of NR2C/D in immature NMDARs that are less sensitive to magnesium block, all of which contribute to relay neuron firing (Liu and Chen, 2008; Hauser et al., 2014). However, whether LTP or LTD is induced is influenced by the concentration and timecourse of the calcium signal: fast, high concentrations of calcium (Ca^{2+}) are needed for potentiation, whereas slow low concentrations of Ca^{2+} can lead to depression (Bienenstock et al., 1982; Lisman, 2001; Ismailov et al., 2004). At the immature synapse the concentration of Ca^{2+} entering NMDARs may not all reach similar concentrations due to the open probability of NMDARs and the concentration of glutamate experienced at the site (Chen et al., 1999; Dingledine et al., 1999). Therefore, it is likely that only receptors near the site of direct glutamate release would have enough NMDARs open to lead to a concentration of Ca^{2+} great

enough to lead to synaptic strengthening. Receptors further away would allow only a lower

concentration of Ca^{2+} through, and therefore may undergo synaptic depression. This type of

scenario would result in a 'center-surround' arrangement of synaptic weights (Diamond, 2002).

Expanding on this idea, extensive AMPAR desensitization has been shown to occur at the

retinogeniculate synapse across development (Chen et al., 2002; Budisantoso et al., 2012;

Hauser et al., 2014). The extent of AMPAR desensitization is linked to the concentration of

glutamate the receptors experience (Patneau et al., 1993; Dzubay and Jahr, 1999). In fact,

some AMPARs exposed to prolonged low concentrations of glutamate can enter an "equilibrium

desensitization" state (Colquhoun et al., 1992), and it has also been suggested that receptors

can be directly driven into a desensitized state before entering an opening state (Robert and

Howe, 2003). Therefore, in addition to having different concentrations of calcium enter the relay

neuron, AMPARs further from the direct release of glutamate are more likely to enter a

desensitized state. If these AMPAR are present opposing a neighboring RGC bouton, and that

bouton subsequently releases glutamate, then the synaptic response of the neighboring contact

will be much less than expected. Therefore, glutamate spillover could potentially act through a

multitude of actions to lead to the proper and relatively precise wiring of the visual circuit.

Summary

The experiments in this dissertation explore the synaptic microenvironment of the immature

retinogeniculate synapse during a dynamic period in development. The data presented here

suggest that extensive glutamate spillover occurs during this remodeling period and challenges

the tenet that strict synaptic specificity is needed for the proper formation of this neural circuit.

Therefore, an interesting topic for future studies will be to identify the principles of plasticity

responsible for this process.

REFERENCES

Bienenstock EL, Cooper LN, Munro PW (1982) Theory for the development of neuron selectivity: orientation specificity and binocular interaction in visual cortex. The Journal of neuroscience : the official journal of the Society for Neuroscience 2:32-48.

Blaschke M, Keller BU, Rivosecchi R, Hollmann M, Heinemann S, Konnerth A (1993) A single amino acid determines the subunit-specific spider toxin block of alpha-amino-3-hydroxy-5-methylisoxazole-4-propionate/kainate receptor channels. Proceedings of the National Academy of Sciences of the United States of America 90:6528-6532.

Budisantoso T, Matsui K, Kamasawa N, Fukazawa Y, Shigemoto R (2012) Mechanisms underlying signal filtering at a multisynapse contact. The Journal of neuroscience : the official journal of the Society for Neuroscience 32:2357-2376.

Butts DA (2002) Retinal waves: implications for synaptic learning rules during development. The Neuroscientist : a review journal bringing neurobiology, neurology and psychiatry 8:243-253.

Chen C, Blitz DM, Regehr WG (2002) Contributions of receptor desensitization and saturation to plasticity at the retinogeniculate synapse. Neuron 33:779-788.

Chen N, Luo T, Wellington C, Metzler M, McCutcheon K, Hayden MR, Raymond LA (1999) Subtype-specific enhancement of NMDA receptor currents by mutant huntingtin. Journal of neurochemistry 72:1890-1898.

Colquhoun D, Jonas P, Sakmann B (1992) Action of brief pulses of glutamate on AMPA/kainate receptors in patches from different neurones of rat hippocampal slices. The Journal of physiology 458:261-287.

Diamond JS (2002) A broad view of glutamate spillover. Nature neuroscience 5:291-292.

Dingledine R, Borges K, Bowie D, Traynelis SF (1999) The glutamate receptor ion channels. Pharmacological reviews 51:7-61.

Dzubay JA, Jahr CE (1999) The concentration of synaptically released glutamate outside of the climbing fiber-Purkinje cell synaptic cleft. The Journal of neuroscience : the official journal of the Society for Neuroscience 19:5265-5274.

Hauser JL, Edson EB, Hooks BM, Chen C (2013) Metabotropic glutamate receptors and glutamate transporters shape transmission at the developing retinogeniculate synapse. Journal of neurophysiology 109:113-123.

Hauser JL, Liu X, Litvina EY, Chen C (2014) Prolonged Synaptic Currents Increase Relay Neuron Firing at the Developing Retinogeniculate Synapse. Journal of neurophysiology.

Hebb DO (1949) The Organization of Behavior: A Neuropsychological Theory: John Wiley & Sons Inc.

Hong YK, Chen C (2011) Wiring and rewiring of the retinogeniculate synapse. Current opinion in neurobiology 21:228-237.

Huberman AD (2007) Mechanisms of eye-specific visual circuit development. Current opinion in neurobiology 17:73-80.

Ismailov I, Kalikulov D, Inoue T, Friedlander MJ (2004) The kinetic profile of intracellular calcium predicts long-term potentiation and long-term depression. The Journal of neuroscience : the official journal of the Society for Neuroscience 24:9847-9861.

Kandel ER, Schwartz JH, Jessell TM (2000) Principles of neural science, 4th Edition. New York: McGraw-Hill, Health Professions Division.

Katz LC, Shatz CJ (1996) Synaptic activity and the construction of cortical circuits. Science 274:1133-1138.

Linden AM, Shannon H, Baez M, Yu JL, Koester A, Schoepp DD (2005) Anxiolytic-like activity of the mGLU2/3 receptor agonist LY354740 in the elevated plus maze test is disrupted in metabotropic glutamate receptor 2 and 3 knock-out mice. Psychopharmacology 179:284-291.

Lisman JE (2001) Three Ca2+ levels affect plasticity differently: the LTP zone, the LTD zone and no man's land. The Journal of physiology 532:285.

Liu X, Chen C (2008) Different roles for AMPA and NMDA receptors in transmission at the immature retinogeniculate synapse. Journal of neurophysiology 99:629-643.

Malenka RC, Nicoll RA (1999) Long-term potentiation--a decade of progress? Science 285:1870-1874.

Matsuzaki M, Honkura N, Ellis-Davies GC, Kasai H (2004) Structural basis of long-term potentiation in single dendritic spines. Nature 429:761-766.

Patneau DK, Vyklicky L, Jr., Mayer ML (1993) Hippocampal neurons exhibit cyclothiazide-sensitive rapidly desensitizing responses to kainate. The Journal of neuroscience : the official journal of the Society for Neuroscience 13:3496-3509.

Robert A, Howe JR (2003) How AMPA receptor desensitization depends on receptor occupancy. The Journal of neuroscience : the official journal of the Society for Neuroscience 23:847-858.

Scimemi A, Tian H, Diamond JS (2009) Neuronal transporters regulate glutamate clearance, NMDA receptor activation, and synaptic plasticity in the hippocampus. The Journal of neuroscience : the official journal of the Society for Neuroscience 29:14581-14595.

APPENDIX

Supplemental Figures
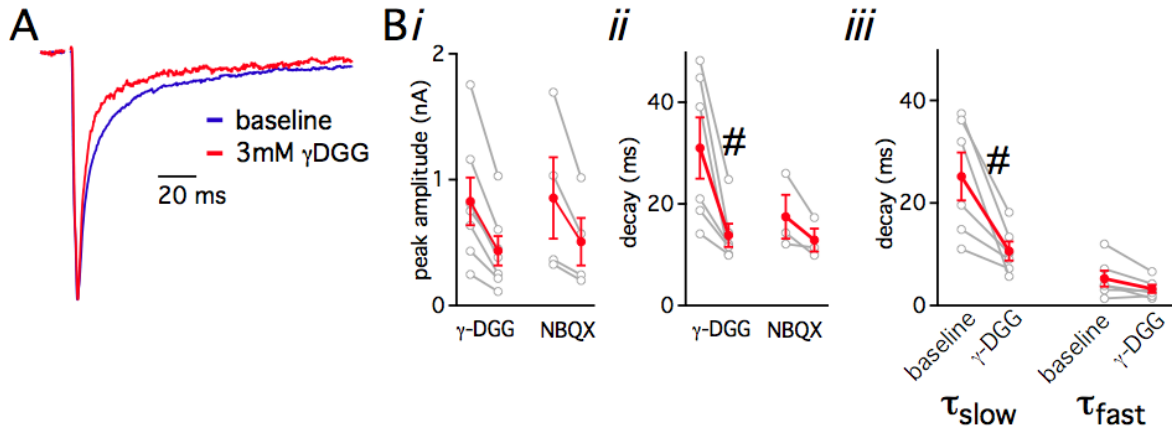
Supplemental Figure 7.1: γ-DGG accelerates the AMPAR EPSC Tau at the immature synapse in $[Ca^{2+}]_o$ of 1.5 mM

(A) Superimposed normalized AMPAR-EPSCs in control (blue) and in the presence of 3mM γ-DGG recorded in extracellular solution containing 1.5 mM $[Ca^{2+}]_o$ / 1.5 mM $[Mg^{2+}]_o$ (B*i*) Peak amplitude of AMPAR EPSC is equally inhibited by both NBQX and γ-DGG (*ii*) γ-DGG accelerates the AMPAR EPSC tau (n=6, p<0.05). (*iii*) EPSC decay was fit to a double exponential relationship: y0 + A_1e(-x/ τ_{fast}) + A_2e(-x/ τ_{slow}), and weighted τ = [τ_{fast} x A_1/(A_1 + A_2)] +[τ_{slow} x A_2/(A_1 + A_2)]. The portion of the decay most sensitive to inhibition is the τ_{slow}. Current recorded in the presence of CTZ and NMDAR antagonists.
Bath temperature: 35 ± 1°C. (#) p<0.05.
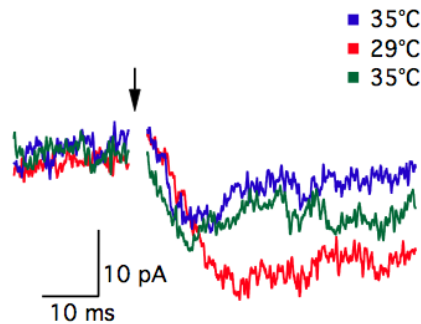
Supplemental Figure 7.2: The peak amplitude of the slow-rising current is sensitive to changes in temperature

The effects of temperature on the response of the purely spillover-mediated slow rising current recorded from an acute slice prepared from a p9 mouse. The AMPAR-mediated response was recorded in the presence of CTZ and NMDAR antagonists at V_h=-70mV. Each trace is the average of 3-4 individual traces. The peak amplitude at 35°C is on average 11.6 pA, whereas the peak amplitude at 20°C is 20.4 pA. (n=1, example).

156